Experimental and numerical investigations of the influence of cracks on mass diffusion in mortar and concrete

Teză destinată obţinerii
titlului ştiinţific de doctor inginer
la
Universitatea Politehnica Timişoara
în domeniul Inginerie Mecanica
de către

Corina Şoşdean

Conducător ştiinţific:	prof.univ.dr.ing. Liviu Marşavina
	prof.univ.dr.ing. Geert De Schutter
Referenţi ştiinţifici:	prof.univ.dr.ing. Dan M. Constantinescu
	prof.univ.dr.ing. Cosmin G. Chiorean
	prof.univ.dr.ing. Nicolae Faur

Ziua susţinerii tezei: 23.10.2015

Seriile Teze de doctorat ale UPT sunt:

1. Automatică
2. Chimie
3. Energetică
4. Ingineria Chimică
5. Inginerie Civilă
6. Inginerie Electrică
7. Inginerie Electronică şi Telecomunicaţii
8. Inginerie Industrială
9. Inginerie Mecanică
10. Ştiinţa Calculatoarelor
11. Ştiinţa şi Ingineria Materialelor
12. Ingineria sistemelor
13. Inginerie energetică
14. Calculatoare şi tehnologia informaţiei
15. Ingineria materialelor
16. Inginerie şi Management

Universitatea Politehnica Timişoara a iniţiat seriile de mai sus în scopul diseminării expertizei, cunoştinţelor şi rezultatelor cercetărilor întreprinse în cadrul Şcolii doctorale a universităţii. Seriile conţin, potrivit H.B.Ex.S Nr. 14 / 14.07.2006, tezele de doctorat susţinute în universitate începând cu 1 octombrie 2006.

România, 300159 Timişoara, Bd. Republicii 9,
Tel./fax 0256 403823
e-mail: editura@edipol.upt.ro

Summary

Even though it was intensely studied in the last decades, chloride ingress into cracked concrete and its influence on reinforced concrete (RC) structures with cracks is still not sufficiently understood, due to its complexity. Along the years, different testing methods were adopted by researchers in order to study the influence of different factors: crack characteristics, environmental parameters, concrete properties and mitigating mechanisms on chloride penetration in cracked concrete. Due to their many advantages, a great interest has been shown in developing a numerical model that can accurately predict chloride penetration into concrete by taking into consideration several aspects of the transport mechanisms of chloride. Still, very limited investigation of the influence of chloride diffusion on samples with real cracks can be found in literature. In this thesis an attempt was made to develop a numerical model that can accurately simulate chloride penetration in structures with real cracks.

Chapter 1 presents the introduction, underlining the motivation and the background of the present research project. General information about chloride penetration in concrete is presented such as the service life of a RC structure, the critical chloride value and corrosion mechanisms are presented. Also an outline of the thesis is presented.

In chapter 2 a brief review of both the experimental and numerical information found in literature regarding chloride ingress in uncracked and cracked concrete is provided. First, several crack preparation methods are presented, followed by the description of the most common experimental methods used to determine chloride penetration in concrete: migration tests and diffusion tests. The main chloride transport mechanisms are then given and briefly discussed. Also the influence of different parameters (crack width, crack depth, water-to-binder ratio, cement content and cement type, and loading conditions) and mitigating mechanisms on chloride penetration in cracked concrete are presented. Finally, a description of the various numerical and modelling techniques found in literature analysing the two or three- dimensional aspects of chloride ingress in cracked concrete taking into account its different transport mechanisms is provided.

Chapter 3 deals with the experimental part of the research. First, an overview of the experimental part is provided. In order to study the influence of real cracks on the chloride penetration in RC structures, 40 cores with 100 mm diameter were drilled from different locations from a previously loaded RC slab, manufactured with a concrete class C30/37 with a maximum size of aggregate of 14 mm. The samples where then prepared to meet the requirements specified in the standard NT BUILD 492 (1999) for the non-steady state migration test (100 mm diameter and 50 mm thickness). Based on their characteristics, the 40 samples were then grouped in four main categories: samples without cracks and without rebars (S), samples with cracks and without rebars (SC), samples without cracks and with rebars (SR), samples with cracks and with rebars (SCR). For each particular sample, geometric characteristics (crack width, crack tortuosity and roughness, rebar position) have been determined, and the position of the carbonation front was also detected. In addition to crack width measurements along the top and bottom surfaces, each core was vertically sectioned in different locations, perpendicular to the surface crack. The crack profile through the specimen's thickness was studied and the crack width through the sample was determined. In order to experimentally determine the chloride ingress, a non-steady state migration test was performed

(NT BUILD 492, 1999) and both the chloride penetration profile and the migration coefficient were determined for each sample. Based on the experimental data it was found that the presence of cracks has a significant influence on chloride ingress, increasing it, but also that chloride penetration is significantly affected by the characteristics of the concrete on the exposed surface. The surface layer of concrete affects the transport characteristics of the material and can enhance the chloride ingress. Also, although a more complex study must be performed, based on the available data, it was found that carbonation influences the chloride front and decreases significantly the chloride concentration. Even though having a limited number of replicas, a statistical analysis at a confidence level of 95% was realized in order to investigate the possible influence of crack width on chloride ingress, but no statistically significant influence was found within the range considered.

Chapter 4 presents a numerical model that can realistically simulate chloride ingress in uncracked and cracked concrete. Initially, a 2D model was developed to simulate chloride transport on mortar samples with artificial cracks (notches), with different widths and depths, using the Abaqus/Standard software based on the finite element method (FEM) using the mass diffusion tool. The algorithm for solving mass diffusion equations in Abaqus is described. The numerical results obtained were compared to the experimental ones and a good agreement between them was found, showing the validity of the proposed model. Also, from these simulations it was found that within the parameter range considered the chloride transport property of concrete is not influenced by the considered crack widths, but only by the crack depths. Furthermore, it was also concluded that chloride penetration depth has a reduced sensitivity to changes in the diffusion coefficient, when simulating chloride diffusion. A 3D model was then used to simulate chloride ingress in the uncracked and cracked samples used in the experimental part previously described. It must be mentioned that as in the case of the 2D model presented above, the model parameters such as the diffusion coefficient D, the initial chloride concentration c and the applied chloride concentration C, were determined experimentally and were used as simulation parameters. Chloride ingress was simulated in uncracked concrete (reference samples type S) and afterwards it was simulated on cracked concrete (Sample 4-of type SC with cracks and without rebars). When comparing the numerical results with the experimental ones, good agreement was found. Also, this chapter presents a 3D model of each sample used in the experimental part, with regards to the individual geometrical characteristics of each sample, including the crack pattern and rebar position.

In chapter 5, final conclusions, personal contributions and some suggestions of further research are presented.

Rezumat

Deşi a fost intens studiat in ultimele decenii, fenomenul de penetrare a clorurilor in betonul fisurat şi influenţa acestuia asupra structurilor fisurate din beton armat (BA), incă nu e suficient inţeles, datorită complexităţii sale. De-a lungul anilor, cercetătorii au folosit diverse metode experimentale pentru a studia influenţa a diverşi factori cum ar fi: caracteristicile geometrice ale fisurilor, factorii de mediu, proprietăţile betonului şi „mecanisme de atenuare" asupra penetrării clorurilor in structuri din beton fisurat. Datorită multiplelor sale avantaje, in ultimul timp s-a arătat un interes ridicat in ceea ce priveşte implementarea unui model numeric care să poată simula cu exactitate penetrarea clorului in beton, luând in considerare diversele mecanisme de transport ale clorului. Cu toate acestea un număr restrâns de informaţii se găseşte in literatură cu referire la simularea penetrării clorului in structuri cu fisuri reale.

Capitolul 1 prezintă o scurtă introducere cu sublinierea scopului şi a importanţei actualului proiect de cercetare. Informaţii generale: durata de viaţă a unei structuri din (BA), valoarea critică a ionilor de clor in beton, referitoare la penetrarea clorului in beton sunt prezentate. De asemenea este realizată o descriere schematizată a tezei de doctorat.

In capitolul 2 este facută o scurtă trecere in revistă atât a datelor experimentale, cât şi a celor numerice existente in literatură cu referire la penetrarea clorului in betonul fisurat şi nefisurat. Mai intâi, sunt prezentate diverse moduri de realizare a fisurilor, după care sunt prezentate cele mai folosite metode experimentale de determinare a clorului in beton: teste de migrare şi teste de difuzie. Principalele mecanisme de transport a clorului sunt prezentate şi descrise sumar. Totodată, influenţa diverşilor factori (lăţimea fisurii, adâncimea fisurii, raportul apă-ciment, conţinutul şi tipul de ciment, caracteristicile de incărcare) şi a mecanismelor de „atenuare" asupra penetrării clorului in betonul fisurat sunt prezentate. In final sunt descrise diversele modele numerice şi tehnici de modelare găsite in literatură care analizează aspectele bi şi tri-dimensionale a penetrarri clorului in beton, luând in considerare diverse metode de transport a clorului.

Capitolul 3 se referă la partea experimentală a actualului proiect de cercetare. Mai intâi este prezentată o descriere schematizată a testelor experimentale. Pentru a fi posibilă studierea influenţei fisurilor reale asupra penetrării clorurilor in structuri din BA, 40 epruvete de 100 mm diametru au fost prelevate prin carotare din diverse locuri dintr-o placă de BA incărcată anterior, realizată dintr-un beton clasa C30/37 cu dimensiunea maximă a agregatelor de 14 mm. Probele au fost apoi pregatite astfel incât să respecte condiţiile impuse in standardul NT BUILD 492 (1999) pentru testul de migrare rapidă (100 mm diametru şi 50 mm grosime). Datorită caracteristicilor probelor, cele 40 de epruvete au fost grupate in patru mari categorii: epruvete fără fisuri şi fara armături (S), epruvete cu fisuri şi fără armături (SC), epruvete fără fisuri şi cu armături (SR) şi epruvete cu fisuri şi cu armături (SCR). Pentru fiecare probă in parte, caracteristicile geometrice (lăţimea fisurii, traiectoria fisurilor, poziţia armăturilor) dar şi poziţia frontului de carbonatare au fost determinate. In plus, pe lânga măsurarea laţimilor fisurilor pe suprafeţele superioară şi inferioară, fiecare proba a fost secţionată vertical in diverse locuri, perpendicular pe fisură. Profilul fisurii a fost studiat pe intreaga grosime a epruvetei, iar totodată, lăţimea fisurii a fost determinată de asemenea pe toată grosimea fisurii. Pentru determinarea experimentală a penetrarii clorului, un test de migrare rapidă nestaţionară a fost efectuat (NT BUILD 492, 1999), in urma căruia

atât valoare frontului de penetrare a fost determinată, cât şi valoarea coeficientului de migrare. Pe baza datelor experimentale s-a ajuns la concluzia că existenţa fisurilor are o influenţă semnificativă asupra penetrării ionilor de clor, ducând la creştera acesteia, dar totodată s-a descoperit o influenţă semnificativă a suprafeţei expuse. Stratul superior al betonului afectează proprietăţile de transport al materialului, favorizând penetrarea clorurilor. Pe baza datelor experimentale obţinute, s-a determinat influenţa carbonatării asupra penetrarii clorului, care duce la scăderea semnificativă a concentraţiei de clor. Cu toate că există un numar limitat de replici, o analiză statistică cu intervalul de incredere de 95% a fost realizată pentru a investiga posibila influenţă a laţimii fisurilor asupra penetrarii clorului, dar nici o influenţă semnificativa din punct de vedere statistic nu s-a obţinut.

Capitolul 4 prezintă un model numeric care permite simularea penetrării ionilor de clor in betonul nefisurat şi fisurat. Iniţial, a fost implementat un model 2D care simulează penetrarea clorului in epruvete de mortar cu fisuri artificiale (crestături), cu laţimi şi adâncimi de diverse valori, cu ajutorul software-ului Abaqus pe baza MEF folosind difuzia de masa. Este prezentat algoritmul de rezolvare al ecuaţiilor de difuzie de masă din Abaqus. Rezultatele numerice obţinute sunt comparate cu cele experimentale şi datorită unei bune concordanţe intre acestea, este dovedită validitatea modelului numeric ales. Totodată, prin aceste simulări s-a demonstrat că pe baza valorilor existente, laţimile fisurilor considerate nu influenţează proprietăţile de transport a clorului, ci doar adâncimea fisurilor. Totodată s-a tras concluzia că in cazul simulării numerice, valoarea penetrării clorului are o influenţa scazută asupra coeficientului de difuzie din Abaqus. Un model 3D a fost apoi implementat pentru a simula penetrarea clorului in probele fisurate şi nefisurate folosite in partea experimentală, descrisă anterior. Trebuie precizat că la fel ca şi in cazul modelului 2D prezentat mai sus, parametrii folosiţi in modelare: coeficicentul de difuzie D, concentraţia iniţială de clor c şi concentraţia aplicată C, au fost determinţi experimental şi folosiţi ca date de intrare in simulare. Penetrarea clorului a fost simulată in beton nefisurat (probe de referinţă tip S), iar dupa aceea a fost simulată in beton fisurat (Epruveta 4 de tip SC cu fisuri şi fără armături). Rezultatele numerice au fost comparate cu cele experimentale şi au fost in buna concordanţă. De asemenea, in acest capitol este prezentat un model 3D pentru fiecare epruvetă folosită in partea experimentală, luând in consideare caracteristicile geometrice ale fiecărei probe, inclusiv ale fisurilor şi ale poziţionării armaturilor.

In capitolul 5 concluziile finale, contribuţiile personale şi câteva sugestii pentru viitoare studii sunt prezentate.

Samenvatting

Hoewel intensief bestudeerd in de afgelopen decennia, is de chloride-indringing in gescheurd beton en de invloed hiervan op gewapende betonconstructies met scheuren nog steeds onvoldoende begrepen vanwege zijn complexiteit. Door de jaren heen werden door vele onderzoekers verschillende testmethoden ontwikkeld om de invloed van verschillende factoren te bestuderen: scheurkenmerken, milieutechnische parameters, betoneigenschappen, evenals maatregelen om de chloridepenetratie in gescheurd beton te beperken. Door de vele voordelen, is er geleidelijk aan een grote interesse ontstaan in het ontwikkelen van een numeriek model dat de chloridepenetratie in beton nauwkeurig kan voorspellen rekening houdend met de verschillende aspecten van de transportmechanismen van chlorides. Toch kunnen in de literatuur slechts zeer beperkte onderzoeksresultaten gevonden worden betreffende de invloed van werkelijke scheuren op de chloridediffusie in beton. In dit proefschrift wordt een numeriek model ontwikkeld voor de nauwkeurige simulatie van chloridepenetratie in constructies met werkelijke scheuren.

Hoofdstuk 1 omvat een inleiding, met een beschrijving van de achtergrond van voorliggend onderzoeksproject, evenals een motivering. Algemene informatie betreffende chloridepenetratie in beton wordt voorgesteld, met inbegrip van de gebruiksduur van gewapende betonconstructies, het kritiek chloridegehalte, en de corrosiemechanismen. Tevens wordt de algemene structuur van de doctoraatsthesis gepresenteerd.

Hoofdstuk 2 geeft een beknopt overzicht van experimentele en numerieke studies betreffende chloridepenetratie in gescheurd en ongescheurd beton, zoals gevonden in de literatuur. Eerst worden verschillende methoden gepresenteerd voor het voorbereiden van scheuren in betonproefstukken. Nadien volgt een beschrijving van de meest gebruikte proefmethoden voor de experimentele bepaling van chloridepenetratie in beton: migratieproeven en diffusieproeven. De voornaamste transportmechanismen relevant voor het chloridetransport in beton worden vermeld en kort besproken. Voorts wordt de invloed besproken van verschillende parameters (scheurwijdte, scheurdiepte, water-cement-factor, cementgehalte, cementtype, en belastingcondities), en worden mogelijke beschermingsmechanismen betreffende chloridepenetratie in gescheurd beton gepresenteerd. Tenslotte worden de verschillende numerieke modelleringstechnieken beschreven, zoals gevonden in de literatuur, aangewend voor de twee- of driedimensionale studie van chloridepenetratie in gescheurd beton, rekening houdend met de verschillende mogelijke transportmechanismen.

Het experimentele proefprogramma van dit doctoraatsonderzoek wordt beschreven in hoofdstuk 3. Eerst wordt een algemeen overzicht gegeven van het proefprogramma. Teneinde de invloed te bestuderen van werkelijke scheuren op de chloridepenetratie in gewapende betonconstructies werden 40 kernen met diameter 100 mm geboord uit verschillende zones van een vooraf belaste gewapende betonplaat vervaardigd met een beton met sterkteklasse C30/37 en maximale korrelmaat 14 mm. De ontnomen proefstukken werden verder voorbereid in overeenstemming met de voorschriften gegeven in de norm NT Build 492 (1999) voor de uitvoering van niet-stationaire migratieproeven (diameter 100 mm, dikte 50 mm). Op basis van hun karakteristieken worden de 40 proefstukken onderverdeeld in vier categorieën: proefstukken zonder scheuren en zonder wapeningsstaven (S), proefstukken met scheuren en zonder wapeningsstaven (SC), proefstukken zonder

scheuren en met wapeningsstaven (SR), proefstukken met scheuren en met wapeningsstaven (SCR). Voor elk proefstuk afzonderlijk werden de geometrische karakteristieken (scheurwijdte, grilligheid en ruwheid van de scheur, positie van de wapeningsstaaf) bepaald, en werd de ligging van het carbonatatiefront gedetecteerd. Aanvullend op de bepaling van de scheurwijdte op boven- en ondervlak, werd elke proefstuk ook verticaal doorsneden in verschillende vlakken loodrecht op de scheur. Het scheurprofiel werd doorheen het ganse proefstuk opgemeten, evenals het verloop van de scheurwijdte doorheen de dikte van het proefstuk. Voor de experimentele studie van de chloridepenetratie werd gesteund op de niet-stationaire migratieproef volgens NT Build 492 (1999), resulterend in de bepaling van het chlorideprofiel en de migratiecoëfficiënt. Op basis van de bekomen proefresultaten werd vastgesteld dat de aanwezigheid van scheuren een significante invloed heeft op de chloridepenetratie, met een toenemende penetratie tot gevolg, doch ook dat de chloridepenetratie significant beïnvloed wordt door de eigenschappen van het beton aan het blootgestelde oppervlak. De oppervlaktelaag beïnvloedt de transportkarakteristieken van het materiaal, wat kan resulteren in een verhoogde chloridepenetratie. Bovendien, alhoewel een meer gedetailleerde studie wat dit betreft aangewezen is, werd vastgesteld dat chloridepenetratie beïnvloed wordt door carbonatatie, met een significante vermindering van de chlorideconcentraties tot gevolg. Alhoewel het aantal proefstukken beperkt was, werd een statistische analyse van de invloed van de scheurwijdte op de chloridepenetratie uitgevoerd met een betrouwbaarheidsniveau van 95%. Hierbij werd geen significante invloed gedetecteerd binnen het bereik van de hier bestudeerde scheurwijdten.

In hoofdstuk 4 wordt een numeriek model voorgesteld voor een realistische simulatie van chloridepenetratie in gescheurd en ongescheurd beton. Initieel werd een tweedimensionaal model ontwikkeld voor de simulatie van chloridetransport in mortelproefstukken met artificiële scheuren (gleufjes), met variabele dikte en diepte, gebruik makend van de diffusiemodule van het eindige-elementen-programma Abaqus. Het algoritme voor het oplossen van de diffusievergelijkingen wordt beschreven. De bekomen numerieke resultaten worden vergeleken met de experimentele resultaten. Hierbij werd een goede overeenkomst vastgesteld, wat de validiteit van het voorgestelde model illustreert. Op basis van numerieke simulaties werd vastgesteld dat de scheurwijdte geen invloed heeft op de chloridepenetratie, althans niet binnen het bereik van de in deze studie beschouwde parameterwaarden. Daarentegen werd wel een invloed vastgesteld van de scheurdiepte. Bovendien werd via een sensitiviteitsanalyse vastgesteld dat de diepte van de chloridepenetratie slechts een beperkte sensitiviteit vertoont ten opzichte van de diffusiecoëfficiënt. Voorts werd een driedimensionaal model gebruikt voor de simulatie van chloridepenetratie in de gescheurde en ongescheurde proefstukken zoals beschouwd in het experimentele programma. Net zoals in het tweedimensionale programma werden de modelparameters begroot op basis van de experimenteel bekomen waarden, zoals bijvoorbeeld de diffusiecoëfficiënt D, de initiële chlorideconcentratie c, en de aangebrachte chlorideconcentratie C. De chloridepenetratie werd gesimuleerd voor ongescheurd beton (referentieproefstukken S), en nadien voor gescheurd beton (proefstuk 4, van het type SC, met scheuren doch zonder wapeningsstaven). Een goede overeenstemming werd bekomen tussen experimentele en numerieke resultaten. Het hoofdstuk toont ook driedimensionale modellen voor elk van de proefstukken beschouwd in het experimenteel programma, met de reële geometrische karakteristieken, inclusief scheurpatroon en positie van de wapeningsstaven.

Globale besluiten worden gegeven in hoofdstuk 5, evenals een beschrijving van de persoonlijke bijdragen en suggesties voor verder onderzoek.

Acknowledgements

It is not easy to compress almost 4 challenging years into a couple of words, but I'm doing my best expressing here some thoughts. The PhD was for sure the greatest adventure I had so far. I have learned a great amount of things, not only science related, but also about me and the surrounding world. I am very grateful for this experience and all it had taught me.
First of all I would like to thank my supervisor Prof. Liviu Marsavina who made this adventure possible. Thank you for all your help and support! I am very grateful for the POSDRU/159/1.5/S/137516 financial support. I am also very grateful to BOF (Funding for candidates for a joint doctorate, Special Research Fund, Ghent University) for funding my research at Ghent University. A sincere thank you goes to my other supervisor Prof. Geert DeSchutter to whom I am really grateful for all his support, help and continuous encouragements.
Sincere aprecieri domnului prof. Dinu Gubencu pentru tot ajutorul si sustinerea oferita ori de cate ori am avut nevoie. Totodata doresc sa-i multumesc domnului prof. Corneliu Bob pentru tot sprijinul oferit.
During my stay in Gent I have met many international people. Jelena, Irena, Florencia, Ioanna, Arnel, thank you for your friendship and support, you are always welcomed to visit me in Romania.
A special thank you goes to the all the staff at Magnel Laboratory, where I had the chance to do my experimental research. Thank you: Philip, Mathias, Didier and Arn for all your advice and suggestions. Thank you: Christel, Stefan and Dieter for your help, smile and kind words. I was really lucky to find a lot of internationals that soon became my friends and family. Even now when I'm thinking of you I am nostalgic. I'm sure you I will always remember our picnics, cooking evenings, chats in the lab, tea rituals, and cultural debates during lunch time, the times we went out...these and yourselves will never be forgotten. Sandra, Jianyun, Kun, Chris, Cornelia, Farid, Tan, Yang, Kai, Raul...thank you.
Le multumesc familiei si prietenilor mei pentru incurajarile si sustinerea oferita.
Lijie, Eleni, Hugo, Joao, you have a special place in my heart; no words could express how lucky I am to have met you. Thank you for everything! Andreea, Mona, multumesc pentru tot suportul moral oferit de la inceputul si pana la sfarsitul acestei etape din viata mea.
Spre sfarsit le multumesc celor care m-au sustinut intotdeauna indifferent de drumul pe care l-am ales, multumesc mama si tata pentru ca imi sunteti mereu alaturi!
Alex, iti multumesc pentru ca desi nu a fost usor, ai fost tot timpul alaturi de mine si m-ai ajutat ba cu un umar pe care sa plang, ba cu o imbratisare, ba schimband rezolutia la o imagine, adaptandu-te fiecarei noi provocari. Iti multumesc!

Timisoara,
09.09.2015

Corina Sosdean

Pentru mama şi tata.

CUPRINS

LIST OF FIGURES

LIST OF TABLES

1. INTRODUCTION

1.1. Background

Being considered the most versatile and robust construction material available, due to its many advantages such as: low cost, convenient raw material source, wide applicability, acceptable performance…reinforced concrete has become the most widely used construction material in the world. As reported by (Lippiat and Ahmad, 2004) about one ton of concrete is produced each year for every human being in the world.

Still, in the last decades a great interest in studying the durability issue of concrete has been shown, as a consequence of the huge amount of money spent on repair or reconstruction of RC structures. According to (Knudsen, 1998) in 1998, a large number of reinforced commercial buildings, domestic dwellings, marine structures, bridges... particularly those over 30 years of age started to show deterioration; the annual cost of repair work on concrete structures was over US$ 5 billion in Western Europe alone. According to the study completed by (Koch, 2002) in 2002, the annual cost of highway bridge repairs and maintenance is over $8.3 billion in the United States. With regard to De Sitter's Law of Fives, (De Sitter,1984) major repair cost is five times more the cost of maintenance repairs if they would have been done on time. Also, all-out replacement cost is five times more the major repairs cost if they would have been done on time.

In general, the durability of a RC is defined by its ability to serve its intended purpose for a designed service life while resisting weathering action, chemical attack, abrasion…In normal conditions, in sound concrete, the cement matrix forms a passive film along the surface of the embedded rebars. Under this condition, the corrosion rate is negligible, even if the concrete is permeated by oxygen and moisture (Bertolini, 2008). During the service life of the structure, this protective layer can be disrupted or destroyed, resulting in the corrosion of the rebar. The volume of rust products is considered to be four- six times larger than the one of the steel, which causes cracking, delamination and spalling.

Chloride ingress and carbonation are considered to be the main causes of steel corrosion. In aggressive environments such as the marine environment or when being exposed to deicing salts, the high concentration of chloride ions causes local depassivation of the reinforcing steel and pitting corrosion occurs. Carbonation-induced corrosion develops due to the neutralization of the alkalinity of the concrete by the carbon dioxide in the atmosphere.

1.2. Chloride penetration in RC structures

1.2.1. Service life and critical chloride value

Several definitions can be found in literature when referring to the service life of a RC structure. According to (Savija, 2014), the service life of a structure can be defined as the period of time after construction during which all properties exceed minimum acceptable values when routinely maintained. (Rostam, 2000) defines the technical service life as the time in service until a defined unacceptable state of deterioration has been reached by the structure. With regards to corrosion of rebars, (Tutti, 1982) defines service life as being the sum of the initiation time and the propagation time; this approach is the most popular and widley adopted by researchers when focusing on chloride attack of RC structures.

(Cao, 2001) defines the service life of a concrete structure in different ways: time from construction until the chloride content at the reinforcement is high enough to initiate steel corrosion; time from construction to time at which signs of distress are observable; time from construction to time at which the structure is considered to be functionally unacceptable or unsafe.

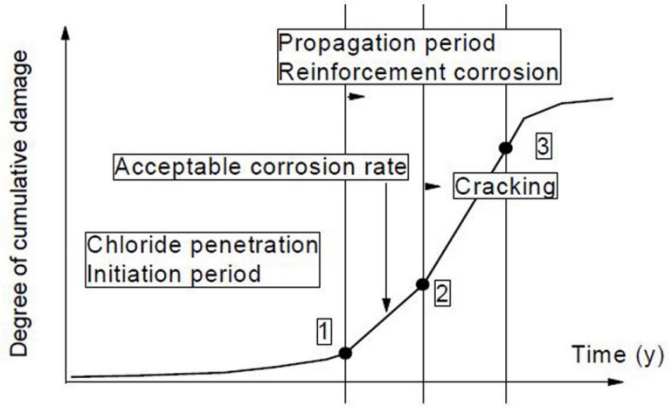

Figure 1.1. Definitions of service life (Cao, 2001)

The initiation phase can be defined by the period of time until the protective passive layer around the rebars is destroyed by either the action of chlorides or by the reduction of alkalinity in the pore solution by carbonation. It is considered that as soon as the maximum allowable chloride value/ chloride threshold concentration/ critical chloride content is reached, propagation starts. According to (Angst, 2009) critical chloride value can be defined as the chloride content required for depassivation of the steel or as the chloride content associated with visible or acceptable deterioration of structure. Due to the fact that the majority of service life models consider the end of the service life of a structure once the propagation period begins, it is very important to know this parameter. Even though there are different codes defining the allowable chloride value in (% weight of binder): 0.4 (BS 8110, 1997), 0.2 (ACI 222, 1994), 0.2- 0.4 for reinforced concrete and 0.1-0.2 prestressed concrete (Eurocode 2, 1992), this parameter is still under a lot of debate.

1.2.2. Corrosion mechanisms

Corrosion of reinforcing steel in concrete is an electrochemical process that requires the presence of an anode, cathode and an electrolyte. Due to the fact that the passive layer is destroyed, the electrochemical potential becomes more negative locally, which causes iron atoms to lose electrons and this part of the rebar becomes the anode, while the rest of the rebar is the cathode. The released electrons move through the reinforcement and are absorbed in the concrete pore solution (electrolyte) and oxygen and water combine producing hydroxyl ions (OH-) (Martin-Perez, 1999). The reactions that take place are (Martin-Perez, 1999):

- anodic reaction:

$$Fe \rightarrow Fe^{2+} + 2e^{-} \quad (1)$$

- cathodic reaction:

$$O_2 + 2H_2O + 4e^{-} \quad (2)$$

The hydroxide ions migrate through the pore solution towards the anode where they combine with the ferrous ions and ferrous hydroxide is created which is transformed to rust if it continues to oxidize:

$$Fe^{2+} + 2OH- \rightarrow Fe(OH)_2 \quad (3)$$

$$4Fe(OH)2 + 2H2O + O_2 \rightarrow 4Fe(OH)_3 \quad (4)$$

Chloride corrosion happens when the chlorides penetrate the passive layer and react with iron ($Fe^{2+} + 2Cl^{-} \rightarrow FeCl_2$). Ferrous chloride combines then with oxygen and water (Martin-Perez, 1999):

$$4FeCl_2 + O_2 + 6H_2O \rightarrow FeOOH + 8HCl \quad (5)$$

The released chloride ions continue to react with ferrous ions, encouraging further oxidation of the iron, so that the process is continuous and the chlorides act as catalyst, increasing the volume of rust. The reactions of corrosion formation are presented in Figure 1.2.

Even though carbonation and chloride ingress are the main causes of rebar corrosion, there are very few publications regarding their combined effect on RC structures. According to (Vesikari, 2009) carbonation pushes the chloride front forward by liberating chlorides that were bound in non-carbonated concrete. (Yoon, 2007) experimentally investigated the interaction between carbonation and chloride penetration and their effects on concrete, under various boundary conditions and found that carbonation of concrete could significantly accelerate chloride penetration. Other studies (Malheiro, 2014) show that carbonation has a direct influence on chloride penetration, decreasing it.

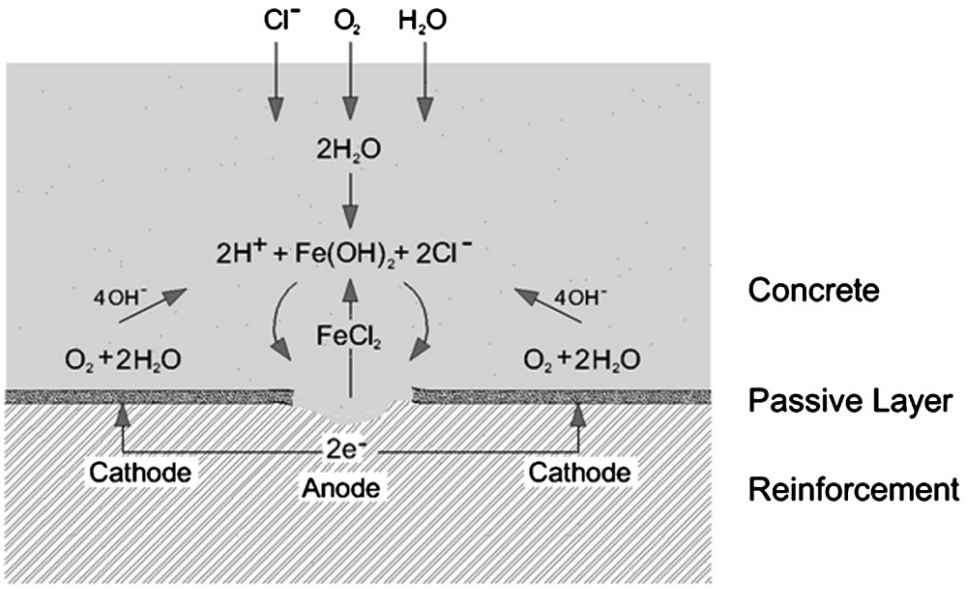

Figure 1.2. Anodic, cathodic reactions for corroding steel (Papakonstantinou, 2013)

1.3. Significance of present research

Even though significant studies were performed in the last years in order to predict the durability of reinforced concrete structures, chloride induced corrosion remains a significant challenge. In order to delay corrosion and to extend the service life of a structure, in present concrete designs several measurements are being taken such as: the usage of low-permeability concrete (low water- binder ratio), the addition of supplementary materials, the usage of different surface coatings…but researchers are still working in developing numerical models in order to have a better understanding of the mechanism and parameters influencing chloride ingress in concrete.

Also, in reality, these structures are frequently cracked either by mechanical loading either as a consequence of chemo-physical effects such as: temperature and moisture gradients, or expansive chemical reactions. Generally it is recognized that the existence of cracks accelerates the ingress of chloride ions. In order to more accurately predict the service life taking into account the potential effect of cracks, it is very important to have a numerical tool which is able to simulate chloride diffusivity in cracked concrete.

Many researchers studied chloride ingress in cracked concrete structures and also many of them proposed different models to simulate chloride ingress, these are presented in Section 2. Yet, due to the fact that real cracks in concrete have a complex 3D geometry and their influence on transport and degradation mechanisms is not straightforward, very limited investigation of the influence of chloride diffusion on samples with real cracks can be found in literature (Lu, 2012, Savija, 2013).

The purpose of the present research is to develop a numerical model that can accurately simulate chloride penetration in uncracked and cracked concrete. Parameters needed as input data in the simulation are determined experimentally and also the geometric characteristics of the samples used are taken into consideration when determining the geometry of the model considered in the numerical simulations.

1.4. Outline of thesis

Chapter 1 underlines the motivation and the background of the research project. In Chapter 2 the state of art is presented, synthetizing relevant literature reviews on the topic of chloride ingress, including crack preparation methods (Section 2.2), testing methods (Section 2.3), the main chloride transport mechanisms (Section 2.4), the most important parameters influencing chloride penetration in cracked concrete (Section 2.5), factors that are delaying rebar corrosion (Section 2.6) and different models of numerical simulation for chloride transport modelling in concrete (Section 2.7).

The following two chapters refer to the experimental, respectively the numerical part of the present work. Chapter 3 refers to the experimental part of the thesis. An overview of the aspects studied here is presented in Section 3.1. The experimental procedure is described in details such as follows: first the materials used and the sample preparation are presented in Section 3.2, while the sample characterisation and the adopted testing methods are presented in Section 3.3, respectively Section 3.4. The influence of carbonation is presented in Section 3.5. The results of the experimental program dealing with different considered aspects are further studied in Section 3.5 as follows: crack width measurements (Section 3.5.1), influence of several parameters on the penetration depth (Section 3.5.2) and on the migration coefficient (Section 3.5.3) and the influence of carbonation (Section 3.5.4). A statistical analyse is further presented in Section 3.5.5, where certain statistical methods are presented (Section 3.5.5.1) in order to determine the influence of various parameters determined experimentally (eg. exposed surface, the presence of rebars, the presence of cracks…) on chloride ingress (Section 3.5.5.2).

Chapter 4 presents the numerical model adopted in order to simulate chloride diffusion in cracked concrete. Section 4.1 presents an overview of the numerical work. Section 4.2 presents the background and the aim of the numerical research, while the development of the numerical model and the simulation of chloride ingress in uncracked and cracked concrete are presented in Section 4.3, Section 4.4, respectively Section 4.5. Final conclusions, personal contributions and recommendations for future research are presented in Section 5.

2. LITERATURE REVIEW

2.1. Introduction

Concrete is one of the most popular construction materials, which has been used ever since the Roman times. The limitations regarding its relatively low tensile strength and ductility have been successfully dealt with by embedding reinforcement in concrete. This usually consists of steel rebars. As a consequence, reinforced concrete (RC) became one of the most widely used modern building materials. In the last decades a great interest has been shown in studying reinforcement corrosion as it became one of the main factors of degradation and loss of structural integrity of RC structures. The degradation process is accelerated in the case of RC structures situated in aggressive environments like marine environments or subjected to de-icing salts or wetting and drying. As previously mentioned in Section 1.2, corrosion occurs when the passive layer protecting the rebar is disrupted or destroyed, causing deterioration of the concrete cover.

Chloride induced corrosion in reinforced concrete structures remains one of the major challenges. Many studies were performed in the last decades in order to predict durability of concrete structures. In reality, these structures are frequently cracked either by mechanical loading either as a consequence of chemo-physical effects such as: temperature and moisture gradients, or expansive chemical reactions. Generally it is recognized that the existence of cracks accelerates the ingress of chloride ions. In order to more accurately predict the service life taking into account the potential effect of cracks, it is very important to understand the mechanisms and phenomena that are taking place.

2.2. Crack preparation methods

Researchers have used different experimental programs in order to create cracks in undamaged concrete. Based on the crack preparation method these studies can be roughly divided into two main categories: destructive and non-destructive methods.

The most popular destructive methods used by researchers are:

- **Brazilian splitting test**: In order to induce cracks in cylindrical specimens, diametrical loading is applied until a predetermined lateral displacement is obtained. The samples are positioned between two press platens on two slim plywoods to prevent crushing at the contact points; two LVDT (linear variable displacement transducer) sensors are clamped to the disc and measure the lateral displacement normal to the load axis along the opposite faces of the sample; their average is called lateral displacement or COD- crack opening displacement. Several lateral displacements under loading are obtained until the desired COD is obtained. Several researchers used this method to produce controlled cracks (Aldea, 1999); (Wang,

1997); (Song, 2006); (Picandet, 2009); (Seung, 2011); (Jang, 2011); (Djerbi, 2008).

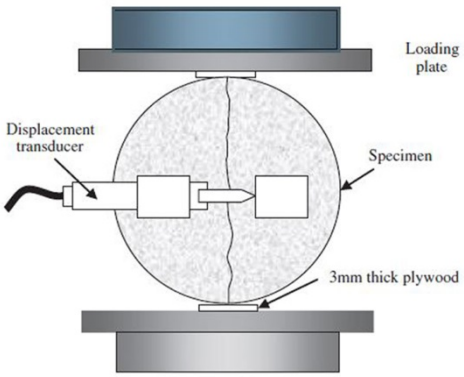

Figure 2.1. Brazilian splitting test (Jang, 2011)

- **Wedge splitting test**: This method which is often used in fracture mechanics has been used by some researchers (Brühwiler, 1990); (Yoon, 2009); (Pease, 2010); (Karihaloo, 2006); (Reinhardt, 2007); (Schlangen, 2007); (Ye, 2012), Due to its advantages such as: it uses relatively small specimens, the test is simple and it doesn't involve sophisticated test equipment. Prismatic specimens which have a cast groove and a notch are being used. Two rollers are placed into the groove and through a wedging device the splitting force is applied. The compressive vertical load is turned by the rollers in two horizontal loads which move away from each other and the crack propagates through the notch. The CMO (crack mouth opening) is measured using LVDT and the crack width can be controlled.

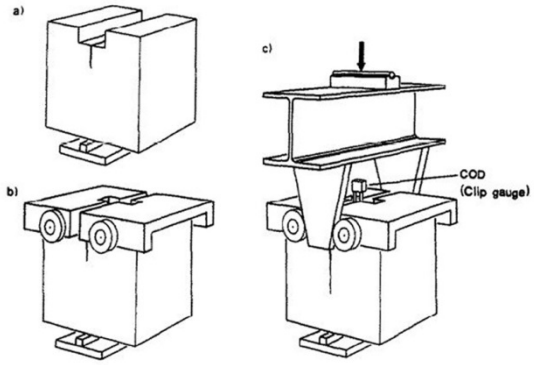

Figure 2.2. Wedge splitting test (Brühwiler, 1990)

- **Expansive core method**: (Ismail, 2004); (Ismail, 2008), used this method to induce controlled cracking in doughnut- shaped brick and mortar samples using a mechanical expansive core. Radial cracks were induced with a mechanical expansive core and an external steel ring. Controlled cracking was obtained by manually

adjusting the deformation of the expansive core which caused deformation of the internal diameter of the sample.

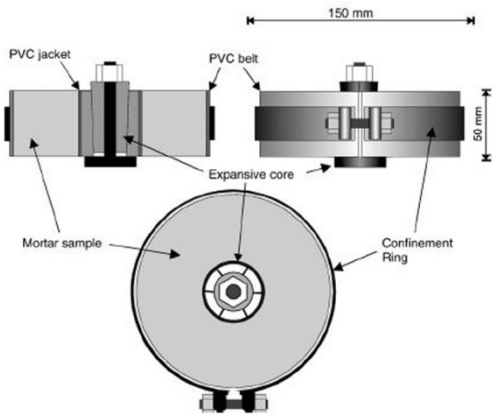

Figure 2.3. Expansive core method (Ismail, 2004)

- **Bending tests**: Reinforced concrete beams subjected to three or four point bending are being used in order to create a single or multiple cracks. Using LVDT sensors the crack widths are controlled by monitoring the CMO (crack mouth opening). This method is considered to give the most realistic cracks and it can be used to study the chloride transport properties in cracked concrete under loading. Various research programs using bending tests in order to produce cracks were carried on (Granju, 2005); (Gowripalan, 2000); (Win, 2004); (Şahmaran, 2007); (Kato, 2005); (Li, 2001); (Mohamed, 2001); (Adiyastuti, 2005); (François, 1998); (Marcotte, 2003); (Otsuki, 2000); (Schießl, 1997); (François, 2006); (Ye, 2013).

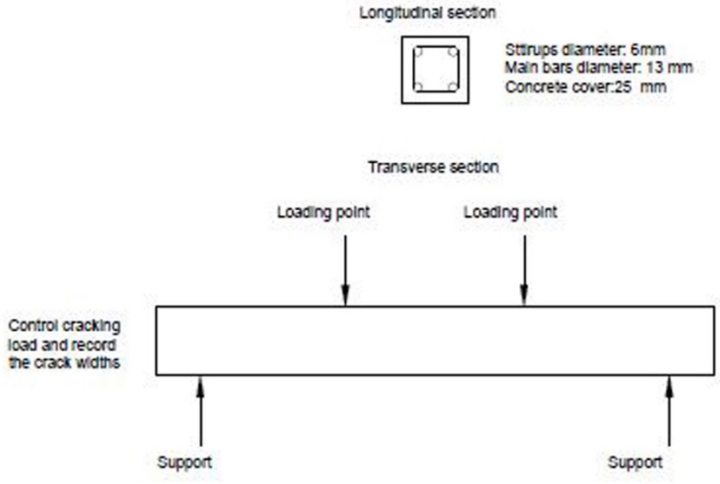

Figure 2.4. Four point bending test (adaptation after Mohamed, 2001)

For non-destructive methods presented in other studies a special casting method is being used in order to simulate a notch-type crack by means of positioning and removal of thin copper sheets before final setting of concrete. Single or multiple notches, with different widths and depths were analysed (Audenaert, 2007); (Audenaert, 2008a); (Audenaert, 2008b); (Marsavina, 2009); (Mu, 2013); (Ma, 2013).

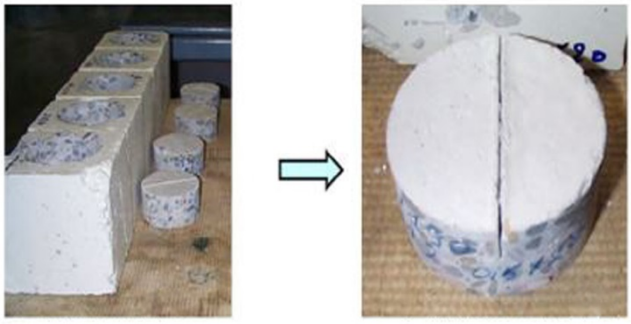

Figure 2.5. Notch method using copper sheets (Marsavina, 2009)

Smooth cracks can also be produced by saw cutting concrete cylinders longitudinally (Rodriguez, 2003); (Pour-Ghaz, 2009a); (Pour-Ghaz, 2009b). In the study of (Rodriguez, 2001), the cracks were created by clamping the cut cylinder parts back together and brass shims of various thickness at the edges were used to keep the gap open.

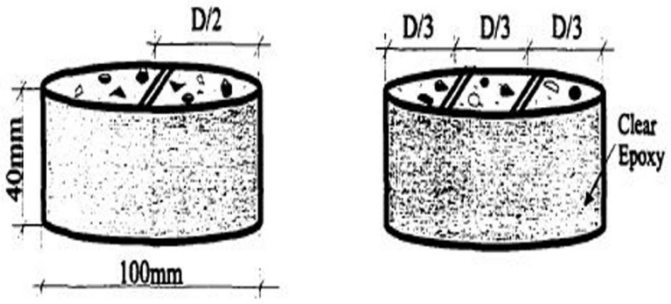

Figure 2.6. Concrete samples containing one and two smooth cracks (Rodriguez, 2001)

Each of the methods presented above has its advantages and its disadvantages. A comparison between the destructive and the non-destructive methods was realized by (Mu, 2012). The notch method has some clear advantages when dealing with the repeatability of tests, the accuracy of obtaining cracks with imposed widths and lengths, which contribute to reliable results. This method can successfully be used in order to study the influence of some parameters such as: crack widths, crack lengths, cement type ….on chloride ingress in concrete.

However, their main disadvantage is that they are not natural shaped cracks, they are parallel walled and this can have some influence on the transport properties. (Marsavina, 2009); (Van den Heede, 2014). Also, the influence of some parameters such as tortuosity, crack connectivity and roughness can't be taken into consideration when dealing with artificial cracks.

The main advantage when using destructive methods consists in obtaining controlled cracks with characteristics comparable to the ones of real cracks, such as crack pattern, tortuosity and connectivity. Still, they are some considerable disadvantages such as: the low repeatability rate, accuracy and reliability.

(Savija, 2014) synthesized the destructive methods based on the possibility of using these methods in order to obtain realistic cracks using reinforced specimens. All the methods presented are being used to study controlled cracks in order to have a better understanding of the chloride ingress in concrete structures. Even though natural cracks obtained from the destructive methods are what can be considered the closest form of real cracks, only very limited information of non-controlled cracking is known. (Taheri- Motlagh, 1998) studies the (micro) cracks induced by thermal stresses in large beams and small cubes subjected to alternate wetting and drying cycles to simulate the marine condition.

2.3. Testing methods

In order to have a better understanding of chloride ingress into concrete, several experimental methods have been used by researchers. These tests are summarized by (Stanish, 1997. Also, a more detailed description of different rapid test methods can be found in (Hooton, 2001).

The most common experimental methods used are: diffusion tests and migration tests. Their main advantages and disadvantages are highlighted by (Mu, 2012).

- **Diffusion tests**: They are considered to be representing the natural chloride diffusion process. They can be divided in: non-steady state diffusion tests and steady-state diffusion tests. Several diffusion tests have been used by researchers. (Audenaert, 2009) carried out diffusion tests using concrete samples with artificial cracks; the specimens were immersed for 10 months in a 3.5% NaCl solution. (Ismail, 2008) used specimens with different crack openings subjected to a diffusion test for 14 days. (Kato, 2005) used reinforced rectangular specimens and conducted accelerated penetration of chloride ions for 91 days either through a wet test or through a drying-wetting test. (Rodriguez, 2001) used the (NordTest NTBuild 443, 1995) bulk diffusion test and exposed concrete cylinders for 40 days. (Mu, 2013) also used the bulk diffusion test to investigate the effect of crack density on chloride transport in cracked concrete using samples with a variable number of notches.
- **Migration tests**: This is a much faster way to study chloride penetration into concrete. However, due to the fact that an external electrical field is applied, migration, and not diffusion, is the main chloride transport mechanism. Therefore, this is not considered to be in accordance to chloride diffusion in real structures. The non-steady state migration test was standardized in (NT Build 492, 1999) and has been used by many researchers. (Audenaert, 2008a) and (Marsavina, 2009) determined the influence of notches with different widths and depths on chloride penetration using an electrical field for different time duration. (Djerbi, 2008) used a steady-state migration test to examine the effects of traversing cracks of concrete

on chloride diffusion. (Jang, 2011) also used steady-state migration to study the effect of crack width on the diffusion.

2.4. Chloride transport mechanisms

The behaviour of chloride ions inside concrete is related to various factors such as: concrete properties (cement type, water-binder ratio, pore structure…), environmental factors (temperature, humidity, concentration of chlorides and the presence of pollutants…), construction practices (concrete cover depth), the moisture content of concrete, the mechanisms of transport of the chloride- bearing solutions and so on.

(Bertolini, 2008) categorized the transport mechanisms of chlorides into concrete as: ionic diffusion, migration, convection/ capillary suction and permeation.

- **Diffusion**: is the movement of chloride ions through saturated concrete due to a chloride concentration gradient and it's usually characterized by Fick's second law;
- **Capillary** suction/ convection: happens due to moisture gradients in partially saturated concrete when the surface of non-saturated concrete comes into contact with a solution containing chlorides which is quickly absorbed into the concrete.
- **Permeation**: is the penetration of chlorides due to a pressure difference.
- **Migration**: is the transport of chlorides due to the presence of electrical fields when the chlorides present in the pore solution migrate into zones with lower electrical potential;

Most studies found in literature consider that only one of these transport mechanisms, usually diffusion, governs chloride ingress. In reality, chloride penetration is a complex combination of all these transport mechanisms.

2.4.1. Diffusion

Diffusion is considered by many researchers to be the main transport mechanism governing chloride ingress in concrete. When the concrete is in a saturated state or in a partially saturated state, chloride ions penetrate the concrete by ionic diffusion due to the existence of a concentration gradient which drives chlorides to move from an area of high concentration to an area of low concentration. An important influencing factor of chloride diffusion is the physical characteristics of the capillary pore structure which can provide fast routes for chloride ions. Due to the fact that diffusion occurs through interconnected moisture-filled pores and fractures, the existence of cracks provides a pathway for diffusion.
Diffusion is based on Fick's first law of diffusion, which relates the diffusion flux (J) to the concentration gradient ($\frac{\partial C}{\partial x}$) and a material property. The negative sign indicates that diffusion occurs in the opposite direction to that of concentration gradient. For a one-dimensional diffusion this is:

$$J = -D\frac{\partial C}{\partial x} \tag{2.1}$$

where:
J- the flux chloride ions, [(amount of substance) per unit area per unit time], e.g. mol/m^{2}s;

D- the diffusion coefficient or diffusivity, in dimensions of [length^2 time^{-1}], e.g. m^2/s;
C- chloride concentration in dimensions of [amount of substance per unit volume], e.g. mol/m^3;
x- the position, [length], e.g. m.
Fick's first law is used for modeling diffusion in steady-state condition assuming that there is no concentration change with time and that pure diffusion occurs in an isotropic environment.
In order to model diffusion in a non-steady state condition, taking into consideration the change of concentration with time, Fick's second law can be used:

$$\frac{\partial c}{\partial t} = D\frac{\partial^2 C}{\partial x^2} \tag{2.2}$$

The following boundary conditions are considered for the semi-infinite case with a single spatial dimension x:

- $C=C_0$ at x=0 and t>0 (boundary condition)
- C=0 at x>0 and t=0 (initial condition).

If a constant diffusion coefficient is considered, Eq. (2.2) has the following analytical solution:

$$C = C_0\left[1 - erf\left(\frac{x}{2\sqrt{Dt}}\right)\right] \tag{2.3}$$

where C_0 is the surface chloride concentration and erf() is the mathematical error function.

Diffusion is a very slow process that normally takes place when concrete is permanently submerged in water, e.g. marine structures. In reality most structures are partially saturated affected by drying-wetting cycles, in this case chloride diffusion depends on the moisture distribution in the concrete cover. In order to have a realistic model it is important to clarify the moisture transport in concrete.

2.4.2. Capillary suction / convection

Capillary suction occurs in non-saturated or in partially saturated concrete when liquids are drawn into the concrete pores due to surface tension acting in capillaries. The capillary suction force occurs near the surface of the concrete where the degree of saturation is zero and it decreases as the degree of saturation increases. Unlike diffusion, capillary suction occurs much faster than diffusion reaching the maximum value some millimetres inside the concrete.

When considering an idealized round pore, capillary pressure can be determined using the Young- Laplace equation:

$$P = -\frac{2v\cos\theta}{r} \tag{2.4}$$

where:
P- the pore pressure;

γ- liquid-vapor surface tension of fluid;
θ- the contact angle between the solid and the fluid;
r- the pore radius.

2.4.3. Permeation

Penetration occurs through the porous medium, from a zone of high hydraulic pressure to one of low hydraulic pressure. This type of chloride transport mechanism usually takes place in the case of offshore or underground concrete structures where hydrostatic pressure increases with depth. It can be determined using Darcy's law:

$$\frac{dq}{dt}\frac{1}{A} = K\frac{dh}{dx} \tag{2.5}$$

where:
dq/dt- flow rate per unit area;
K- coefficient of permeability;
dh- pressure difference across the specimen thickness, *x*.

2.4.4. Migration

Migration occurs when an electrical field is applied, forcing the ions (cations and anions) to move towards the applied (negative or positive) electrical charge. In the case of chlorides ingress in concrete, when an electrical field is applied positive ions (cations) migrate in the direction of the applied current, while the negative chloride ions (anions) move in the opposite direction. Migration is considered an accelerated diffusion test and due to the fact that provides a fast and easy way to determine the chloride ingress in concrete it has been widely used in laboratory test. A standardized method for the determination of the chloride migration coefficient in concrete is presented in (NTBuild 492, 1999).

2.4.5. Chloride binding

Chloride ingress in concrete is also affected by chloride binding. When chloride ions penetrate into concrete, a part of them will be retained by the cement hydration products, phenomenon called chloride binding.

As (Yuan, 2009 a) underlines, it is very important to consider chloride binding when studying the service life of concrete structures, because: reduction of free chloride concentration in the vicinity of the reinforcing steel reduces the chance of corrosion; removal of chloride from the diffusion flux retards the penetration of chloride to the level of the steel; formation of Friedel's salt results in a less porous structure and slows down the transport of chloride ion.

According to (Hirao, 2005) chloride ions can be found in concrete in two forms: as free chloride in the pore solution and as bound chloride in some form to cement paste. Free chlorides are usually associated with the corrosion initiation period while physically and chemically bound chlorides are more related to the propagation period of corrosion due to chloride ingress.

2.5. Influencing parameters

There are several factors influencing chloride penetration in cracked concrete. As follows, some of the most important parameters are presented.

2.5.1. Crack width

Crack width can be considered the most controverted parameter that can influence the penetration of chloride in cracked concrete. The influence of crack width is still under debate even though there are different codes prescribing an allowable crack width ranging from 0.5 to 0.3 mm (ACI Manual of Concrete Practice, 1999), (British Standards Institution ENV, 1992); (British Standards BS, 1997). (Gérard, 2000) show that in the case of steady state migration tests, the coefficients of concrete with different crack widths are one order of magnitude higher than for uncracked concrete. (Djerbi, 2008) found, while evaluating cracks with average widths ranging from 30 to 250 μm using a steady-state migration test, that the diffusion coefficient of cracked concrete increased with increasing crack width, but becomes constant when the crack width is higher than ~80μm. Using steady-state migration tests, (Jang, 2011) found that the threshold crack width for diffusion is around 55-80 μm and above this threshold value, the diffusion coefficients start to increase with crack width. (Ismail, 2008) determined that for crack opening lower than the critical mechanical opening (30μm), no chloride diffusion occurs along the crack path. (Yoon, 2009) found that for a rapid test, cracks smaller than 0.013 mm have no influence of penetration depth, while in a long-term test, the threshold width was found to be 0.04mm. Other studies conducted by (Marsavina, 2009) and (Audenaert, 2008a), on notched specimens with (artificial) crack widths between 0.2-0.5 mm, found no pronounced influence of crack width on chloride penetration. (Rodriguez, 2003) also concluded that chloride diffusion in concrete was independent of crack width for the 0.08-0.68 mm width range considered.

2.5.2. Crack depth

Another parameter affecting chloride ingress is crack depth. However, not many studies have been carried on in order to have a better understanding of the influence of this parameter. (Marsavina, 2009) and (Audenaert, 2008a) found in their studies that penetration depth is increasing with an increasing notch depth and that this effect is more pronounced for longer test durations.

2.5.3. Water-to-binder ratio

In order to determine the influence of w/b on chloride diffusivity, (Djerbi, 2008) conducted a steady-state migration test in which three concrete mixes were used: one ordinary concrete (OC) with a w/c of 0.5 and two high performance concretes with two different mix designs, the first had a w/c of 0.32 (HPC), the second had a w/c of 0.38 and contains 6% of silica fume (HPCSF). The results concluded that chloride ion penetration through the crack is considered to occur more easily in OC than in HPC and HPCSF. (Win, 2004) investigated the influence of different parameters on chloride diffusion including w/c ratio and it was determined

that the increasing of w/c led to a higher ingression rate of Cl^- ions, not only from the exposed surface but also around the cracks. (Konin, 1998) used three concrete types: the first one was (Ordinary Concrete), while the second one produced a high strength concrete (HSC) and the third one a very high strength concrete (VHSC). In the second and third compositions, part of the cement was replaced by silica fume. It was observed that HSC with a low water/cement ratio reduces the chloride ingress level.

2.5.4. Cement content and cement type

(Konin, 1998) concluded in their studies that the addition of silica fume reduces the penetration of chloride ions into concrete. (Jang, 2011) also found that the addition of fly ash also decreases the diffusion coefficient. (Rodriguez, 2001) observed that concrete containing 25 % replacement of cement by blast furnace slag possesses a better ability to resist the ingress of chloride ions than LOO % OPC concrete. (Otiento, 2010) found that the increase of corrosion rates was smaller in Corex slag specimens (increases of 40% or more) than in OPC specimens (increases 210% or more).

2.5.5. Loading conditions

(Gowripalan, 2000) studied the effect of flexural loading on chloride diffusion in both the tension and compression zones of cracked concrete. Their research showed that the apparent chloride diffusion coefficient in the tension zone was higher than in the compression zone, which can be attributed to the reduction in the porosity of the concrete in compression, which slows down diffusion. (Antoni, 2008) studied the effect of static and cyclic loading on the chloride penetration into plain concrete (PC) and fiber reinforced concrete (FRC). The results of the static loading showed that there was a slight reduction in the chloride penetration under low level of compressive stress while an increase in the chloride penetration was found at higher stress level. Also, he concluded that the increase in the chloride penetration is more pronounced when the concrete is subjected to cyclic compressive loading. In the studies of (Saito, 1995) normal weight concrete was subjected to static and repeated compressive loading in order to evaluate the chloride permeability. The results of concrete under static loading showed that the application of loads up to 90 % of the ultimate strength had little effect on the chloride permeability. It was found from the results of concrete under repeated loading that load repetitions at the maximum stress levels of 60 % or more caused the chloride permeability to increase significantly. The test results also indicated that the chloride permeability of concrete subjected to static and repeated loading increased at an increasing rate with its residual strain.

(Deif, 2010) conducted a study in which a small-scale RC slab was subjected to wet and dry cycles with a saturated chloride solution while sustaining static service loads in order to investigate the effect of sustained load on chloride ingress in concrete. The experimental results indicate that there is a dependence of chloride ingress properties on the type and level of sustained load. The same conclusion was reached by (Karam, 2014) while investigating the influence of sustained compressive and tensile stresses on chloride ingress into concrete. (Cousin, 2010) studied the effect of chloride-induced corrosion on pre-tensioned pre-stressed

beams. First, the beams were exposed to a saturated chloride solution while sustaining a flexural load. The results show that the higher the load, the higher the rate of chloride ingress. Afterwards, the influence of corrosion of the strands on the loading capacity of the beams was investigated. (Results show that the loading capacity of the beams can be impaired up to 60% for the higher corrosion degrees studied. For low corrosion degrees for which no or minor external signs of corrosion damage were apparent, the loading capacity decreased up to 20% only in the cases where the anchorage length was affected by corrosion.). (Wang,H., 2011) studied the effects of compressive and flexural loads on chloride transport. The experimental results indicated that the chloride concentration and apparent chloride diffusion coefficient decreased with the increase of the compressive stress, up to 55% of the compressive strength, and they increased with the increase of the flexural stress. (Fu, 2015) conducted an investigation regarding the loading effects on chloride diffusion in saturated concrete. Two types of concrete mixes were investigated for chloride diffusion tests under compressive and tensile loads at different magnitudes. It was concluded that the chloride diffusivity increases with the increase in tensile strain, while it decreases with the increasing compressive strain within a limit range.

(Jaffer, 2009) conducted a study in order to examine the composition and distribution of chloride-induced corrosion products at the rebar–concrete interfaces and on crack surfaces in reinforced ordinary Portland cement concrete (OPCC) and high performance concrete (HPC) subjected to different loading conditions. The results show that dynamic loading caused a greater detachment of the aggregate–paste bond in OPCC than static loading. The opening and closing of the cracks in salt solution under dynamic load forced corrosion products to flow from the rebar–concrete interface into the cracks in both OPCC and HPC. As a result, corrosion products diffused from the crack into the cement paste in the dynamically loaded OPCC but remained in the cracks in the dynamically loaded HPC, where they induced branched cracks.

(Wang, J., 2014) conducted a study in order to have a better understanding of the influence of micro-cracks on chloride induced corrosion. 24 reinforced concrete beams with 4 different concrete mixes were subjected to three levels of sustained lateral loading (0%, 50% and 100% of the load that can induce 0.1 mm wide cracks on the tension surface of beam—F0.1) and to weekly cycles of wetting-drying with 10% NaCl solution. These results have shown that macro-cracks (at load F0.1) and micro-cracks (at 50% of F0.1) largely accelerated both the initiation and propagation stages of the corrosion of steel in the concrete beams. Large crack widths for the F0.1 load cases caused higher corrosion rates initially, but after about 38 weeks of exposure, there was a decrease in the rate of corrosion. However, such trends could not be found in 50% F0.1 group of beams. The extent of chloride ingress also was influenced by the load level. These findings suggest that the effect of micro-cracking at lower loads are very important for deciding the service life of reinforced concrete structures in chloride exposure environments.

2.6. Mitigating mechanisms

Nowadays, a great interest in the so called mitigating mechanisms of concrete has been shown due to the fact that they can "repair" cracks, delay or reduce the rate of corrosion.

2.6.1. Autogenous (self) healing

Autogenous self-healing is the ability of concrete cracks to heal themselves with time. Several definitions of self-healing can be found in literature (Igarashi, 2011); (De Rooij, 2011). It seems that the intrinsic self-healing property of concrete was first observed in immersed condition by the French Academy of Science in 1836, which concluded that self-healing is the conversion of calcium hydroxide exuded from the hydrated cement and converted to calcium carbonate on exposure to the atmosphere. (Mihashi, 2012). In the recent 20 years researchers focused on the study of autogenous self-healing of concrete as it became an alternative solution to repair and rehabilitation of deteriorated reinforced structures. It seems that this complex phenomenon that can occur due to different possible mechanisms: further reaction of the unhydrated cement, expansion of the concrete in the crack flanks, crystallization of calcium carbonate, closing of the cracks by solid matter in the water, closing off the cracks by spalling-off of loose concrete (Ramm, 1998). (Reinhardt, 2013) divided the mechanisms contributing to autogenous self-healing in: physical, chemical and mechanical causes:

- Physical causes: When water is absorbed by the hydrated cement paste (HCP) and reaches the spaces between the constituents of HCP, swelling of the HCP near the crack faces occurs. This causes only a small reduction of the cracks.
- Chemical processes: So far, three chemical processes are attributed to self-healing of concrete. When further hydration of unhydrated cement particles develops, the new hydration products occupy about double the space of the original cement grain, growing into the free space of the crack. This can have a significant impact of self-healing of crack widths smaller than 0.1 mm. The second chemical process, which is considered to have the highest capacity to result in autogenous healing is the formation of calcium carbonate which precipitates on the crack faces, due to the dissolution of calcium hydroxide. This mechanism has been investigated in great detail by (Edvarsen, 1999). (Mohammed, 2003) found in their studies a thirds chemical process that occurs in the case of marine environment, the narrower cracks are healed due to the deposition of ettringite, calcite and brucite in the crcak regions.
- Mechanical causes: Two mechanical causes seem to contribute to self-healing: the presence of fine particles in the water which leaks through the crack and the fracturing of small concrete particles from the crack faces.

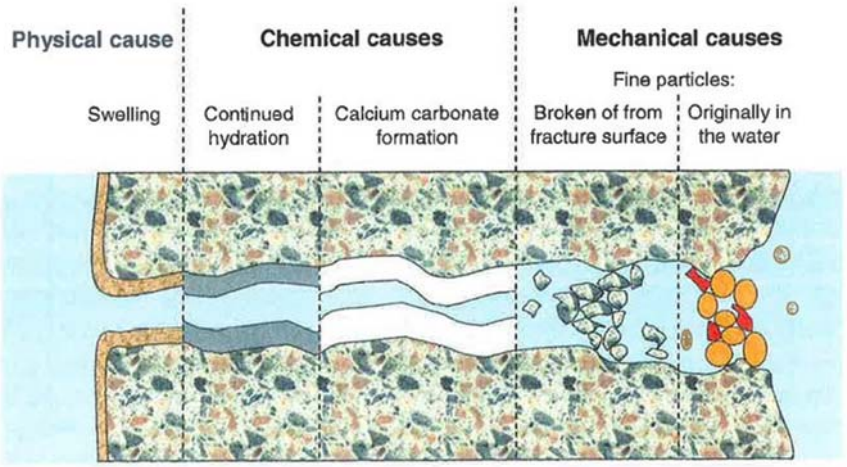

Figure 2.7. Causes of autogenous self-healing (Reinhardt, 2013)

Even though many studies were carried on that are reported in (Mihashi, 2012), the total contribution of these mechanisms is still a matter of debate. What became clear is the fact that no autogenous self-healing is possible without the presence of water inside the crack and that it depends on the concrete age at the time of cracking.

Also, a lot of studies using different preparation methods of cracks under different test conditions were carried on in order to determine the maximum crack width that can be closed by autogenous healing. Different values were obtained: 5 to10 μm (Jacobsen, 1996 b); (Şahmaran, 2008a), 53 μm (Ismail, 2004), 100 μm (Reinhardt, 2003), 200 μm (Edvardsen, 1999), 205 μm (Aldea, 2000) and 300 μm (Clear, 1985). In the studies presented above autogenous self-healing was carried in static water, flowing water or under wet-dry cycles.

Even though autogenous self-healing could have an important impact on chloride penetration in cracked concrete, only few studies were carried on.
(Ismail, 2008) suggested that autogenous self-healing reduces chloride diffusion along the crack path. (Jacobsen, 1996 a) concluded that the rate of chloride migration in the self-healed concretes was reduced by 28–35 % and penetration time was increased compared to newly cracked concrete. In the studies conducted by (Şahmaran, 2007) a significant amount of self-healing was observed within the cracks with width below 50 μm subjected to NaCl exposure. In the studies conducted by (Yoon, 2009) autogenous healing was quantified as a reduction of crack width by optical microscopy.

2.6.2. Crack blocking by corrosion products

This type of mitigating mechanism was reported by (Marcotte, 2003) who found in their research that crack blocking by corrosion products occurred in concrete made using 10% silica fume replacement. Further investigation is needed due to the fact that by blocking the further ingress of chlorides, the propagation period could be increased.

2.7. Numerical simulations for chloride transport modelling in cracked concrete

More and more researchers conduct their studies on developing a numerical model in order to simulate chloride ingress. Numerical simulations have many advantages: they can be used when experimental research is impossible or difficult, the costs and the amount of time needed is highly reduced compared to the experimental ones, simulations can be conducted taking into consideration a various number of factors and they can predict more accurately the service life when taking into account the potential effect of cracks.

Various numerical and modelling techniques can be found in literature, analysing the two or three- dimensional aspects of chloride ingress in cracked concrete taking into account its different transport mechanisms. Most of these studies consider the transport of chloride ions into concrete as pure diffusion and it's solved as a one-dimensional in a semi-infinite medium according to Fick's 2nd law of diffusion. Also, most numerical models adopt the geometrical patterns of the cracks in accordance with the samples used in the experiments. The most common way to simulate chloride transport in cracked concrete involves three steps:

1. determining the crack geometry;
2. determining the chloride transport mechanism in both the crack and the sound concrete;
3. applying the numerical method to simulate chloride diffusion.

Based on the different existing procedures, (Gu, 2015) classified them in:

1. Rectangular crack, cracking wall acts as exposed surface.

(Marsavina, 2009) studied both experimentally and numerically the influence of artificial cracks, with different crack widths and depths on the chloride penetration. The artificial cracks were realized experimentally using the method of notches by inserting and removing afterwards of thin copper sheets inside the specimens (De Schutter, 1999 a); (De Schutter 1999 b) and were modelled as rectangular cracks. Based on the experimental results they concluded that the cracks behave like exposed concrete surface and the influence of the notch width was not clear. Chloride penetration was simulated with the FEM method using a transient analysis and a concentration dependent diffusion coefficient. The chloride diffusion coefficient used was determined experimentally by the non-steady state migration test. The experimental results were in good agreement with the simulation ones.

2. Rectangular cracks, width-dependent chloride diffusion coefficient in crack.

In the experiments of (Djerbi, 2008) cracks with average widths ranging from 30 to 250 μm were induced using a splitting tensile test. The experimental results showed that the chloride diffusion coefficient of cracked samples is influenced by the crack width; this approach was adopted in the simulations. Also, the crack was presumed to propagate across the sample and was delimited by parallel planes perpendicular to the disc faces.

Based on the data reported by (Djerbi, 2008), (Jin, 2010) proposed a model in which chloride diffusion varies with the crack width. In the simulations the crack was assumed to be rectangular and diffusion was considered to be the only mechanism for chloride ions.

(Wang, L., 2011) developed a meso-scale model based on the lattice network approach for modelling mass transport in concrete and numerically evaluated the chloride diffusion coefficients of chlorides through cracks of different widths by the trial and error method. The range of investigated crack width is from 20 to 600 μm covering the available experimental data found in literature. A pure diffusion process described by Fick's second law was adopted in order to verify the precision and applicability of the proposed model. The crack was considered to be parallel-walled with approximately constant width.

(Bentz, 2013) studied the influence of transverse cracking directly above the steel reinforcement on chloride penetration and concrete service life comparing the simulation results with the experimental ones obtained by (Şahmaran, 2008b). Assuming that all cracks are rectangular shaped and considering a simple 2-D COSMOL model in order to simulate diffusion he considered a chloride diffusion coefficient in the zone near the crack and another one within the crack itself. The influence of chloride binding was also studied.

(Ishida, 2009) proposed a model for chloride diffusivity based on computed micro-pore structure, for undamaged and cracked concrete, the crack being modeled by introducing large void spaces in a control volume.

3. Realistic crack, width-dependent chloride diffusion coefficient in crack.

In the studies of (Lu, 2012) a 3-D image-based microstructure simulation procedure was developed to model the chloride ingress in cracked mortar. They used notched mortar samples exposed in a chloride ponding test for 30 days. The chloride concentration profile was obtained by a micro-X-ray fluorescence (XRF) test. In order to obtain a realistic crack geometry, two microstructures were used: a 3-D X-ray computed tomography (CT) image-based mortar microstructure was measured and a 3-D a spherical harmonic-based microstructure was created. These 3-D models were then converted into a FE mesh and then used to study the crack effect on chloride transport. Chloride diffusion was simulated taking into account chloride binding, using the COSMOL software. They concluded that cracks act as an accelerator, while binding acts as a moderator.

4. Load induced crack, width-dependant chloride diffusion coefficient in crack.

(Wang, L., 2008) proposed a numerical method which can appropriately take into account the effect of load-induced cracking on diffusivity of concrete. In their study concrete is simulated on the meso-scale as a three-phase composite: aggregate particles, mortar and the interfacial transition zone (ITZ) and a rigid body spring model (RBSP) is used in order to carry out the mechanical analysis to simulate the distribution and width of micro racks under compressive and tensile loading. After using the truss network model to numerically simulate chloride transport, the diffusion property of chloride ions in cracks is evaluated and the formulation of diffusion coefficient in cracks with regard to crack width is proposed according to experimental results found in literature.

(Savija, 2013) proposed a 3-D lattice model capable of simulating chloride transport in saturated sound and cracked concrete, taking into account the aggregate, mortar and ITZ of concrete. The lattice model was used to simulate a four-point bending test in order to produce cracks of various widths. Different analyses were performed based on experimental data found in literature and a relationship between the effective diffusion coefficient of cracked lattice elements and the crack width was adopted.

As mentioned earlier, most studies focused on simulating chloride penetration by taking into consideration only diffusion as a transport mechanism. But as presented in Section 2.4, the transport of chlorides into concrete is a much more complex mechanism involving not only diffusion but also migration, convection/capillary suction, permeation, and chloride binding. Furthermore, different concrete properties are relevant for the transport mechanisms. These aspects were taken into consideration by some researchers in order to develop a model which can more accurately predict chloride ingress into RC.

(Ozbolt, 2010) developed a 3D numerical model for transport of capillary water, oxygen and chloride through the concrete. taking into account the interaction between the non-mechanical processes and mechanical properties of concrete in order to investigate: the influence of damage of concrete on depassivation time of reinforcement, the influence of concrete quality, cracking and water saturation in concrete on the current density (Ozbolt, 2011), the transient analysis of corrosion processes before and after depassivation and the corrosion induced damage of steel reinforcement (Ozbolt, 2014).

(Park, 2012) proposed an analytical model for an evaluation of chloride behavior in cracked concrete considering both chloride diffusion and water permeation in a Representative Element Volume (REV) model. The results of the numerical simulation were compared to the experimental ones obtained after performing an accelerated migration test in non-stationary condition using concrete samples with various crack widths.

(Ye, 2012) elaborated a model describing chloride ion penetration into cracked concrete subjected to cyclic drying-wetting condition using the alternating-direction implicit (ADI) finite difference method for solving the chloride transport problem. The advection part was simulated by moisture transport in rough cracks considering crack width, crack surface roughness, tortuosity and capillary pores at crack surface.

(Yuan, 2010) used a multispecies model based on the finite-difference method inputting parameters such as porosity, density, chemical composition of pore solution, diffusion coefficient and chloride-binding isotherm in order to describe chloride transport in saturated concrete. Also, a depth-dependent diffusion coefficient instead of a fixed- diffusion coefficient was used in this model.

(Guo, 2012) proposed a new multi-scale FE model coupling equations of the degree of freedoms of meso-scale model of interfacial transition zone (ITZ) and macroscopic model of bulk pastes in analysing chloride diffusion in concrete. Three benchmark examples were performed to verify both the accuracy and efficiency of the proposed model. They concluded that both the local geometry and physical characteristics of ITZs significantly affect chloride diffusion in concrete.

(Iqbal, 2009) conducted in laboratory controlled conditions different experiments in order to obtain a model which can simulate saturated conditions in a typical marine environment in order to alternate wetting and drying as well as for single long wetting exposure. In the model, both advective-diffusive phenomenon and moisture migration were considered.

(Kato, 2005) experimentally investigated chloride ion transport in cracked concrete and numerically simulated the effects of the crack width by considering an apparent chloride ion diffusion coefficient through the cracks. Furthermore, the proposed model was able to simulate chloride ion profiles in cracked concrete under wet and periodic drying-wetting conditions if the crack width, the chloride content at the exposed surface and the diffusion coefficient of chloride ions in the whole concrete were known.

(Paul, 2014) proposed a model based on virtual RCPT (rapid chloride penetration test) and FEM in order to analyse the effects of fly ash and slag on the diffusion coefficient and chloride penetration depth in various mixes of concrete.

(Lin, 2010) developed an integrated FE- based numerical model for predicting the service life of RC structures exposed to chloride environments, taking into consideration environmental humidity, temperature fluctuation, chloride binding, diffusion and convection, as well as the decay of concrete structural performance. The numerical results were validated by comparison with analytical solutions and experimental observations.

2.8. Conclusions

Chloride ingress into concrete was intensely studied in the last decades and even so, due to its complexity it remains a major challenge. Moreover, the influence of cracks on chloride penetration in RC structures is still not sufficient understood.

Different testing methods (eg. diffusion tests, migration tests) were developed in order to study the influence of different factors: crack characteristics, environmental parameters and concrete properties on chloride penetration in cracked concrete. The transport mechanism of chlorides into concrete is a complex combination of ionic diffusion, migration, convection/ capillary suction and permeation) and most studies consider that only one of these transport mechanisms, usually diffusion, governs it. A great interest in the so called mitigating mechanisms of concrete has been shown lately, as it is considered that these can "repair" cracks, delay or reduce the rate of corrosion.

Due to their advantages (they can be used when experimental research is impossible or difficult, the costs and the amount of time needed is highly reduced compared to the experimental ones, simulations can be conducted taking into consideration a various number of factors and they can predict more accurately the service life when taking into account the potential effect of cracks), many researchers conduct their studies on developing a numerical model in order to simulate chloride ingress by analysing the two or three- dimensional aspects of chloride ingress in cracked concrete and by taking into account its different transport mechanisms.

Still, very limited investigation of the influence of chloride diffusion on samples with real cracks can be found in literature.

3. EXPERIMENTAL APPROACH

3.1. Overview of experimental program

As earlier mentioned in Section 1.2, the aim of the present research is to develop a numerical model which can accurately simulate chloride ingress in structures with real cracks. In order to be able to do that, relevant experimental data is required.

In the experimental program, the main challenge was to use samples with the same characteristics as in structures from the real environment. With regard to this, cores were drilled from a 14.30m RC slab exposed to a simulated accidental failure of the central support and subsequent vertical loading until collapse.

In this study 40 cores, drilled from different locations of the slab subjected to compressive stress, where cracks with different geometries occurred, were analysed. For each particular sample, geometry characteristics (e.g. crack width, crack tortuosity and roughness, rebar position) and also the detection of carbonation was realized. In addition to crack width measurements along the top and bottom surfaces, each core was vertically sectioned in different locations, perpendicular to the surface crack and the crack profile through the specimen's thickness was studied and the crack width through the sample was determined.

After completing the sample characterization, the non-steady state migration test was performed, according to (NT Build 492, 1999), in order to determine the chloride profile. Using the colorimetric method (Otsuki, 1993), the chloride depths were measured and the migration coefficient was determined for each sample. A schematic overview of the experimental program is presented in Figure 3.1.

The provided experimental data is then used in the numerical part, further discussed in Section 4.

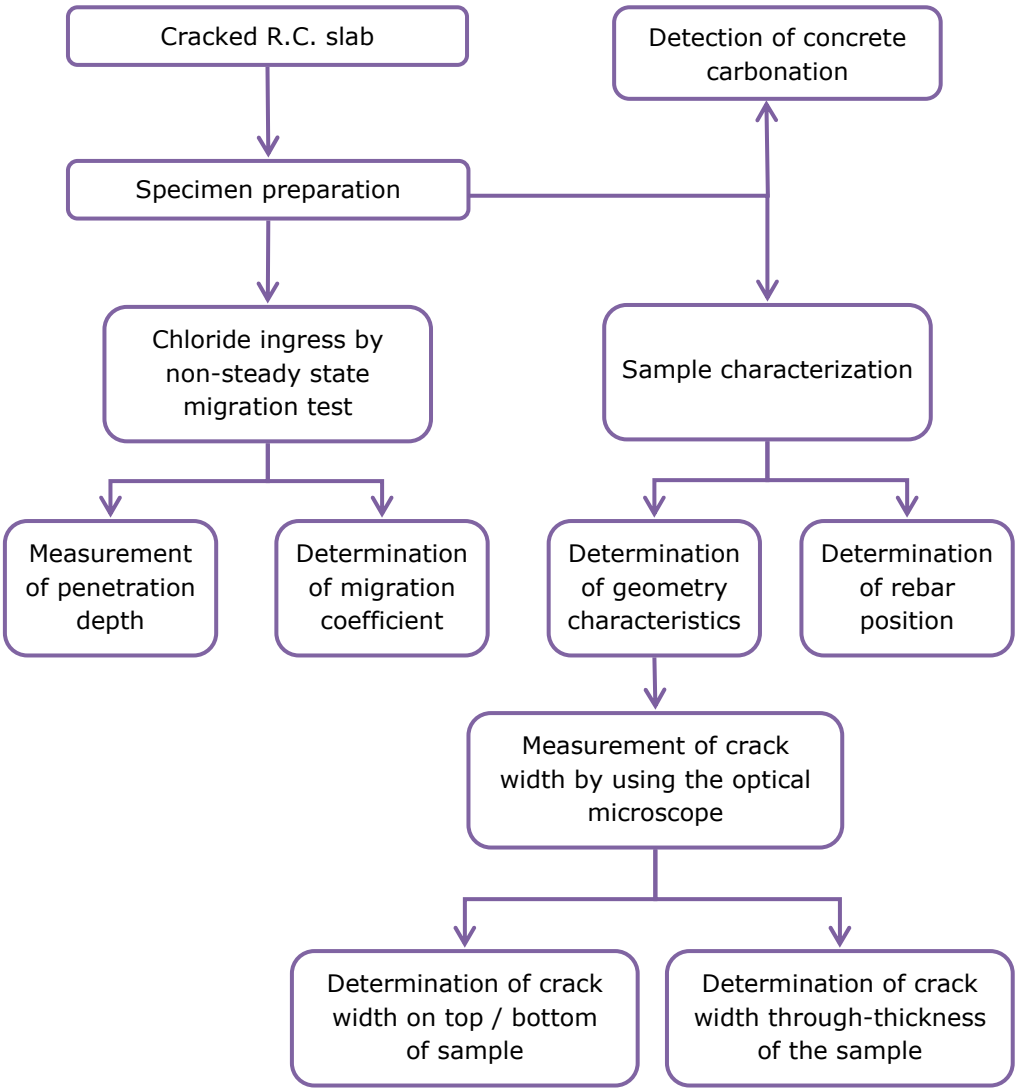

Figure 3.1. Schematic overview of the experimental program

3.2. Materials and specimen preparation

3.2.1. Concrete composition

The samples used in this study were obtained from a cracked RC slab of 140 mm thickness and 1800 mm wide, having the total length of 14.30 m. This slab was exposed to an artificial failure of the central support and subsequent vertical loading until collapse. A detailed description of the test set-up and the results for the experimental large-scale tests are described in (Gouverneur, 2014).

A concrete class C30/37 with a maximum size of aggregate of 14 mm was used to manufacture the slab. The concrete composition and the material properties for this slab are given in Table 3.1, respectively Table 3.2.

Table 3.1. Concrete mix used in this study (Gouverneur, 2014)

Material	Composition
crushed limestone 6.3/14	849 kg/m^3
crushed limestone 2/6.3	150 kg/m^3
sea sand 0/2	483 kg/m^3
limestone sand 0/4	366 kg/m^3
cement CEM III/A 42.5 LA	275 kg/m^3
fly ash	25 kg/m^3
superplasticizer	0.85 %/cement
water	174 kg/m^3

Table 3.2. Sample characteristics of material properties for concrete (Gouverneur, 2014)

	Slab		
	$f_{c,cube}$	f_c	E_{ci}
	(Mpa)	(Mpa)	(Gpa)
mean value	42.6	36.7	31.9
standard deviation	2.1	1.4	1.6
COV	0.05	0.04	0.05

3.2.2. Sample preparation

Drilling plan

Cores of 100 mm in diameter were taken from the slab, from locations where cracks appeared due to the applied external loading (Figure 3.2).

The concrete cores were obtained using a drilling machine. The direction of drilling was the same as the applied load and in the plane of the cracks. From a total of more than 80 drilled samples, only 40 samples could be used in this study.

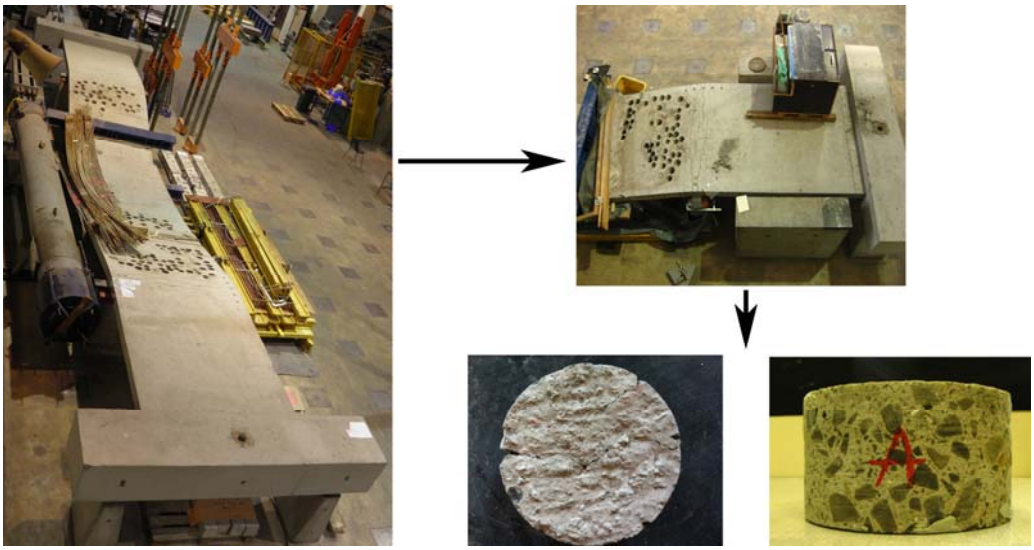

Figure 3.2. Slab after the drilling of the cores

Samples used in the non-steady state migration test

In order to meet the requirements specified in (NT BUILD 492, 1999), the samples were cut by wet sawing method, reducing them from an initial thickness of 140 mm to 50 mm (Figure 3.3).

The samples can be categorized in four main groups: samples without cracks and without rebars (S) (a), samples with cracks and without rebars (SC) (b), samples without cracks and with rebars (SR) (c), samples with cracks and with rebars (SCR) (d), as it can be observed in Figure 3.4, where a representative sample for each group is presented. Table 3.3 presents the total number of samples for each of the mentioned categories.

Table 3.3. Number of samples per category

Sample type	Number of test pieces
S	12
SC	4
SR	6
SCR	18

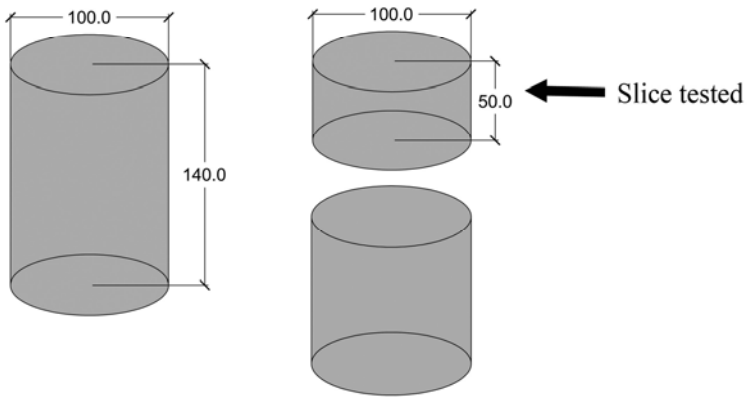

Figure 3.3. Preparation of the concrete sample

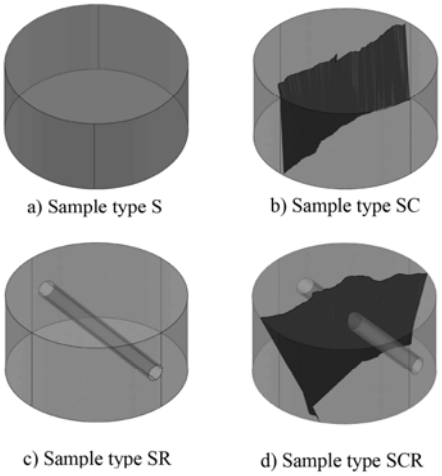

Figure 3.4. Sample categories

3.3. Sample characterization

Due to the fact that the samples were drilled from various locations of the slab, where real cracks with different patterns occurred, each sample used in this study has unique crack characteristics. Except for the reference samples, all samples have diametric transecting cracks. Various efforts were made in order to have a precise comprehension of the main distinctive aspects of each of these real cracks.

At a first visual investigation it could be observed that as a result of the drilling process some of the cracks were partly filled with dust. Therefore, before the cracks were thoroughly analysed, the specimens were brushed without water and blasted with pressurized air.

3.3.1. Crack characterization

As previously mentioned in Section 2.5, the crack geometric parameters are known to have a considerable effect on the transport mechanism of chlorides. Most studies consider only the evaluation of the crack width, depth or length in relation to chloride diffusion, while other factors such as tortuosity, connectivity, density and crack distribution are disregarded. There is very few information about these last aspects. In his study, (Mu, 2013) adopted a non-steady state diffusion test to investigate the relationship between the diffusion coefficient and crack density. Samples with different crack densities are prepared by the non-destructive notch method. A piecewise function is proposed to indicate the relationship between diffusion coefficient determined by water soluble chloride and crack density. (Arya, 1996) investigated the effect of crack frequency on the corrosion of reinforcing steel. RC beams with a varying number of parallel sided cracks with equal width were exposed by spraying to a 3% chloride solution. The results suggest that decreasing the frequency of cracking leads to a decrease in corrosion. (Akhavan, 2012) conducted a study about the transport properties of cracks taking into consideration: crack connectivity, roughness and tortuosity. Plain and fiber reinforced cement paste and mortar samples with simulated cracks exposed to permeability and diffusion tests are used. Crack connectivity was found to be linear dependent on crack width for small crack and constant for large crack.

In order to have more information about the geometric patterns of cracks and their influence on chloride ingress an appreciable effort was made to centralize the geometric aspects of the cracks from the samples used in the present study.

3.3.1.1. Crack width characterization

Crack width on top and bottom surfaces

The crack width of each sample was measured according to a three step procedure:

- first of all, both the top and the bottom surface of the sample were marked starting with the middle of the sample and continuing towards the edges, at a 2 cm distance from each other;
- then, in order to make the crack more visible, a colorimetric method was used; the samples were marked with a black marker in the vicinity of the crack, and afterwards a barium sulphate ($BaSO_4$) powder was applied;

- finally, the crack width was measured using an optical microscope; several readings were made in each of the 5 marked spots (0,1,2,3,4) and a mean value was obtained.

A sketch of this procedure is illustrated in Figure 3.5.

Table 3.4. Crack widths in samples

Sample	Crack opening (μm)		
	Top	Bottom	Average
A	211	337	274
B	165	387	276
C	90	277	184
D	172		172
E	177	340	259
F	100	301	201
G	96	647	372
H	191	323	257
I	168	328	248
J	187	442	314
K	190	396	293
L	269	359	314
M	211	389	300
N	338	232	285
4	143	79	111
6	154	160	157
7	169	68	119
13	164	131	148
16	130	108	119
25	141	66	104
A2	173	148	161
B2	93	155	124

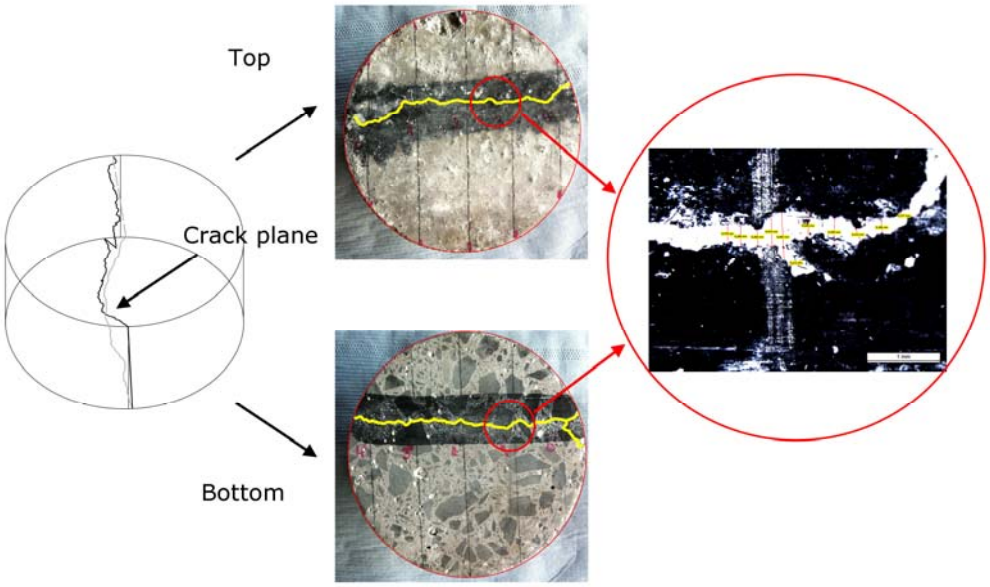

Figure 3.5. Measurement of the crack width determination procedure

Table 3.4 shows the crack width measured on the top and bottom surfaces of each sample and their average widths. The determined crack widths for the top and bottom is the average of the mean value of the measurements in each of the 5 marked places along the crack path.

Crack width through- thickness of the sample

After the non-steady state migration test, further presented in Section 3.4, in order to have a more accurate image about the crack pattern, each sample was vertically cut in 6 parts (this is further presented in Figure 3.15.a and Figure 3.15.b), in order to determine the crack width through the thickness of the sample. Each part was then divided in 5 marked equal parts where several readings were made in each of the 4 marked spots (1,2,3,4) using the optical microscope and a mean value was obtained according to Figure 3.6. It is important to mention that while cutting by wet sawing method, some parts of the samples broke along the crack, making the measurements less accurate. Still, considering that the measured average crack width through- thickness of the sample was determined for each of the 6 cut parts each divided in 5 parts, the author considers that the result is accurate enough.

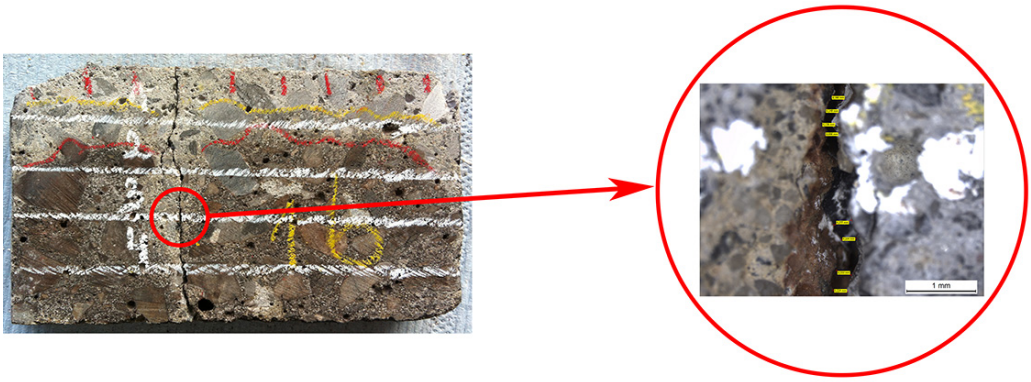

Figure3.6. Measurement of through-thickness crack width procedure

The average crack width determined through the thickness of the sample along splitting planes 0, 1, 2, 3 and 4, is presented in Table 3.5.

Table 3.5. Crack widths through- thickness of the sample for the entire sample

Crack opening (μm)			
Sample		Sample	
A	235	L	63
B	149	M	145
C	103	N	102
D	84	4	195
E	309	6	311
F	214	7	63
G	108	13	122
H	128	16	146
I	149	25	106
J	73	A2	182
K	105	B2	160

3.3.1.2. Surface roughness and crack tortuosity

Figure 3.7 presents pictures taken during crack width measurement on the optical microscope. It can be noticed that the edges of the crack seem to be rather rough. This roughness may be a result of the damage to the walls of the crack caused by drilling and saw cutting the sample. If we look deeper into the crack, it can be noticed that the inside part of the crack is quite smooth and has a constant gap. When measuring the width of the crack this internal gap was taken into consideration and not the outer broken edges of the crack.

Figure 3.7. Measurement of crack width under the optical microscope

It can be clearly seen from Figure 3.8 that the crack width is less consistent along the sample, having a tortuous profile. This is the reason why a consistent number of measurements, from different sections along the crack, were performed in order to obtain a mean value that can accurately indicate the crack width. For the rough crack samples, both places with the lowest and highest consistency in crack width were chosen for the measurement.

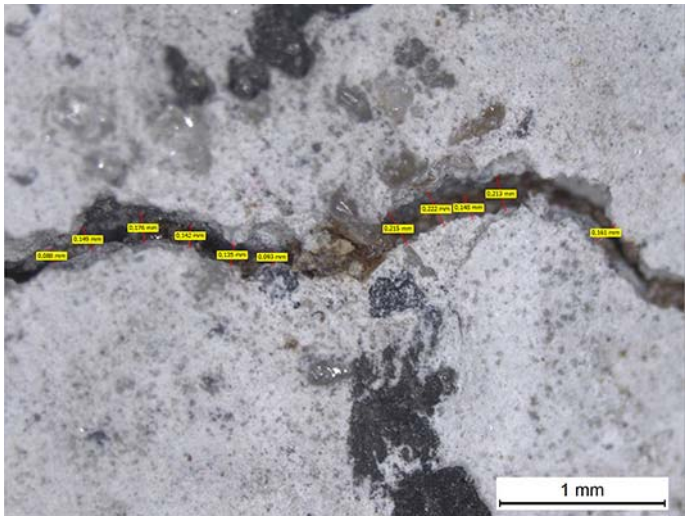

Figure 3.8. Tortuous profile of the crack

3.3.2. Rebar position

Due to the reinforcement arrangement of the slab (Gouverneur, 2014) it was almost impossible to obtain samples without rebars. After the non-steady state migration test (Section 3.4), once the samples were cut, (Figure 3.a and Figure 3.b), it was possible to detect the position of the rebar in relation to the crack. Taking this into consideration the next main situations can be observed: some samples have the rebar perpendicular to the crack, other have it parallel to the crack and some have both a perpendicular and a parallel rebar in rapport to the crack (Figure 3.9). A detailed rebar characterization is presented in Table 3.6.

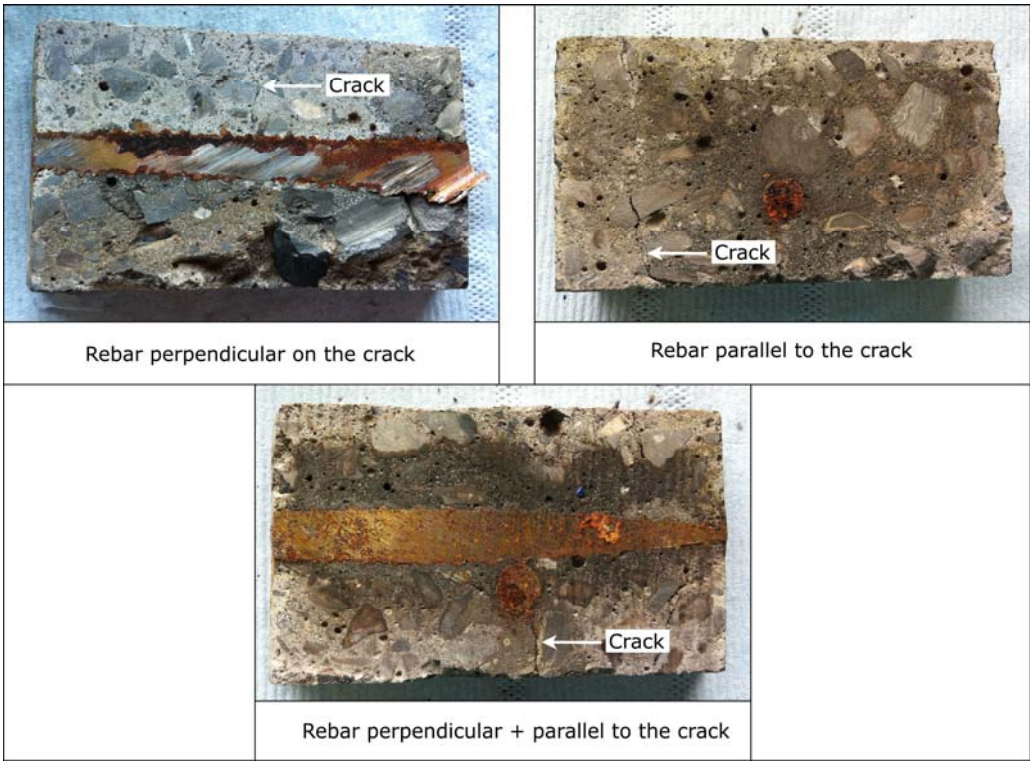

Figure 3.9. Rebar in relation to the crack

Table 3.6. Rebar characterization for cracked samples

Sample	Number of rebars	Rebar position rapported to the crack	Rebar diameter (mm)
A	1	perpendicular	10
B	no rebar		
C	no rebar		
D	1	perpendicular	10
E	2	1 perpendicular	10
		1 parallel	8
F	2	1 perpendicular	10
		1 parallel	8
G	1	perpendicular	10
H	1	perpendicular	10
I	1	perpendicular	10
J	1	perpendicular	10
K	2	perpendicular	2x 10
L	1	perpendicular	10
M	1	perpendicular	10
N	1	perpendicular	10
4	no rebar		
6	1	perpendicular	10
7	1	perpendicular	10
13	2	1 perpendicular	10
		1 parallel	8
16	1	perpendicular	10
25	1	perpendicular	10
A2	2	1 perpendicular	10
		1 parallel	8
B2	1	perpendicular	10

The rebar characteristics for samples type SR are presented in Table 3.7.

Table 3.7. Rebar characterization for cracked samples type SR

Sample	Number of rebars	Rebar diameter (mm)
Sample 1R	1	10
Sample 2R	1	10
Sample 3R	1	10
Sample 4R	2	10+8
Sample 6R	1	10
Sample 7R	1	10

3.4. Testing method of chloride transport: the non-steady state migration test

3.4.1. Introduction

Due to the fact that the mechanism of chloride transportation in concrete is a process that requires a long time and conventional diffusion tests need long-term exposure of concrete samples to salt solution, researchers tried different accelerated methods based on the application of electric potential gradient. One of these accelerated methods is the non-steady state migration test, one of the most popular methods used to determine the chloride ingress. Its main advantages include a simple calculation and a short duration of time. Even though it is different from the real situation of chloride diffusion, being an accelerated process which uses an electrical field as the driving force to move chloride ions, it is still considered to be an effective way to measure the chloride resistance of concrete. In this case, migration is considered to be the only chloride transport mechanism. The movement of chloride ions in a solution under an electrical field is governed by the Nernst-Planck equation, from which the chloride migration coefficient of concrete can be calculated. Chloride ions migrate into the concrete very rapidly, and this allows a quick estimation of effective chloride diffusion coefficient, however, because of the short duration of the test and application of strong electric field, the amount of bound chloride in a rapid-migration test is very low compared to the natural diffusion test (Rahman, 2012). (Rodriguez, 2001) emphasizes the idea that the depth determined by the colorimetric method represents the average penetration front of free chlorides, e.g. chlorides dissolved in the concrete pore solution and that the colorimetric method is a simple and fast technique to indicate whether or not free chlorides are present in the concrete.

This test was proposed by (Tang and Nilsson, 1993) and it was standardized as (NT BUILD 492, 1999). Samples of 50 mm thickness and 100 mm diameter are

being used in the test. In order to ensure they are fully saturated, the samples are stored for 24 hours in a vacuum saturator containing $Ca(OH)_2$ solution. After that, they are placed in the migration cell, where the catholyte solution is 10% NaCl and the anolyte solution is 0.3 NaOH. An electrical voltage (ranging from 10-60V, depending on the concrete quality) is applied across the thickness of the sample, pushing the chloride ions towards the anode. Based on the applied current, the time duration of the test is from 6 to 96 hours. This method was used by several authors: (Yoon, 2009), (Djerbi, 2008), (Marsavina, 2009), (Audenaert, 2009), (Rahman, 2012), to study the effects on chloride ingress in concrete. The steel bars could have an influence on the electric field, but this was not taken into consideration in the present research.

3.4.2. Experimental test setup and test procedure

A non-steady state migration test was performed on the obtained concrete samples, according to (NT Build 492, 1999). A schematic representation of this procedure can be observed in Figure 3.10.

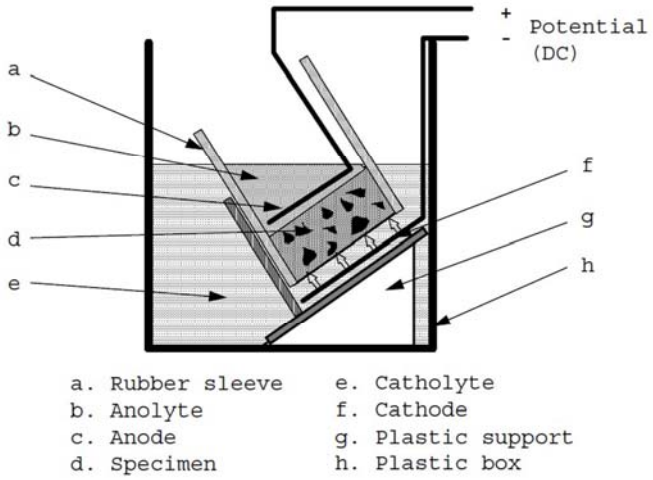

Figure 3.10. Test setup of non-steady state migration test (according to NT Build 492, 1999)

Before testing, the samples were placed in a vacuum container for vacuum treatment for three hours to a pressure in the range of 10-50 mbar; afterwards, with the vacuum pump still running, the container was filled with saturated $Ca(OH)_2$ solution so as to immerse all specimens, which was maintained for a further hour before allowing air to reenter the container. The specimens were kept in the solution for 18±2 hours. (Figure 3.11).

After the vacuum saturation the samples were placed in the reservoir and an external electrical potential of 30 V to 35 V was applied for 24 hours, forcing the chloride ions from the 10% NaCl solution to migrate into the specimens (Figure 3.12).

Figure 3.11. Equipment used for vacuum saturation

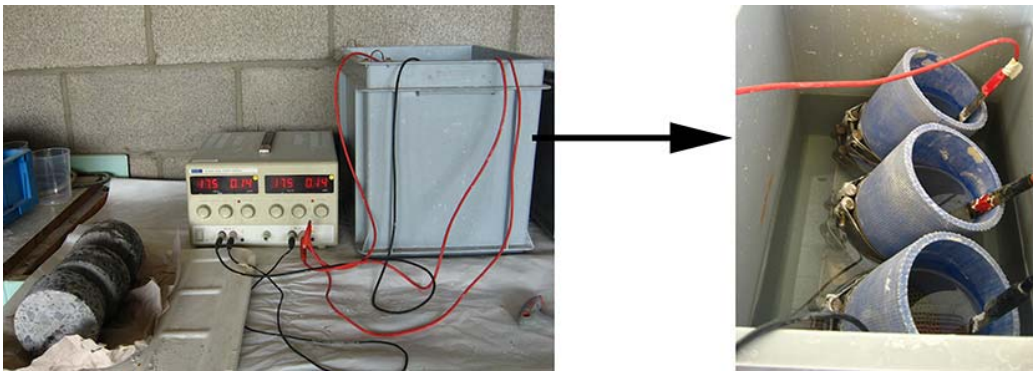

Figure 3.12. The Rapid Chloride Migration Test setup

Two sets of accelerated migration tests were conducted. The main difference between them consists in the sample's surface chosen to be in contact with the NaCl solution (Figure 3.13).

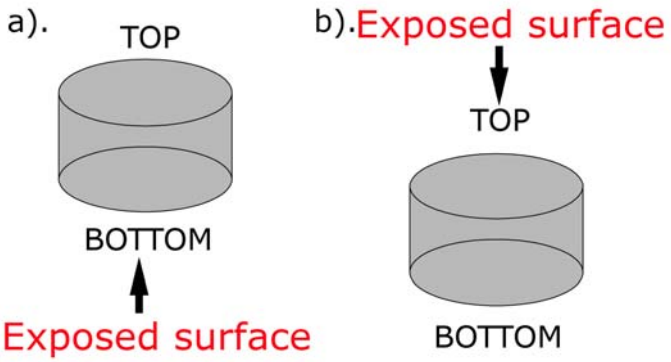

Figure 3.13. Surfaces tested in the accelerated migration test

In the first set of experiments 18 samples were used, while in the second set of experiments 22 samples were used. The total number of samples per category for both the first and second set of experiments is given in Table 3.8, respectively in Table 3.9.

Table 3.8. Number of samples used in the first set of experiments

Sample type	Number of test pieces
S	6
SC	3
SR	3
SCR	6

Table 3.9. Number of samples used in the second set of experiments

Sample type	Number of test pieces
S	6
SC	1
SR	3
SCR	12

3.4.3. Penetration depth

After the migration test all samples were split in order to determine the chloride penetration depth: samples type S were split in two, while samples type SR, SC and SCR were cut in 6 parts each perpendicular to the crack according to Figure 3.15. A 0.01 N Ag NO_3 solution was sprayed on each of the freshly cut surfaces and the chloride penetration depths were measured based on the colorimetric method according to (Otsuki, 1993). The penetration depth was measured at intervals of 10 mm, measuring the distance between the core end and the chloride front (colour boundary defined by the silver nitrate), as shown in Figure 3.10.c. In order to avoid the edge effect due to a non-homogeneous degree of saturation or possible leakage, no measurements were considered close to the edge. Taking into consideration the exposed surface and the sample category, the chloride penetration depth was measured. For each concrete sample 10 chloride penetration profiles were obtained and based on these, an average chloride penetration depth (x_d) was determined. For samples type SC and SCR, the average chloride depth (x_d), the diametric chloride depth (x) and the chloride depth near the crack (x_c) were determined, (Table 3.10 and Table 3.11). For sample type S, only x_d was determined (Table 3.12 and Table 3.13), while for sample type SR both x_d and x_c were determined Table 3.14 and Table 3.15). It needs to be clarified that x is determined only in the middle of each sample, where the core was vertically sectioned at the mid-point along a diameter perpendicular to the surface crack, while x_d and x_c are average values determined for the entire sample. A schematic representation of the chloride depths measurement in the middle of the sample is presented in Figure 3.14

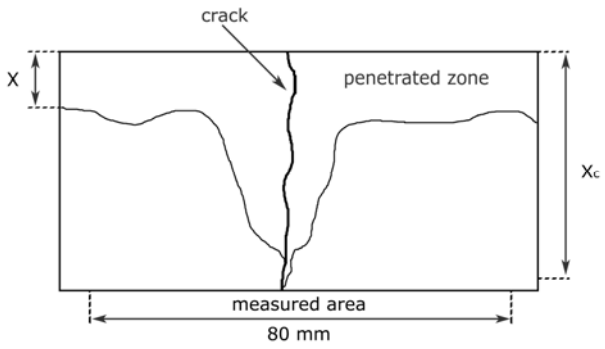

Figure 3.14. Chloride front measurement in the middle of the sample

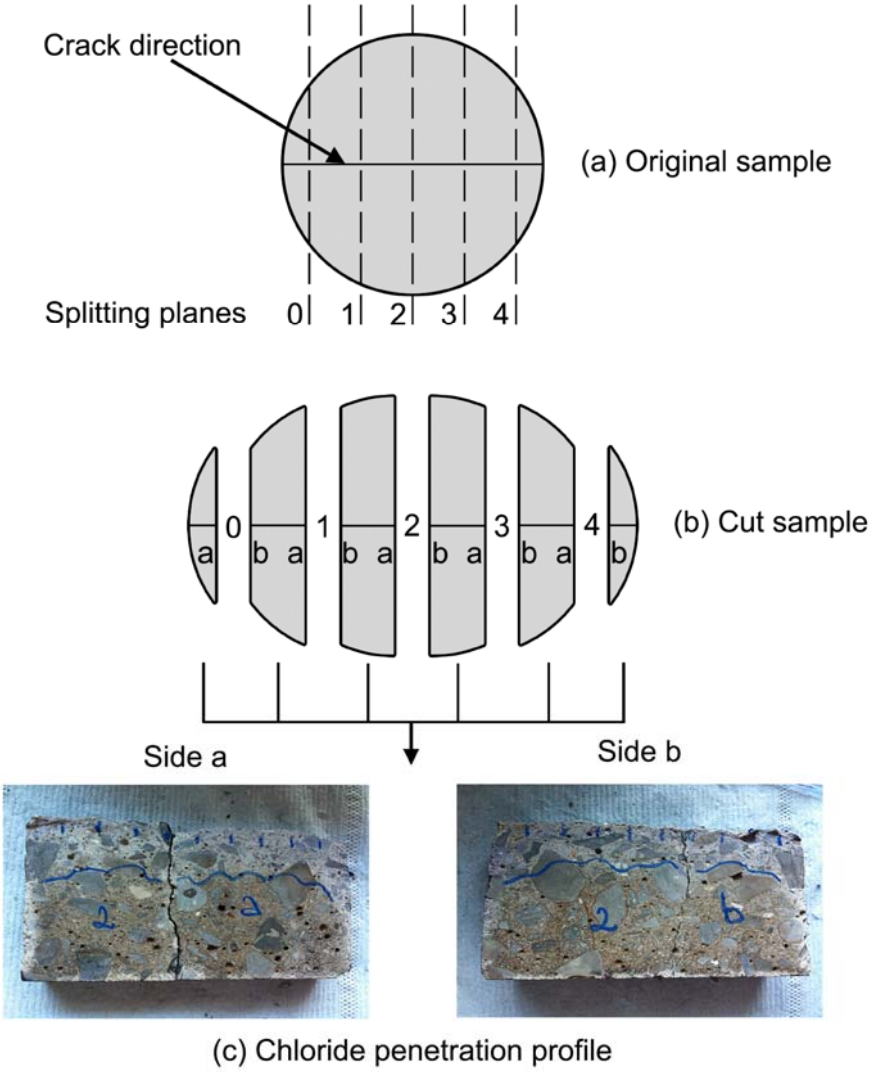

Figure 3.15. Splitting of concrete samples

Table 3.10. Penetration depth for samples having the top surface exposed

Sample	Chloride penetration		
	x_d (mm)	x_c (mm)	x (mm)
J	23.1	28.4	20.8
K	28.0	36.8	24.9
L	22.3	27.7	22.1
M	23.9	26.4	24.8
N	20.1	20.6	18.8
4	22.4	26.8	24.1
6	15.2	28.4	17.0
7	28.1	37.0	23.6
13	25.9	30.9	21.4
16	24.0	31.3	23.3
25	21.1	31.9	22.3
A2	23.7	26.5/27.2	25.9
B2	25.2	34.8	26.0

Table 3.11. Penetration depth for samples having the bottom surface exposed

Sample	Chloride penetration		
	x_d (mm)	x_c (mm)	x (mm)
A	9.3	22.7	9.8
B	9.6	25.2	8.4
C	9.0	22.0	7.9
D	10.7	12.2	10.0
E	12.7	27.1	12.5
F	11.6	21.0	8.8
G	-	-	-
H	13.5	21.1	11.5
I	-	-	-

Table 3.12. Penetration depth for reference samples type S having the top surface exposed

Sample	Chloride penetration
	x_d (mm)
Ref IV a	21.4
Ref V	24.2
Ref VI	26.3
Ref IV b	15.7
Ref VII	17.6
Ref VIII	18.7

Table 3.13. Penetration depth for reference samples type S having the bottom surface exposed

Sample	Chloride penetration
	x_d (mm)
Ref I a	12.6
Ref II a	17.6
Ref III a	20.5
Ref I b	20.6
Ref II b	13.7
Ref III b	10.3

Table 3.14. Penetration depth for reference samples type SR having the top surface exposed

Sample	Chloride penetration	
	x_d (mm)	x (mm)
Sample 4R	18.1	14.1
Sample 6R	21.2	12.8
Sample 7R	24.2	25.0

Table 3.15. Penetration depth for reference samples type SR having the bottom surface exposed

Sample	Chloride penetration	
	x_d (mm)	x (mm)
Sample 1R	12.0	9.9
Sample 2R	11.8	11.1
Sample 3R	11.3	9.7

As (Yuan, 2009 b) already emphasized it is not easy to measure the penetration depth by colorimetric method accurately by visual judgment. The colour change boundary is quite irregular and it is not easy to distinguish it by visual observation. Taking this in consideration the images for which it was difficult to determine the chloride penetration front were processed (Figure 3.14).

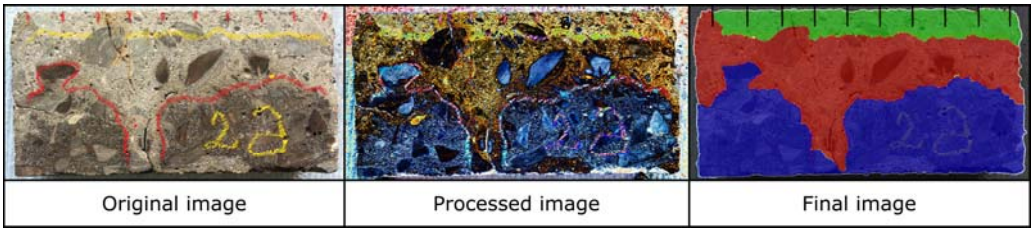

Figure 3.16. Example of image processing

3.4.4. Migration coefficient

Using the average penetration depth the non-steady state migration coefficient can be calculated according to (NT Build 492, 1999).

$$D_{nssm} = \frac{RT}{zFE} \cdot \frac{x_d - a\sqrt{x_d}}{t} \tag{3.1}$$

where :

$$E = \frac{U-2}{L} \tag{3.2}$$

$$a = 2\sqrt{\frac{RT}{zFE} \cdot erf^{-1}\left(1 - \frac{2C_d}{C_0}\right)} \tag{3.3}$$

C_d = chloride concentration at which the color changes (= 0.07N);

C_0 = chloride concentration in the catholyte solution (= 2N)

erf^{-1} = inverse of error function

F = Faraday constant (=9.648 x 10^4 J/(V·Mol))

L = thickness of the specimens (m)

R = gas constant (= 8.314 J/(K·Mol))
x_d = average value of the penetration depths (m)
t = test duration (sec)
T = average value of the initial and final temperatures in the anolyte solution (K)
U = absolute value of the applied voltage (V)
z = absolute value of ionic valence (= 1 for chloride)

Since $erf^{-1}\left(1-\frac{2x0.07}{2}\right)=1.28$, the following simplified equation can be used:

$$D_{nssm}=\frac{0.0239(273+T)L}{(U-2)t}\left(x_d-0.0238\sqrt{\frac{(273+T)Lx_d}{U-2}}\right) \quad (3.4)$$

where:
D_{nssm} = non-steady-state migration coefficient, x10^{-12} m^2/s;
U = absolute value of the applied voltage (V)
T = average value of the initial and final temperatures in the anolyte solution (°C)
L = thickness of the specimens (mm)
x_d = average value of the penetration depths (mm)
t = test duration, hour

Based on the relations presented above and on the penetration depths previously presented in Section3.4.2., the migration coefficients corresponding to the average chloride depth (D_d), the diametric chloride depth (D) and the chloride depth near the crack (D_c) were determined for each type of sample and taking into consideration the exposed surface. Table 3.16 corresponds to the migration coefficients determined for type SC and SCR, Table 3.17 and Table 3.18 for samples type S and Table 3.19 and Table 3.20 for sample type SR.

Table 3.16. Migration coefficient for samples having the top surface exposed

Sample	Migration coefficient (x10^{-12} m^2/s)		
	D_d	D_c	D
J	9.3	11.6	8.3
K	11.4	15.2	10.1
L	9.0	11.3	8.9
M	11.2	12.4	11.6
N	9.3	9.6	8.7
4	8.8	10.7	9.6
6	5.9	11.4	6.6
7	11.3	15.0	9.3
13	12.0	14.5	9.8
16	9.5	12.6	9.2
25	9.7	15.0	10.3
A2	10.9	12.29/12.63	12.0
B2	10.0	14.1	10.4

Table 3.17. Migration coefficient for reference samples type S having the top surface exposed

Sample	Migration coefficient
	D_d (x10^{-12} m2/s)
Ref IV a	8.6
Ref V	9.8
Ref VI	10.7
Ref IV b	5.4
Ref VII	6.1
Ref VIII	6.5

Table 3.18. Migration coefficient for reference samples type S having the bottom surface exposed

Sample	Migration coefficient
	D_d (x10-12 m2/s)
Ref I a	4.9
Ref II a	7.0
Ref III a	8.3
Ref I b	7.2
Ref II b	4.6
Ref III b	3.4

Table 3.19. Migration coefficient for reference samples type SR having the top surface exposed

Sample	Migration coefficient (x10-12 m2/s)	
	D_d	D
Sample 4R	7.0	5.4
Sample 6R	8.7	4.9
Sample 7R	9.5	10.0

Table 3.20. Migration coefficient for reference samples type SR having the bottom surface exposed

	Migration coefficient (x10-12 m2/s)	
	D_d	D
Sample 1R	4.6	3.7
Sample 2R	4.5	4.2
Sample 3R	4.3	3.6

3.5. Carbonation

3.5.1. Influence of carbonation on concrete

As previously presented in Section 1.2.2, carbonation has an important impact on the corrosion initiation process of the embedded rebars in concrete, being one of the main factors causing structural damage.

It is acknowledged that cement paste contains 25-50 wt% calcium hydroxide, providing a high alkaline layer on top of the steel rebars, protecting them against corrosion. Concrete carbonation occurs due to the presence of carbon dioxide from air or from water, which reacts with calcium hydroxide, reducing the pH of concrete and forming calcium carbonate:

$$Ca(OH)_2 + CO_2 \rightarrow CaCO_3 + H_2O \quad (3.5)$$

$$C\text{-}S\text{-}H + 2CO_2 \rightarrow SiO_2 + 2CaCO_3 + H_2O \quad (3.6)$$

According to the reactions above, CO_2 reacts with $Ca(OH)_2$ and by consuming the $(OH)^-$ ion, the pH in the pore solution may decrease which can increase the rate of corrosion (Ramezanianpour, 2014).

As CO_2 from the environment reacts with the carbonatable constituents, it diffuses through the concrete or mortar pores, from regions of high concentration to those of low. To react with CO_2, solid calcium hydroxide is dissolved from the cement gel into the pore water and diffuses in it from regions of high alkalinity to those of low. When at a certain point within the concrete mass all the amount of $Ca(OH)_2$ has been converted to $CaCO_3$, the pH value of the pore water drops below the threshold of steel depassivation.

When $Ca(OH)_2$ is removed from the paste, hydrated CSH will produce CaO which will also carbonate. According to (Papadakis, 1992), in pozzolanic cements or in concrete mixes using pozzolan as an additive, part of this calcium hydroxide is consumed by the pozzolanic activity and only the remaining quantity is available for carbonation.

According to (Borges, 2010), the HCO_3^- and CO_3^{2-} ions present in the pore solution react with the Ca^{2+} from calcium hydroxide (CH), but also from calcium silicate hydrate (C-S-H) and hydrated calcium aluminates and ferro-aluminates. And also, it is believed that the microstructural consequences of C-S-H carbonation are very different from the porosity reducing effect of CH carbonation. According to (Kropp, 1989) upon carbonation of the hydrated cement paste, concrete shrinkage happens due to the fact that the silica chains in C-S-H are polymerized, decreasing the volume and consequently causing cracks.

For non-reinforced concrete, carbonation is an advantage, due to the fact that the decrease of porosity makes the carbonated paste stronger; but for RC, due to the fact that the pH of carbonated concrete drops to about 7, which is below the passivation threshold of steel.

The main factors affecting carbonation are: the chemical and mineralogical composition of cement, the water/cement (w/c) and aggregate/cement (a/c) ratios and the main environmental factors are: the ambient CO_2 concentration, the relative humidity and the cycles of rain and snow for outdoor concrete.

Carbonation does not occur when the concrete is fully saturated or completely dry. According to (Sagues, 1997) the carbonation process is more severe on the concrete structures exposed to an environment where the RH is in the range

of 50-70 %. When the RH is higher than 70%, the concrete pores tend to saturate with water, making the diffusion of the CO_2 through the concrete very slow. On the other hand, when the relative humidity is lower than 50%, the pores tend to become dry and the dissolution of $Ca(OH)_2$ and CO_2 necessary for the carbonation reaction does not take place.

3.5.2. Influence of carbonation on chloride ingress

Even though carbonation and chloride ingress are considered to be to be the main causes of rebar corrosion, there are few publications regarding their combined effect on RC structures.

(Yoon, 2007) experimentally investigated the interaction between carbonation and chloride penetration and their effects on concrete, under various boundary conditions and concluded that carbonation of concrete could significantly accelerate chloride penetration.

(Ramezanianpour, 2014) investigated the effect of an accelerated test method of simultaneous carbonation and chloride ion ingress on mechanical properties and durability of ordinary concrete. The results show that specimens maintained in CO_2 gas have higher compressive strength compared to the specimens maintained in the tidal zone containing both CO_2 gas and saline water.

(Liu, 2014) conducted a study regarding the influence of the carbonation on chloride- induced reinforcement corrosion in a simulated concrete pore solution with different concentration of bicarbonate ions. The study concluded that a high HCO_3^- concentration will enhance the stability of the passive film and the corrosion resistance of the steel specimen, while the low concentration of HCO_3^- ions accelerates corrosion.

(Malheiro, 2014) studied the influence of carbonation on the chloride diffusion of mortar specimens. Cubic mortar specimens were cast with a 0.55 water-cement ratio and were subjected to 56 days of wetting and drying cycles. Samples were immersed for a day in 3.5% NaCl solution and half of them placed afterwards in a carbonation chamber (4% CO_2), while the other half was kept in laboratory environment. When evaluating the depth of chlorides and CO_2 penetration, the results showed that carbonation had a direct influence on chloride penetration, decreasing it.

(Ngala,1997) studied steady-state diffusion kinetics of dissolved oxygen and chloride ions in well-cured, partially dried, non-carbonated and fully carbonated specimens of OPC, OPC/30% PFA and OPC/65% BFS pastes. They observed that the diffusion coefficient of chloride increases significantly after carbonation.

(Tumidajski, 1996) considered the combined actions of chloride, sulfate and CO_2 on the ingress of chloride ion into OPC and concrete incorporating the partial replacement of the cement with slag. The results concluded that for concrete, when CO_2 is bubbled through the sulfate-chloride bath, the chloride penetration is decreased for Portland cement, but increased for concrete incorporating slag.

Corrosion initiation can be considered the main parameter when determining the service life of a structure, therefor, when chloride ingress and carbonation occur at the same time, the prediction of the distribution of chloride ions in concrete is essential. According to (Kobayashi, 1991) concrete degradation due to chloride ion ingress and carbonation is as follows:

1. generation of Friedel's salt due to the reaction of monosulphate with chloride ions;

2. carbonation of Friedel's salt;
3. dissolution of chloride ions into pore solution that have been immobilized in Friedel's salt;
4. increase in the concentration of chloride ions in pore solution, resulting in the further ingress of chloride ingress into the internal part of concrete caused by concentrating and diffusion cycles.

In his research, (Saeki, 2002) investigated the immobilization of chloride ions in cement hydrates and their release due to carbonation order to estimate the effect of carbonation on chloride penetration in concrete by. He developed a model in which he considered the effect of change in micro-structure due to carbonation on chloride penetration was able to predict the distribution of chloride ion in concrete when simultaneously subjected to carbonation and chloride ion ingress.

It is considered that carbonation pushes the chloride front forward and affects chloride binding by liberating chlorides that were bound in non-carbonated concrete. In his studies, (Reddy, 2002) concluded that due to the fact that high amount of bound chlorides may release when pH goes below 12, these are considered as a potential risk for corrosion.

3.5.3. Experimental determination of carbonation depth

After the non-steady state migration test previously presented in Section 3.4, an examination was carried out in order to check whether concrete carbonation affected the specimens used for the chloride analysis. Samples type SR (reference samples) were spilt in two and while one half was used to determine the chloride profile according to Section 3.4.2, the other one was tested for carbonation. The method used for determining the carbonation profile was the colorimetric method based on phenolphthalein spraying which assess a carbonation depth corresponding to a pH value roughly equal to 9 and it's applied either on cores of real structures or on specimens carbonated in laboratory conditions (Bertolini, 2008). The phenolphthalein solution turns pink in non-carbonated concrete and remains colorless in carbonated concrete. The results illustrated in Figure 3.16 and Figure 3.17 show that carbonation only occurred on the surface exposed to the external environment (top surface). Even at first sight, without determining any measurements, it can be noticed that the carbonation profile (yellow line) is quite advanced, even though the slab's age at the time of the experimental determination was only about 2 years. A possible explanation could be the influence of the air relative humidity (RH). According to (Bertolini, 2008) the highest penetration rate of carbonation is normally found on sheltered concrete exposed to 60% to 70% relative humidity (e.g. inside a building).

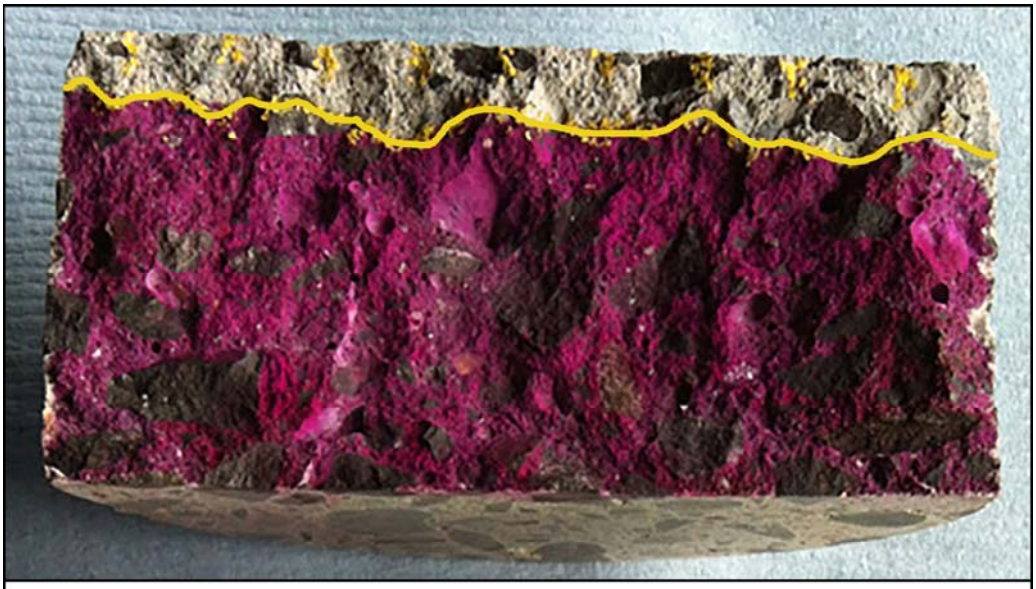

Carbonation depth

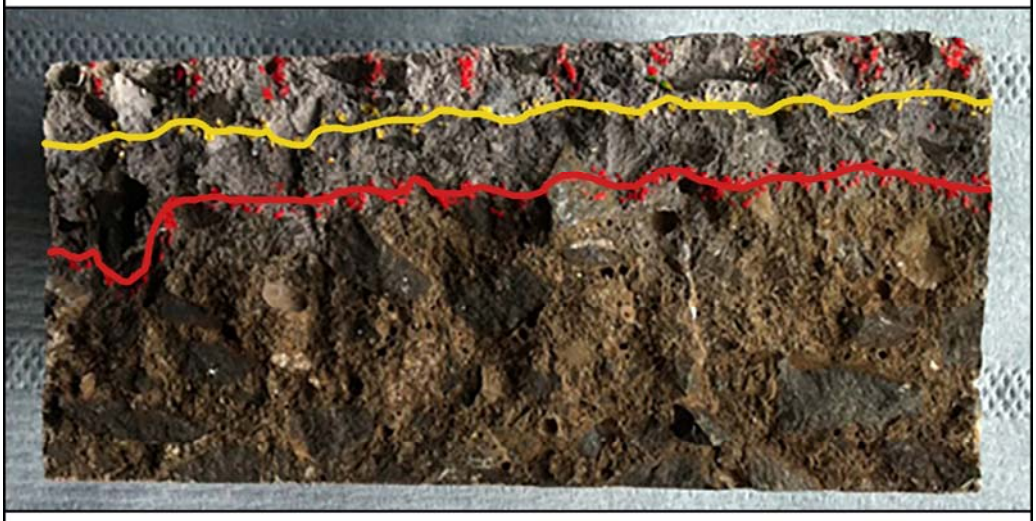

Carbonation depth + chloride profile

Figure 3.17. Carbonation depth and chloride profile for sample SIV- top surface exposed

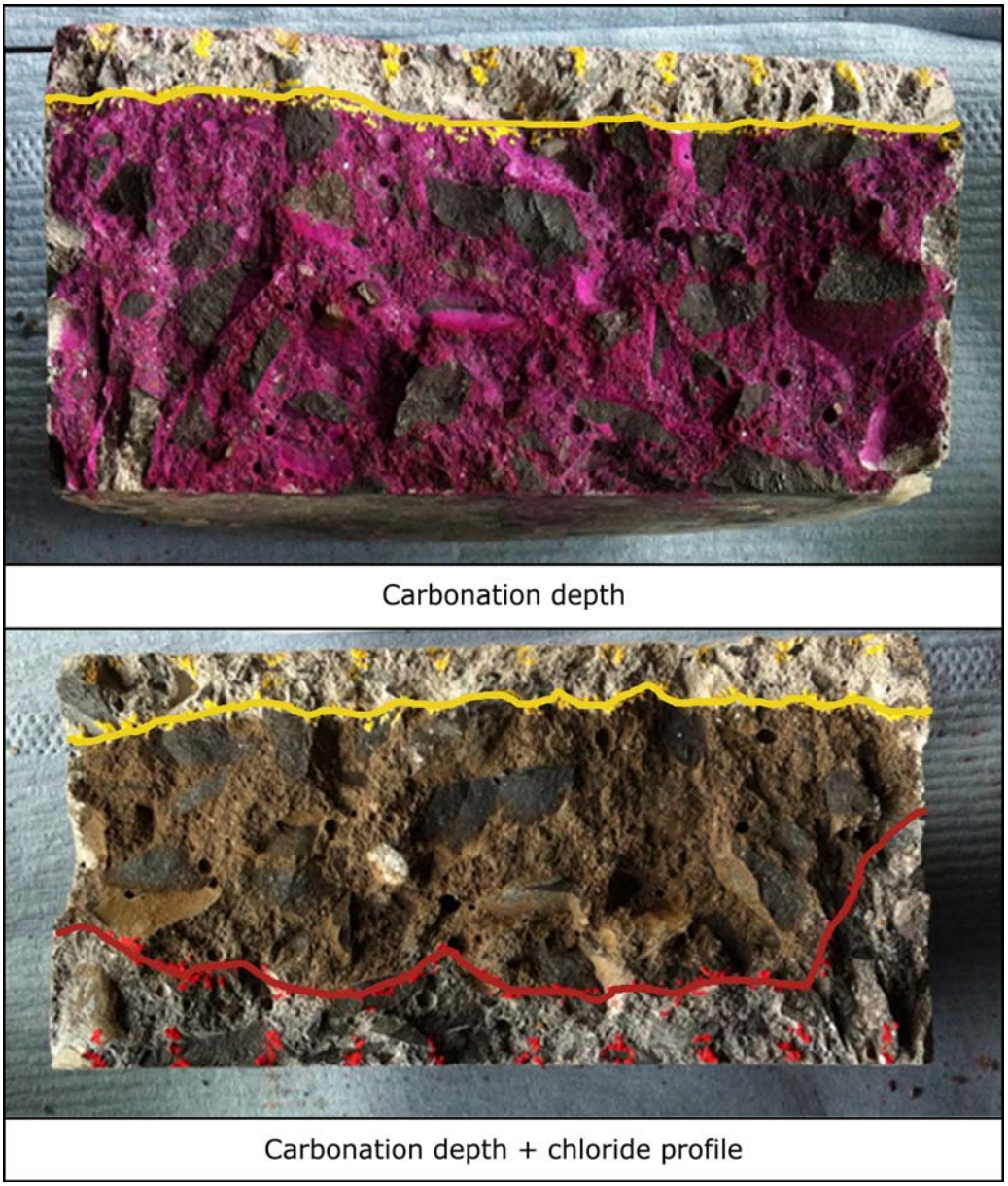

Figure 3.18. Carbonation depth and chloride profile for sample SIII- bottom surface exposed

The carbonation depths, in *mm*, were determined at intervals of 10 mm, by measuring the distance between the core end and the carbonation front (color boundary defined by phenolphthalein), as shown in Figure 3.18. For each type S sample the maximum (x_{max}), minimum (x_{min})and average (x_c) carbonation depths were determined (Table 3.21 and Table 3.22). The possible effect of carbonation on chloride ingress will be further discussed in Section 4.

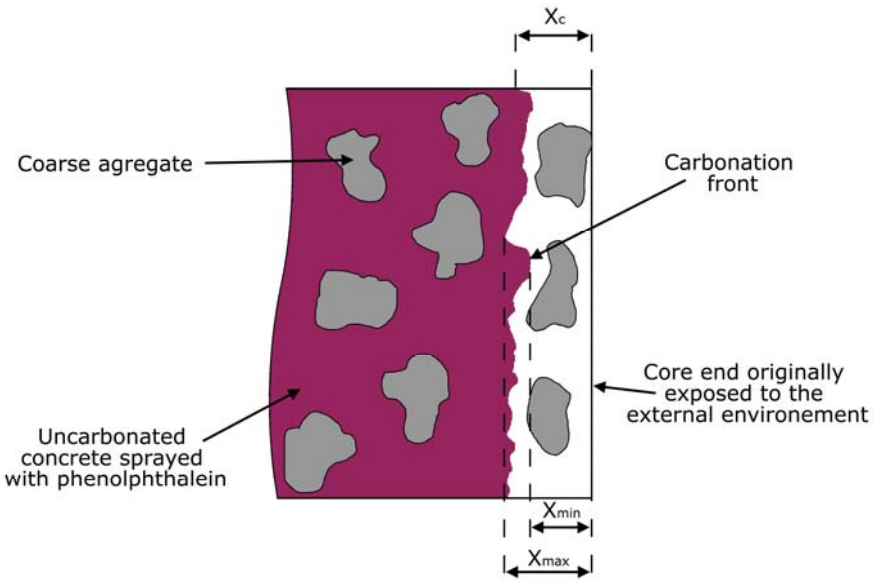

Figure 3.19. Schematic representation of the carbonation depth (x_c) measured on a concrete core (adaptation after Sagues, 1997)

Table 3.21. Carbonation depth measurements- first set of experiments

Sample	x_{min}(mm)	x_{max} (mm)	x_c (mm)
Ref I a	6.0	9.0	7.7
Ref II a	-	-	-
Ref III a	6.0	10.0	8.2
Ref IV a	8.0	12.0	9.0
Ref V	5.0	11.0	7.0
Ref VI	5.0	10.0	8.4

Table 3.22. Carbonation depth measurements- second set of experiments

Sample	x_{min}(mm)	x_{max} (mm)	x_c (mm)
Ref I b	8.0	10.0	8.8
Ref II b	8.0	11.0	8.9
Ref III b	8.0	10.0	8.6
Ref IV b	7.0	10.0	7.9
Ref VII	4.0	10.0	8.1
Ref VIII	7.0	10.0	8.3

3.5. Results and discussions

3.5.1. Measurement of crack width

The average crack widths obtained with the use of the optical microscope were previously described in Section 3.3.1. Surface measured average crack widths range from 104 to 372 μm for the top and bottom surfaces of the samples and from 63 to 311 μm for through- thickness of the sample. In order to statistically analyse the influence of crack widths on chloride penetration (Section 4.5), where a considerable number of replicas is required in order to perform the analysis, these values were rounded. Table 3.21 presents the average values of the crack widths determined as a sum of the measurements determined at the top and bottom surface, while Table 3.22 presents the average values of the crack widths determined through-thickness of the samples.

Table 3.21. Rounded values of crack widths for top/bottom surfaces

Sample	Crack opening (mm)	Sample	Crack opening (mm)
A	0.3	L	0.3
B	0.3	M	0.3
C	0.2	N	0.3
D	0.2	4	0.1
E	0.3	6	0.2
F	0.2	7	0.1
G	0.4	13	0.1
H	0.3	16	0.1
I	0.2	25	0.1
J	0.3	A2	0.2
K	0.3	B2	0.1

Table 3.22. Rounded values of crack widths for through-thickness of the sample

Sample	Crack opening (mm)	Sample	Crack opening (mm)
A	0.2	L	0.1
B	0.2	M	0.2
C	0.1	N	0.1
D	0.1	4	0.2
E	0.3	6	0.3
F	0.2	7	0.1
G	0.1	13	0.1
H	0.1	16	0.2
I	0.2	25	0.1
J	0.1	A2	0.2
K	0.1	B2	0.2

3.5.2. Penetration depth

3.5.2.1. Influence of exposed surface

The results of the chloride depth penetration were previously presented in Section 3.4.3. According to (NT Build 492, 1999) three specimens should be used for each test. Due to the unique characteristics of each sample and the reduced repeatability rate, beside the reference samples, this criterion could not be met. The average values of the penetration depth for reference samples type S are presented in Table 3.23. The first average values obtained for each of the exposed surfaces correspond to the chloride penetration depth measurements from the first set of experiments, while the other ones to the second set of experiments. It can be seen that the (average) values obtained per sample vary from 10.3 to 26.3 mm.

Table 3.23. Average penetration depths for samples type S

	Chloride penetration depth (mm)						
	Sample 1		Sample 2		Sample 3		Average
Top	Ref IV a	21.4	Ref V	24.2	Ref VI	26.3	23.9
	Ref IV b	15.7	Ref VII	17.6	Ref VIII	18.7	17.3
Bottom	Ref I a	12.6	Ref II a	17.6	Ref III a	20.5	16.9
	Ref I b	20.6	Ref II b	13.7	Ref III b	10.3	14.8

A representation of these average values is presented in Figure 3.20. It can be observed that the values obtained for samples having the top surface exposed are significantly higher than the ones obtained for those having the bottom surface

exposed. In the case of the first set of experiments the average value obtained for the exposed top surface is 29% higher than the bottom surface, while for the second set of experiments, the top surface is 15% higher than the bottom one.

It is a known fact that while casting, the surface layer of concrete is more porous due to the existence of a higher amount of cement paste compared to the bulk material, which is more compact; this may affect the transport characteristics of the material and can enhance the chloride ingress. Also, another factor that could facilitate the chloride ingress at the exposed top surface is carbonation. The possible influence of carbonation is further discussed in Section 3.5.4.

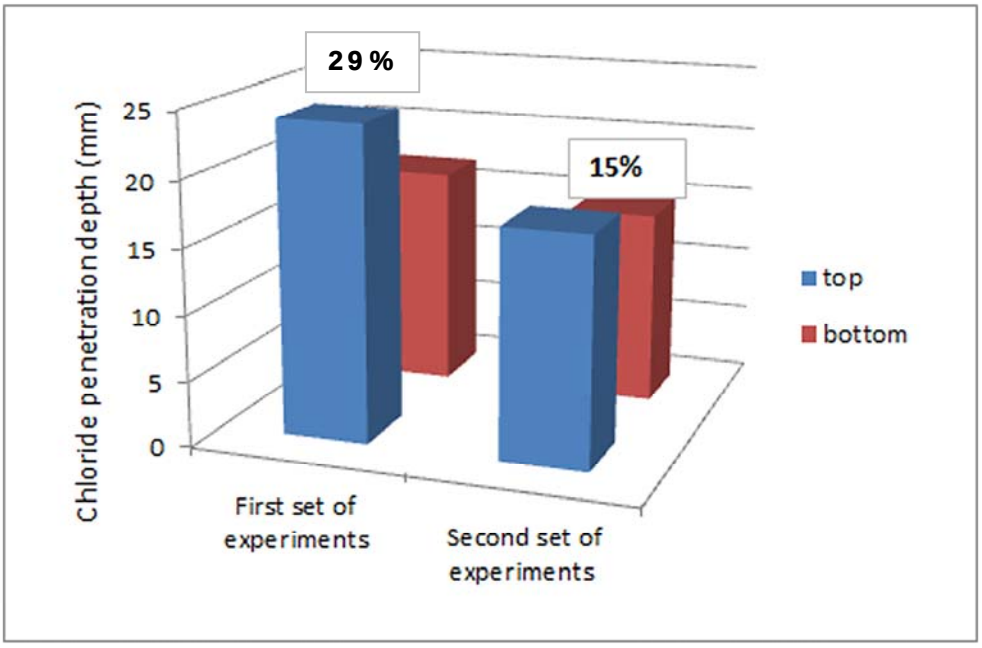

Figure 3.20. Comparison between the top and bottom surface exposure for samples type S- penetration depth

As previously mentioned, for the other sample types: SR, SC and SRC, it was not possible to obtain the required average chloride penetration per test value due to either the unique pattern of the crack, the existence of rebars or both. Figure 3.21 represents a comparison between the values of the chloride penetration depth x_d (average value of the chloride penetration depth for the entire sample) and x (average penetration depth determined in the diametric section of the sample) obtained for the top and bottom exposed surface for samples type SR, previously presented in Table 3.14 and Table 3.15. It can be clearly observed that the penetration depths are significantly higher for the samples having the top surface exposed). From Figure 3.21 it can be seen that the highest value of x_d for the top surface exposed is 24.2 mm (Sample 7R), compared to 12.0 mm (Sample 1R), the highest value for the bottom surface exposed. The penetration depth obtained for the exposed top surface is ≈50% higher than the one for the bottom surface exposed. The lowest value for x_d obtained from the top surface exposed is 18.1 mm

(Sample 4R) which is ≈38% higher than 11.3 mm (Sample 3R), the lowest value obtained for the bottom surface exposed. In the case of x, the highest values for top/bottom surfaces are 25.0 mm (Sample 7R), respectively 11.1 mm (Sample 2R), and meaning a difference of ≈56%. The lowest values obtained for x are 12.8 mm (Sample 6R) for the top surface, compared to 9.9 mm (Sample 1R) for bottom surface exposed, meaning a difference of ≈23 %.

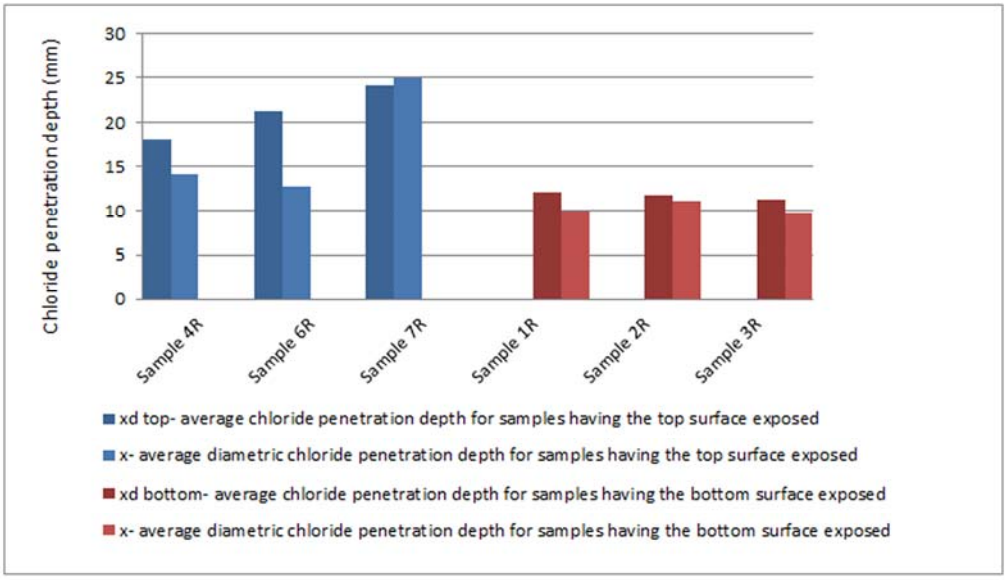

Figure 3.21. Comparison between the top and bottom surface exposure for samples type SR- penetration depth

3.5.2.2. Influence of rebars

With regards to the exposed surface, a comparison between reference samples type S and reference samples type SR was realized, based on the measured average chloride penetration depths (x_d) previously presented in Table 3.12, Table 3.13, Table 3.14 and Table 3.15, in order to determine the possible influence of rebars on chloride penetration. The obtained results are presented in Figure 3.23 and Figure 3.24.

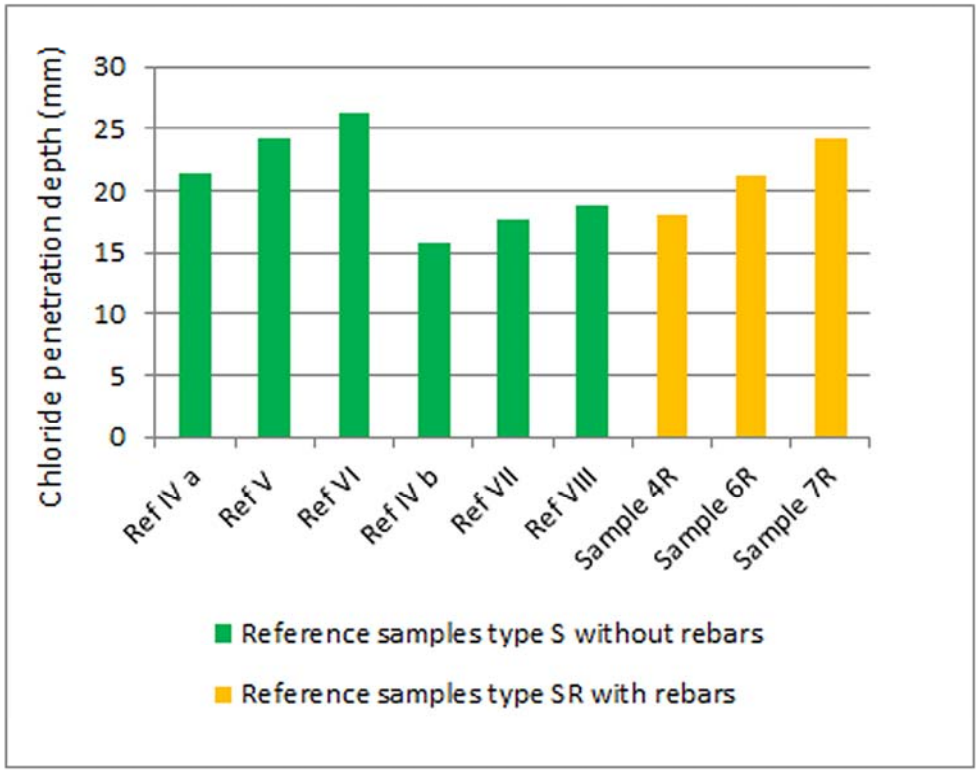

Figure 3.23. Comparison between samples type S and type SR- top surface exposed- penetration depth

It appears that in the case of samples having the bottom surface exposed, the penetration depth is higher in the case of samples containing rebars, while in the case of samples having the top surface exposed, no significant difference between the values of the penetration depths obtained for the two types of samples can be noticed. It is possible that the presence of rebars obstructs the penetration of chloride. Still, based on the limited number of samples, no significant conclusion can be drawn regarding how chloride diffusion is affected by the presence of rebars.

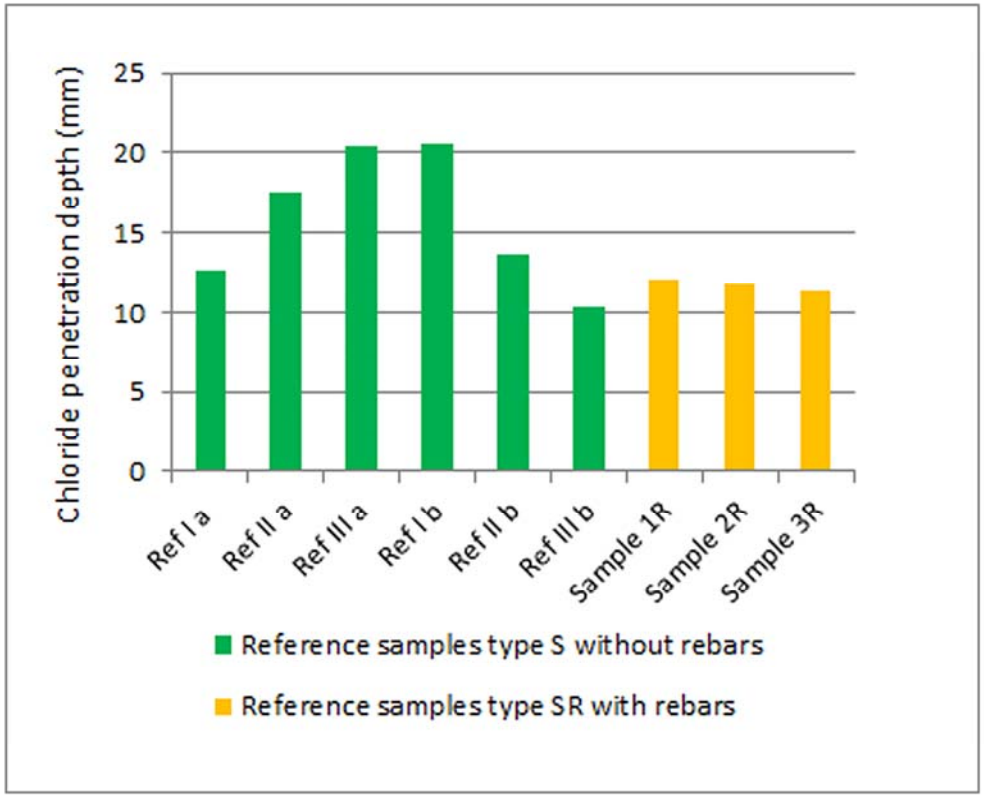

Figure 3.24. Comparison between samples type S and type SR- bottom surface exposed- penetration depth

3.5.2.3. Influence of cracks

Based on the measured average chloride penetration depths previously presented in Table 3.10 and Table 3.11, a comparison was made between the values obtained for x_d (average penetration depth determined for the whole sample in the uncracked region) and x_c (average penetration depth determined for the whole sample determined near the crack). It can be clearly seen from Figure 3.25 and Figure 3.26 that the penetration depth obtained near the crack is 2.5 % (Sample N) up to 87% (Sample 6) higher than the migration coefficients in the uncracked region, for samples having the top surface exposed, while in the case of the samples having the bottom surface expose the values obtained for x_c are 14% (Sample D) up to 163 % (Sample B) higher than x_d.

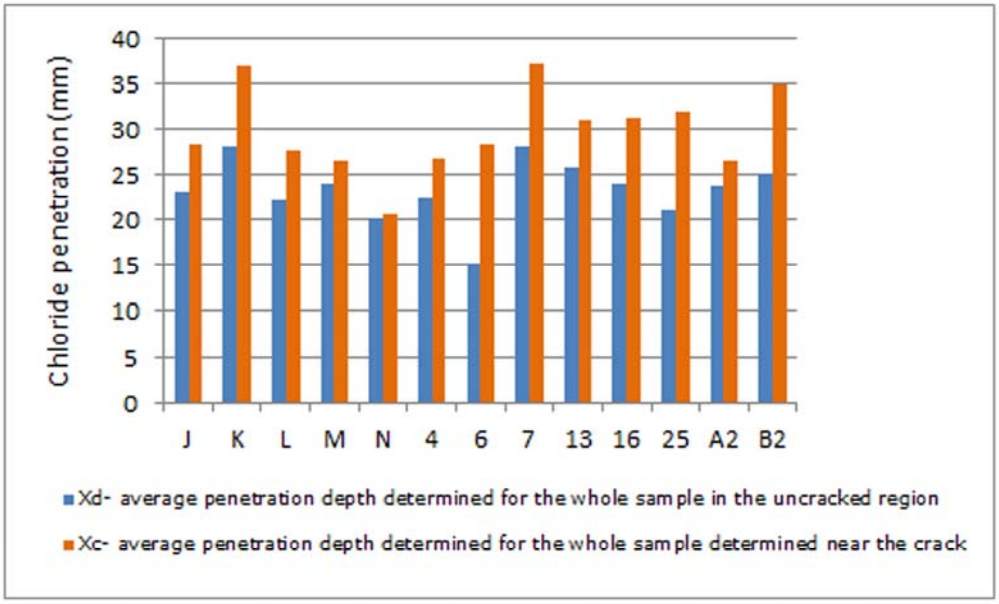

Figure 3.25. Comparison between chloride penetration depths for samples type S having the top surface exposed

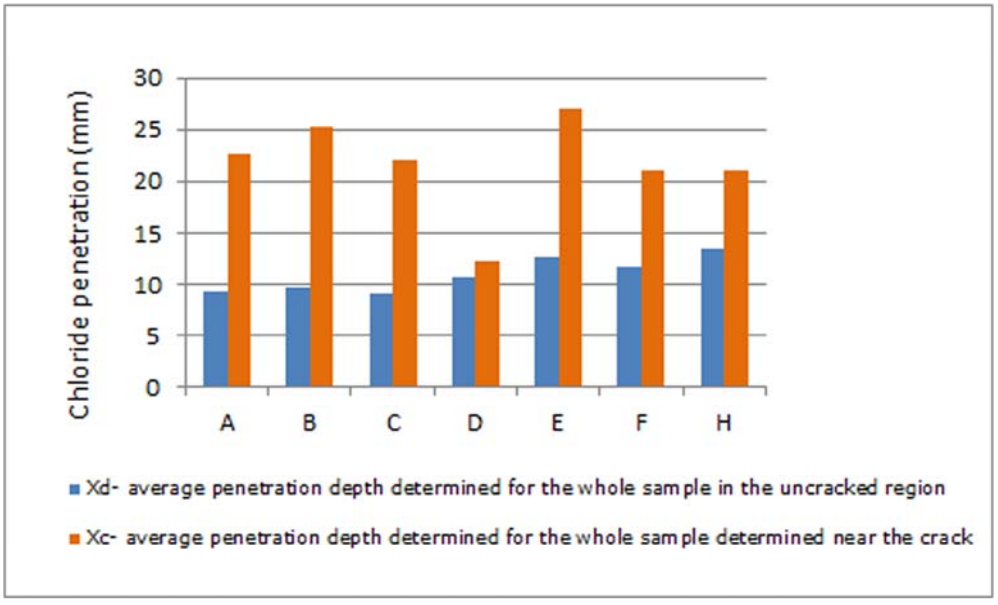

Figure 3.26. Comparison between chloride penetration depths for samples type S having the bottom surface exposed

3.5.3. Migration coefficient

3.5.3.1. Influence of exposed surface

According to the measured penetration depth, migration coefficients were determined for all samples except for samples type SCR having the bottom surface exposed, as previously mentioned in Section 3.4.4. Migration coefficients could not be determined for samples type SCR having the bottom surface exposed, due to an incident that led to loss of information regarding the values of the temperature and voltage used in the non-steady state migration test. Table 3.24 presents the migration coefficients for samples type S in accordance to the penetration depths previously resented in Table 3.23.

Table 3.24. Average migration coefficients for samples type S

	Migration coefficient (x 10^{-12} m^2/m)						
	Sample 1		Sample 2		Sample 3		Average
Top	Ref IV a	8.6	Ref V	9.8	Ref VI	10.7	9.7
	Ref IV b	5.4	Ref VII	6.1	Ref VIII	6.5	6.0
Bottom	Ref I a	4.9	Ref II a	7.0	Ref III a	8.3	6.7
	Ref I b	7.2	Ref II b	4.6	Ref III b	3.4	5.1

As expected, the migration coefficients obtained for samples having the top surface exposed is significantly higher than for those having the bottom one exposed. In the case of the first set of experiments the average value obtained for the exposed top surface is 31% higher than the bottom surface, while for the second set of experiments, the top surface is 15% higher than the bottom one (Figure 3.27).

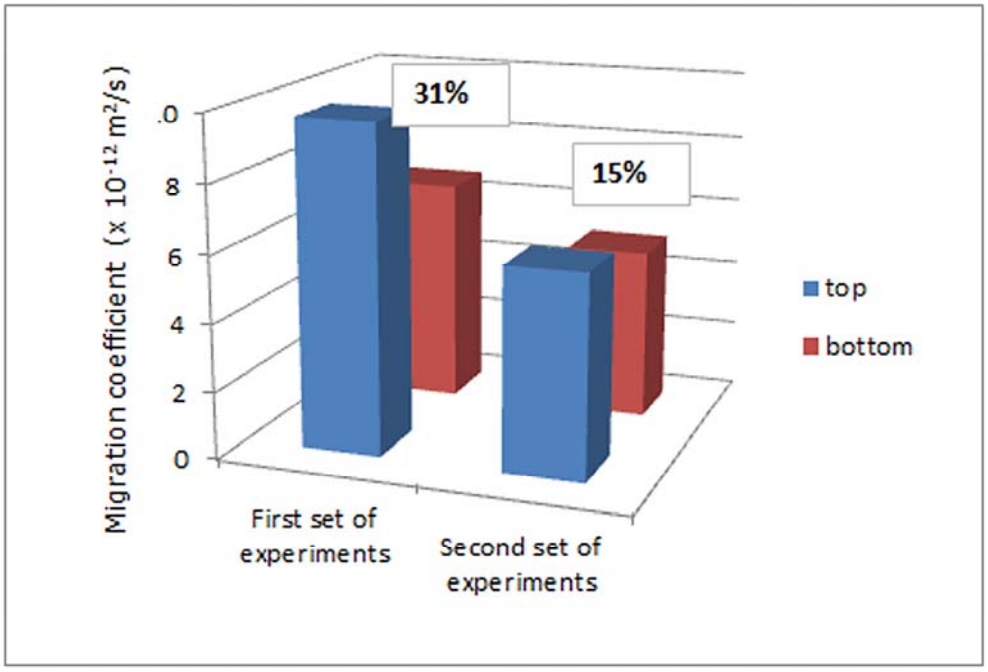

Figure 3.27. Comparison between the top and bottom surface exposure for samples type S- migration coefficient

Figure 3.28 represents a comparison between the values of the migration coefficients D_d (migration coefficient for the entire sample) and D (diametric migration coefficient) obtained for the top and bottom exposed surface for samples type SR, previously presented in Table 3.19 and Table 3.20. It can be clearly observed that the penetration depths are significantly higher for the samples having the top surface exposed). From Figure 3.28 it can be seen that the highest value of D_d for the top surface exposed is 9.5 x 10^{-12} m^2/s (Sample 7R), compared to 4.6x 10^{-12} m^2/s (Sample 1R), the highest value for the bottom surface exposed. The penetration depth obtained for the exposed top surface is ≈52% higher than the one for the bottom surface exposed. The lowest value for D_d obtained from the top surface exposed is 7.0 x 10^{-12} m^2/s (Sample 4R) which is ≈39% higher than 4.3 x 10^{-12} m^2/s (Sample 3R), the lowest value obtained for the bottom surface exposed. In the case of D, the highest values for top/bottom surfaces are 10 x 10^{-12} m^2/s (Sample 7R), respectively 4.2 x 10^{-12} m^2/s (Sample 2R), meaning a difference of ≈58%. The lowest values obtained for D is 4.9 x 10^{-12} m^2/s (Sample 6R) for the top surface, compared to 3.6 x 10^{-12} m^2/s (Sample 3R) for bottom surface exposed, meaning a difference of ≈27 %. As expected, the results are in agreement with the results obtained for the chloride penetration depth.

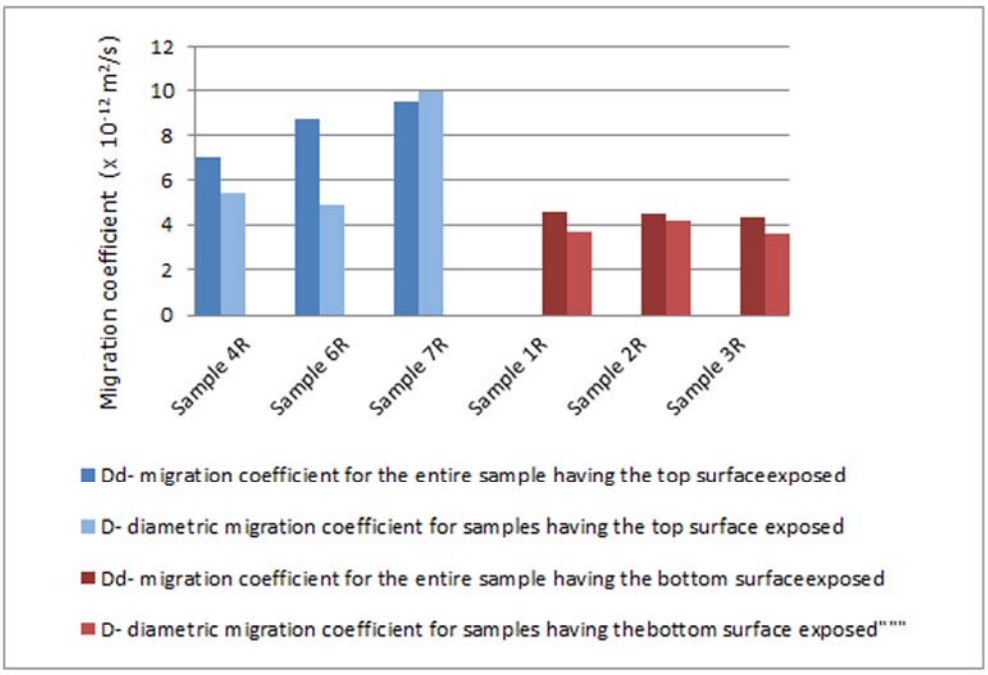

Figure 3.28. Comparison between the top and bottom surface exposure for samples type SR- migration coefficient

3.5.3.2. Influence of rebars

Figure 3.29 and Figure 3.30 present the migration coefficients obtained for samples type S and SR in order to determine the possible influence of rebars on the determination of the non-steady state migration coefficient.

It appears that in the case of samples having the bottom surface exposed, the penetration depth is higher in the case of samples containing rebars, while in the case of samples having the top surface exposed, the data obtained from the first set of experiments indicates a higher value for samples having the top surface exposed, while the data from the second set of experiments indicates the opposite, therefore no significant conclusion can be drawn regarding how chloride diffusion is affected by the presence of rebars.

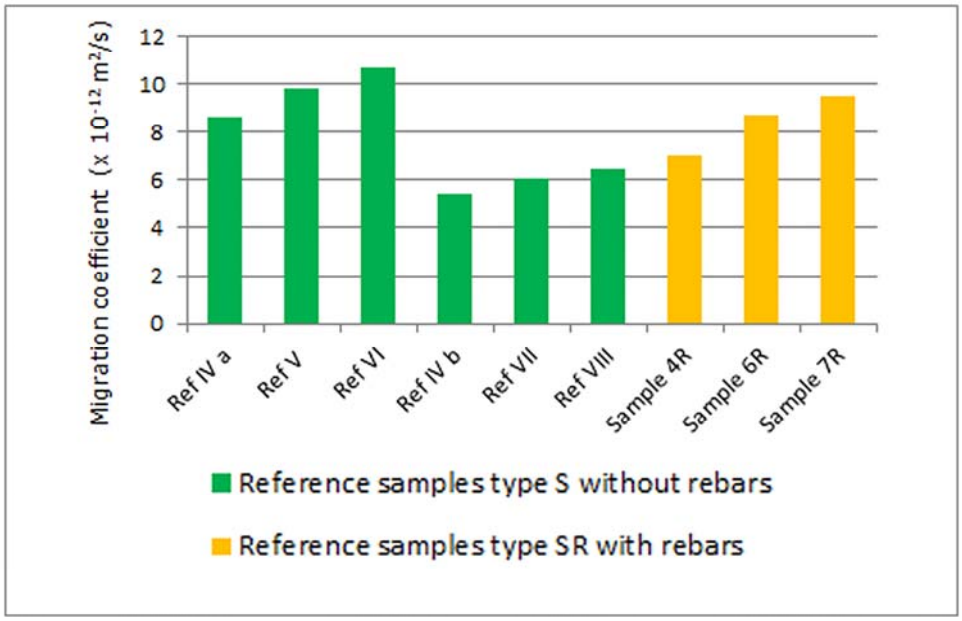

Figure 3.29. Comparison between samples type S and type SR- top surface exposed- migration coefficient

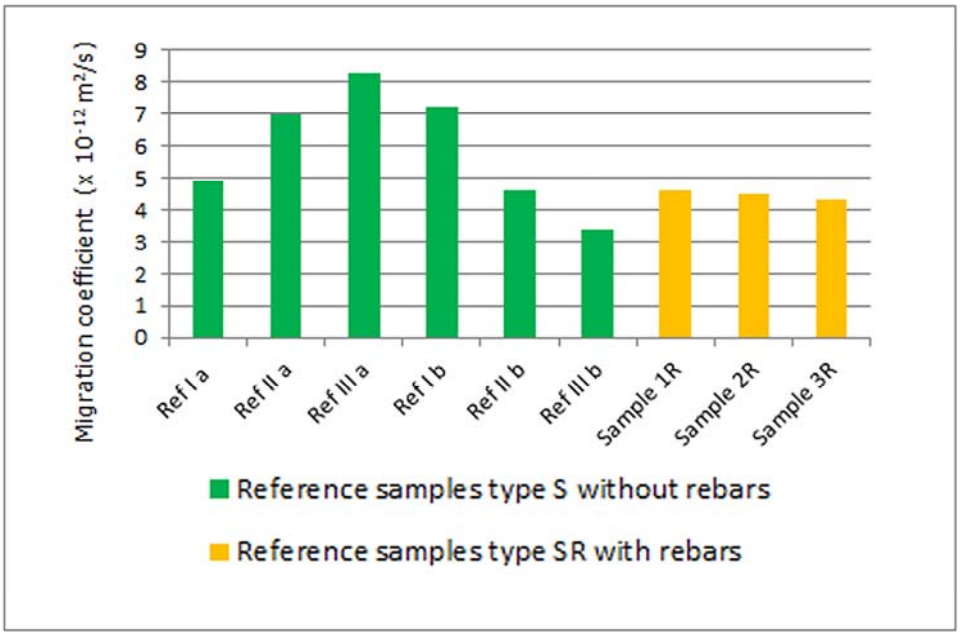

Figure 3.30. Comparison between samples type S and type SR- bottom surface exposed- migration coefficient

3.5.3.3. Influence of cracks

Based on the migration coefficients determined for cracked samples having the top surface exposed (Table 3.16) a comparison between D_d (migration coefficient in the uncracked region) and D_c (migration coefficient determined near the crack) was made. It can be clearly seen from Figure 3.31 that the values of the migration coefficients near the crack are 3 % (Sample N) up to 93% (Sample 6) higher than the migration coefficients in the un-cracked region of the sample.

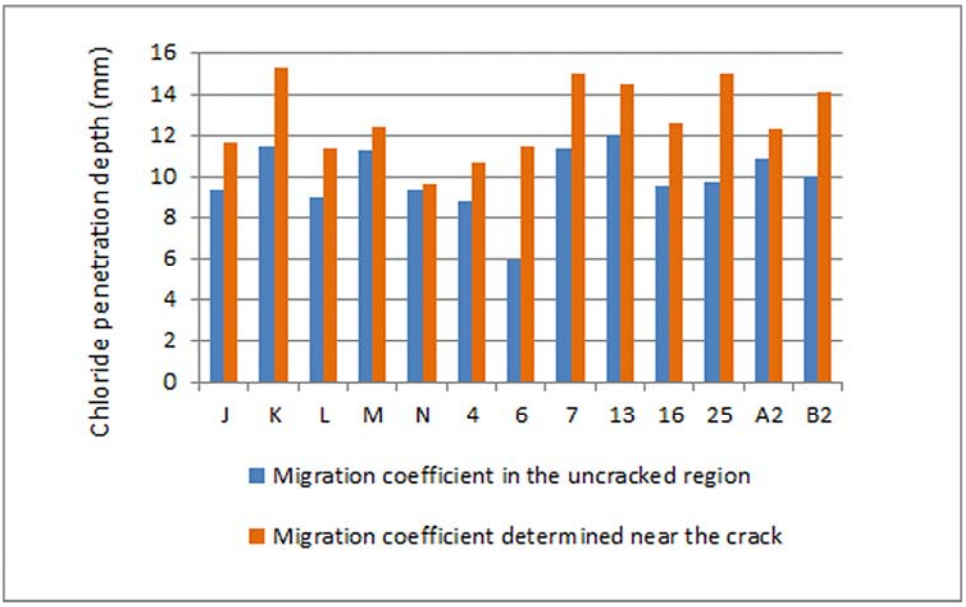

Figure 3.31. Comparison between migration coefficients for samples type S having the top surface exposed

3.5.4. Carbonation

3.5.4.1. Procedure for determination of chloride concentration for acid soluble chloride

After the non-steady state migration test previously described in Section 3.4, six of the reference samples type S used for the determination of chloride penetration, three having the top surface exposed, three having the bottom surface exposed, were used to determine the total chloride concentration. Since each sample was broken in two parts for the colorimetric method, only one half was used for the determination of the chloride concentration.

For profile grinding, each half of sample was mounted on the Arboga Maskinen, a vertical drilling machine with a movable table that controls displacement in two directions, and levelled. Powder samples were produced by

grinding layers of 2 and 4 mm layers with the aid of a 12 mm diameter diamond core (Figure 3.32).

While collecting the powder samples, care was taken to prevent contamination of the powder samples either from the previously ground layers or from any other sources. For each sample 10 layers were ground according to Figure 3.33. The total chloride concentration was determined by means of titration following the method of (Yuan, 2009 b).

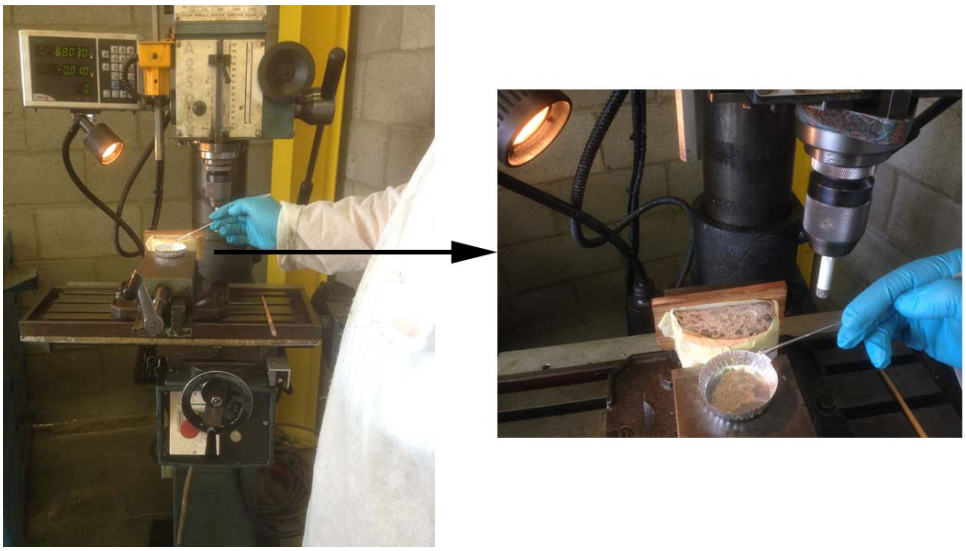

Figure 3.32. Profile grinding machine

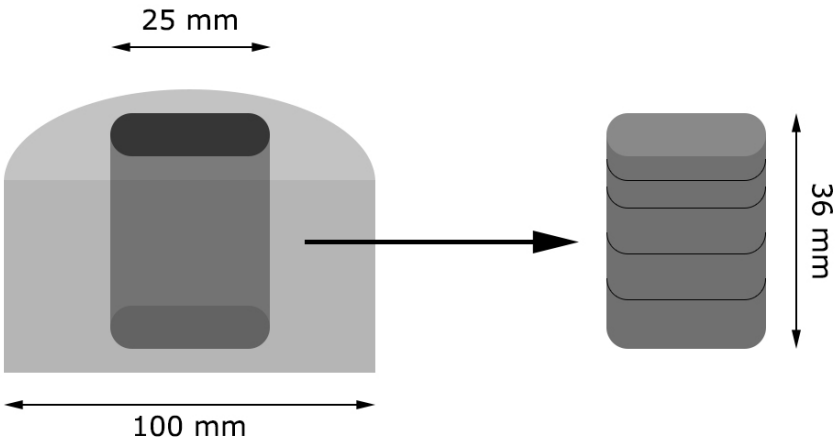

Figure 3.33. Grinding of the concrete layers

3.5.4.2. Chloride concentration

The results obtained for the acid soluble chloride for both carbonated and non-carbonated samples are presented in Figure 3.34. It can be seen that all chloride profiles decrease with increasing distance from the exposure surface, which is a typical gradient driven process with high concentrations close to the surface and low concentrations at the centre. It can be observed that the chloride concentration stabilizes at around 0.03%, due to the reduction in the chloride concentration gradient towards the centre.

It can be observed that in case of the carbonated samples, the trend of the chlorides seem to be very similar, the maximum chloride concentration of 0.38 %wt. was obtained at about 12 mm from the exposed surface, while in the case of the non-carbonated samples the highest concentration was reached at about 6 mm from the exposed surface and it's about 0.49 % wt. for non-carbonated samples Ref II. Also, it can be seen that the chloride profiles of the carbonated and non-carbonated samples are parallel. It appears that carbonation pushes the chloride front and decreases significantly the chloride concentration.

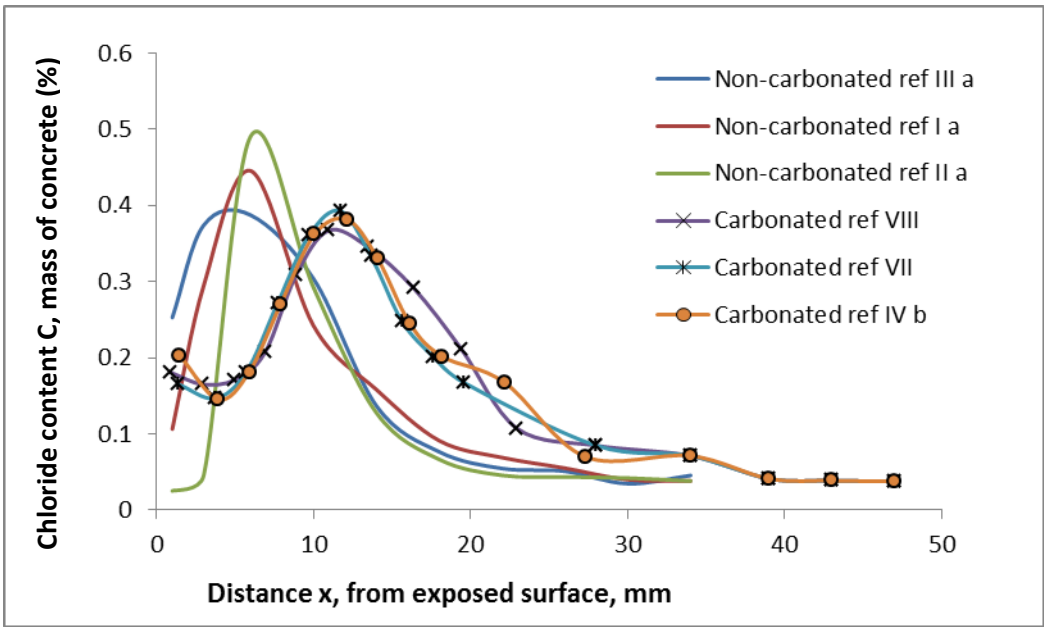

Figure 3.34. Concentration of acid soluble chloride

Figure 3.35 presents the results obtained by (Saeki, 2002) when studying the chloride distribution in OPC mortar under cyclic complex deterioration test (2 days in salt solution and 6 days in carbonation chamber). For the comparison, the cyclic CO_2 free wet-dry test was performed, where the specimens were exposed in the air at the same temperature and RH with accelerated carbonation test. It can be

seen from this picture that carbonation controls the chloride ingress which seems to be happening due to a decrease in the pore volume due to the changed micro-structure of concrete due to carbonation.

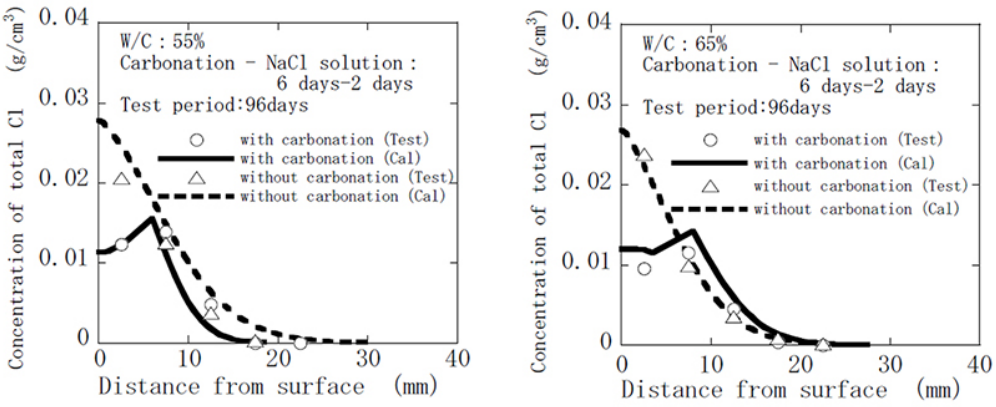

Figure 3.35 Chloride distribution after the combined effect of carbonation and chloride according to (Saeki, 2002)

3.5.5. Statistical analysis

3.5.5.1. Introduction and aim of the statistical analysis

Even though the behavior of many natural phenomena was described by means of mathematical and statistical models, when referring to civil engineering and especially for the analysis of chloride penetration, few data can be found in literature (Benedetti, 2012; Maes, 2013; Nieves-Mendoza, 2012).

As earlier mentioned, it is possible that different parameters, such as: exposed surface, crack existence, rebar presence, different crack widths, might influence chloride penetration in concrete and, consequently, have a significant importance in the determination of the migration coefficient. Therefore, a statistical analysis of the chloride penetration data was performed, using different methods: the comparison of means, the comparison of standard deviation and the analysis of variance tests (ANOVA). In order to determine whether the exposed surface, respectively the existence of cracks has a significant influence on the chloride penetration depth, the comparison of means method was used by comparing the means of the different test series using t-tests with a significance level of 0.05. For determining the influence of both exposed surface and rebar presence or the possible influence of different crack widths, on the chloride penetration depth, respectively on the diffusion coefficient, multifactor and one-way ANOVA analysis were performed with a level of significance of 0.05.

It must be mentioned that in order to obtain an accurate result, a sufficient number of replicas is needed for each of the performed tests. As previously described in Section 3, all samples have 100 mm diameter and 50 mm thickness and were subjected to the non-steady state diffusion test according to (NT Build 492, 1999). But, considering the fact that the crack geometries were not induced artificially and are in fact real cracks obtained as a result of the collapsing of a real-

scale slab, the number of equal replicas for each test is almost impossible. Still, based on the existent information, the statistical analysis was realized in order to investigate the possible influence of crack width on chloride ingress.

The methods used for the statistical analysis are further presented.

3.5.5.1.1. Comparison of two means

This statistical tool is used in many cases when a researcher is interested in gathering information about two samples of data and compares them in order to determine whether there is a statistically significant difference between them, by calculating various statistics and graphs for each sample and by running several tests. The outcome of these tests is the acceptance or rejection of the null hypothesis

The first step of this procedure is determining the confidence intervals for the difference between two means by specifying a range of values within which the difference between the means of the two samples of data may lie. These confidence intervals are then used in Student's t-test and help establishing whether the null hypothesis is accepted or rejected. If the null hypothesis is accepted this means that the differences between the two samples of data is random and does not have a statistically significant importance; if the null hypothesis is rejected there is a significant statistical difference between the two samples of data (Montgomery, 2008). t is calculated according to (4.1):

$$t = \frac{\bar{x}_1 - \bar{x}_2 - \Delta}{\sqrt{\frac{s_1^2}{n_1} + \frac{s_2^2}{n_2}}} \tag{4.1}$$

$\bar{x}_1, \bar{x}_2$ = the means of the two samples;

Δ = the hypothesized difference between the population means (0 if testing for equal means);

s_1, s_2 = standard deviations of the two samples;

n_1, n_2 = the sizes of the two samples.

The number of degrees of freedom for the problem is $df = min(n_1, n_2) - 1$.

In the case that the two sample distributions can be assumed to have the same variance and therefore the same standard deviations s_1, s_2 can be pooled together:

$$s_p^2 = \frac{(n_2 - 1)s_1^2 + (n_2 - 1)s_2^2}{n_1 + n_2 - 2} \tag{4.2}$$

The statistic t_{exp} (experimental t value) is obtained according to (4.3):

$$t_{calc} = \frac{\bar{x}_1 - \bar{x}_2 - \Delta}{s_p\sqrt{\left(\frac{1}{n_1} + \frac{1}{n_2}\right)}} \tag{4.3}$$

After obtaining t_{calc}, this value is compared with the critical, theoretical t_{th} value corresponding to the desired confidence level and the given degrees of

freedom. The critical t value can be found in any books of statistical analyses. Also, for a hypothesis test, t can be converted to a P-value using table of t statistics. If for the considered confidence level and the given degrees of freedom, $t_{calc}>t_{th}$, then the null hypothesis is rejected, else it is considered random (Montgomery, 2008).

3.5.5.1.2. Comparison of standard deviations

This statistical tool is usually used when measurements are made in different conditions and the problem of the accuracy of these measurements is under debate. As a particular case it can be used to determine the measurement precision of two different methods or different measurement tools. In this case an F-test is used to compare if two variances of standard deviations are equal. If the null hypothesis is accepted, then the variances and the standard deviations are equal which means that there is no significant statistical difference between them and so, with a 95% confidence level, the precision of two series of measurements is the same; if not, there is a significant statistical difference between variances (Montgomery, 2008).

In order to perform Fisher's F-test, the samples variances s_1^2, s_2^2 determined and considering: $s_1^2 > s_2^2$, the F-value is calculated as the ratio of the two variances:

$$F_{calc} = \frac{s_1^2}{s_2^2} \tag{4.4}$$

where:

s_1^2, s_2^2 = sample variances.

The degrees of freedom for the numerator and denominator are $n_1 - 1$ and $n_2 - 1$, respectively. Based on the considered significance level, F_{calc} is then compared to a theoretical F_{th} to see if the null hypothesis is rejected or not. If $F_{calc}>F_{th}$, the null hypothesis is rejected, else it is considered there is no significant difference between the accuracy of the two series of measurements.

3.5.5.1.3. Analysis of variance test (ANOVA)

The one-way analysis of variance (ANOVA) is a technique used to compare means of three or more samples (using the F distribution) with the purpose of determining whether there are any significant differences between them. This method tests the null hypothesis (Montgomery, 2008):

$$H_0=\mu_1=\mu_2=\ldots=\mu_k \tag{4.5}$$

where:

μ= group mean;

k= number of groups.

If the one-way ANOVA offers a statistically significant result the alternative hypothesis is accepted, which means that there are at least two groups that are significantly different from each other.

Performing a one-way ANOVA test is more accurately than performing multiple t-tests. While conducting a t-test there is a chance of a 5% error (Type 1 error); while

running two t-tests, the error chance increases to 10% and so on. ANOVA controls these errors within the range of 5% (Type 1 error).

In order to perform a one-way ANOVA test, certain requirements must be satisfied:

1. The populations from which the samples were obtained must be normally or approximately normally distributed;
2. The samples must be independent;
3. The variances of the populations must be equal.

When performing a one-way ANOVA test, the F value and P value are obtained based on the mean square (MS) values, sum of squares (SM) and the degrees of freedom (df) and taking into consideration the null hypothesis and the 95% confidence level. To determine which specific groups differ from each other, post-hoc tests are performed. In the present analysis, Fisher's Least Significant Difference (LSD) test is used as a post-hoc test with the level of significance of 0.05). Taking into account the sample sizes of two groups being compared, it computes a standard error of the difference between those two means and then it computes a t ratio by dividing the difference between the means by the standard error of that difference.

A multi-factor ANOVA is used to detect statistically significant factors in a multi-factor model. This method is normally used in designed experiments where values for each of the factor variables are set in order to measure the response variable. The model decomposes the response into contributions due to various factors. The model assumes that the error term should follow the assumptions for a univariate measurement process, which means that the contribution of each factor is measured having removed the effects of all other factors. The P-values test the statistical significance of each of the factors within the 95% considered confidence level (Montgomery, 2008).

3.5.5.2. Results and interpretations of the statistical analysis

It must be noted that the following data analysis presented in this section were performed using the (Statgraphics, 1997) software.

3.5.5.2.1. Influence of exposed surface

Two-sample comparison tests based on the comparison of two means and the comparison of standard deviation methods were realized in order to determine the possible influence of the exposed surface. These comparisons were made for different considered cases using the values of x_d (chloride mean penetration depth) and x_c (chloride penetration depth near the crack).

3.5.5.2.1.1. Two-sample comparison: depth x_d by exposed surface for reference samples

The two samples of data considered in this case are the values of x_d obtained for reference samples type S and SR which had the top and respectively the bottom surface exposed. These values were previously presented in Table 3.12 and Table 3.13.

Sample 1, representing the bottom surface exposed, consists in 9 values ranging from 10.3 to 20.6 while sample 2, representing the top surface exposed, and consists in 9 values ranging from 15.7 to 26.3. These two samples of data are compared by means of various statistics and graphs and by running several tests in order to determine whether there are statistically significant differences between the two samples.

The samples characteristics are further presented in Table 3.25.

Table 3.25. Summary statistics: depth x_d by exposed surface for reference samples

	Surface Exposed=bottom	*Surface Exposed=top*
Count	9	9
Average	14,4889	20,8222
Standard deviation	4,00763	3,56783
Coeff. of variation	27,66%	17,1347%
Minimum	10,3	15,7
Maximum	20,6	26,3
Range	10,3	10,6
Stnd. skewness	1,00155	0,191175
Stnd. kurtosis	-0,69528	-0,742232

The standardized skewness and standardized kurtosis can be used to determine whether the samples come from normal distributions. Values of these statistics outside the range of -2 to +2 indicate significant departures from normality, which would tend to invalidate the tests which compare the standard deviations. In this case, both standardized skewness values are within the range expected and both standardized kurtosis are within the range expected.

Comparison of means for depth x_d

A t-test is run to compare the means of the two samples and it also constructs confidence intervals for each mean and also for the difference between the means. Of particular interest is the confidence interval for the difference between the means, which extends from -10.149 to -2.54175. Since the interval does not contain the value 0, there is a statistically significant difference between the means of the two samples at the 95% confidence level. The test is also used to investigate the null hypothesis about the difference between the means of the populations from which the two samples come. Considering that in the present test t=-3.54102 and P=0.00271757, meaning P<0.05 the null hypothesis is rejected in favour of the alternative.

Comparison of standard deviations for depth x_d

The previously presented results assume that the variances of the two samples are equal. These assumptions are made based on the results of an F-test to compare the standard deviations presented in Table 3.26.

Table 3.26. Comparison of standard deviations: depth x_d by exposed surface for reference samples

	Surface Exposed=bottom	*Surface Exposed=top*
Standard deviation	4,00763	3,56783
Variance	16,0611	12,7294
Df	8	8

An F-test is run to compare the variances of the two samples and it also constructs confidence intervals for each standard deviation and for the ratio of the variances. The standardized skewness and standardized kurtosis values shown in table 4.6, confirm that the samples came from normal distributions.
Of particular interest is the confidence interval for the ratio of the variances, which extends from 0.284605 to 5.59357. Since the interval contains the value 1, there is not a statistically significant difference between the standard deviations of the two samples at the 95% confidence level. The test is also used to investigate the null hypothesis about the standard deviations of the populations from which the two samples come. Considering that in this test F=1.26173 and P=0.750223, meaning P>0.05 and the ratio of the standard deviation equals 1.26, the null hypothesis cannot be rejected, so it can be concluded that the precision of the two samples measurements is the same.

The conclusion of this two-sample comparison test is that there is a statistically significant difference between the x_d values of the compared two samples, meaning that, at 95% confidence level, the chloride penetration in the case of reference samples (with no cracks) is influenced by the exposed surface.

3.5.5.2.1.2. Two-sample comparison: depth x_d by exposed surface for samples with cracks

The two samples of data considered in this case are the values of x_d obtained for samples with cracks type SC and SCR which had the top and respectively the bottom surface exposed. These values were previously presented in Table 3.10 and Table 3.11.
Sample 1, representing the bottom surface exposed, consists in 7 values ranging from 9.0 to 13.5 while sample 2, representing the top surface exposed, consists in 13 values ranging from 15.2 to 28.1. These two samples of data are compared by means of various statistics and graphs and by running several tests in order to determine whether there are statistically significant differences between the two samples.

The samples characteristics are further presented in Table 3.27.

Table 3.27. Summary statistics: depth x_d by exposed surface for samples with cracks

	Surface Exposed=bottom	*Surface Exposed=top*
Count	7	13
Average	10,9143	23,3077
Standard deviation	1,75065	3,40403
Coeff. of variation	16,04%	14,6048%
Minimum	9,0	15,2
Maximum	13,5	28,1
Range	4,5	12,9
Stnd. skewness	0,460479	-1,25079
Stnd. kurtosis	-0,815477	1,28369

The standardized skewness and standardized kurtosis can be used to determine whether the samples come from normal distributions. Values of these statistics outside the range of -2 to +2 indicate significant departures from normality, which would tend to invalidate the tests which compare the standard deviations. In this case, both standardized skewness values are within the range expected and both standardized kurtosis are within the range expected.

Comparison of means for depth x_d

A t-test is run to compare the means of the two samples and it also constructs confidence intervals for each mean and also for the difference between the means. Of particular interest is the confidence interval for the difference between the means, which extends from -15.3063 to -9.48052. Since the interval does not contain the value 0, there is a statistically significant difference between the means of the two samples at the 95% confidence level. The test is also used to investigate the null hypothesis about the difference between the means of the populations from which the two samples come. Considering that in the present test t=-8.93878 and P=4.87479e-8, meaning P<0.05 the null hypothesis is rejected in favour of the alternative.

Comparison of standard deviations for depth x_d

The previously presented results assume that the variances of the two samples are equal. These assumptions are made based on the results of an F-test to compare the standard deviations presented in Table 3.28.

Table 3.28. Comparison of standard deviations: depth x_d by exposed surface for samples with cracks

	Surface Exposed=bottom	*Surface Exposed=top*
Standard deviation	1,75065	3,40403
Variance	3,06476	11,5874
Df	6	12

An F-test is run to compare the variances of the two samples and it also constructs confidence intervals for each standard deviation and for the ratio of the variances. Of particular interest is the confidence interval for the ratio of the variances, which extends from 0.0709414 to 1.41932. Since the interval contains the value 1, there is not a statistically significant difference between the standard deviations of the two samples at the 95% confidence level. The test is also used to investigate the null hypothesis about the standard deviations of the populations from which the two samples come. Considering that in this test F=0.26449 and P=0.113549, meaning P>0.05 and the ratio of the standard deviation equals 0.26449, the null hypothesis cannot be rejected.

The conclusion of this two-sample comparison test is that there is a statistically significant difference between the x_d values of the compared two samples, meaning that, at 95% confidence level, the chloride penetration depth in the case of samples with cracks is influenced by the exposed surface.

3.5.5.2.1.3. Two-sample comparison: depth x_c by exposed surface for samples with cracks

The two samples of data considered in this case are the values of x_d obtained for samples with cracks type SC and SCR which had the top and respectively the bottom surface exposed. These values were previously presented in Table 3.10 and Table 3.11.

Sample 1, representing the bottom surface exposed, consists in 7 values ranging from 12.2 to 27.1 while sample 2, representing the top surface exposed, consists in 13 values ranging from 20.6 to 37.0. These two samples of data are compared by means of various statistics and graphs and by running several tests in order to determine whether there are statistically significant differences between the two samples.

The samples characteristics are further presented in Table 3.29.

Table 3.29. Summary statistics: depth x_c by exposed surface for samples with cracks

	Surface Exposed=bottom	*Surface Exposed=top*
Count	7	13
Average	21,6143	29,8077
Standard deviation	4,71785	4,63797
Coeff. of variation	21,8275%	15,5596%
Minimum	12,2	20,6
Maximum	27,1	37,0
Range	14,9	16,4
Stnd. skewness	-1,49336	-0,0674505
Stnd. kurtosis	1,62526	0,0187035

The standardized skewness and standardized kurtosis can be used to determine whether the samples come from normal distributions. Values of these statistics outside the range of -2 to +2 indicate significant departures from

normality, which would tend to invalidate the tests which compare the standard deviations. In this case, both standardized skewness values are within the range expected and both standardized kurtosis are within the range expected.

Comparison of means for depth x_c

A t-test is run to compare the means of the two samples and it also constructs confidence intervals for each mean and also for the difference between the means. Of particular interest is the confidence interval for the difference between the means, which extends from -12.7879 to -3.59896. Since the interval does not contain the value 0, there is a statistically significant difference between the means of the two samples at the 95% confidence level. The test is also used to investigate the null hypothesis about the difference between the means of the populations from which the two samples come. Considering that in the present test t=-3.74664 and P=0.00147696, meaning P<0.05 the null hypothesis is rejected in favor of the alternative.

Comparison of standard deviations for depth x_c

The previously presented results assume that the variances of the two samples are equal. These assumptions are made based on the results of an F-test to compare the standard deviations presented in Table 3.30.

Table 3.30. Comparison of standard deviations: depth x_c by exposed surface for samples with cracks

	Surface Exposed=bottom	*Surface Exposed=top*
Standard deviation	4,71785	4,63797
Variance	22,2581	21,5108
Df	6	12

An F-test is run to compare the variances of the two samples and it also constructs confidence intervals for each standard deviation and for the ratio of the variances. Of particular interest is the confidence interval for the ratio of the variances, which extends from 0.277538 to 5.55268. Since the interval contains the value 1, there is not a statistically significant difference between the standard deviations of the two samples at the 95% confidence level. The test is also used to investigate the null hypothesis about the standard deviations of the populations from which the two samples come. Considering that in this test F=1.03474 and P=0.899146, meaning P>0.05 and the ratio of the standard deviation equals 1.03474, the null hypothesis cannot be rejected.

The conclusion of this two-sample comparison test is that there is a statistically significant difference between the x_c values of the compared two samples, meaning that, at 95% confidence level, the chloride penetration depth in the case of samples with cracks is influenced by the exposed surface.

3.5.5.2.1.4 Two-sample comparison: depth x_d by exposed surface for all samples

The two samples of data considered in this case are the values of x_d obtained for all sample types which had the top and respectively the bottom surface

exposed. These values were previously presented in Table 3.10, Table 3.11, Table 3.12 and Table 3.13.

Sample 1, representing the bottom surface exposed, consists in 16 values ranging from 9.0 to 20.6 while sample 2, representing the top surface exposed, and consists in 22 values ranging from 15.2 to 28.1. These two samples of data are compared by means of various statistics and graphs and by running several tests in order to determine whether there are statistically significant differences between the two samples.

The samples characteristics are further presented in Table 3.31.

Table 3.31. Summary statistics: depth x_d by exposed surface for all samples

	Surface Exposed=bottom	*Surface Exposed=top*
Count	16	22
Average	12,925	22,2909
Standard deviation	3,62574	3,61042
Coeff. of variation	28,0522%	16,1968%
Minimum	9,0	15,2
Maximum	20,6	28,1
Range	11,6	12,9
Stnd. skewness	2,10587	-0,715271
Stnd. kurtosis	0,670406	-0,422092

The standardized skewness and standardized kurtosis can be used to determine whether the samples come from normal distributions. Values of these statistics outside the range of -2 to +2 indicate significant departures from normality, which would tend to invalidate the tests which compare the standard deviations. In this case, surface exposed=bottom has the standardized skewness values otside the normal range, but both standardized kurtosis are within the range expected.

Comparison of means for depth x_d

A t-test is run to compare the means of the two samples and it also constructs confidence intervals for each mean and also for the difference between the means. Of particular interest is the confidence interval for the difference between the means, which extends from -11.776 to -6.95581. Since the interval does not contain the value 0, there is a statistically significant difference between the means of the two samples at the 95% confidence level. The test is also used to investigate the null hypothesis about the difference between the means of the populations from which the two samples come. Considering that in the present test t=-7.8814 and P=2.37537e-9, meaning P<0.05 the null hypothesis is rejected in favor of the alternative.

Comparison of standard deviations for depth x_d

The previously presented results assume that the variances of the two samples are equal. These assumptions are made based on the results of an F-test to compare the standard deviations presented in Table 3.32.

Table 3.32. Comparison of standard deviations: depth x_d by exposed surface for all samples

	Surface Exposed=bottom	*Surface Exposed=top*
Standard deviation	3,62574	3,61042
Variance	13,146	13,0352
Df	15	21

An F-test is run to compare the variances of the two samples and it also constructs confidence intervals for each standard deviation and for the ratio of the variances. Of particular interest is the confidence interval for the ratio of the variances, which extends from 0.398026to 2.76357. Since the interval contains the value 1, there is not a statistically significant difference between the standard deviations of the two samples at the 95% confidence level. The test is also used to investigate the null hypothesis about the standard deviations of the populations from which the two samples come. Considering that in this test F=1.0085 and P=0.964714, meaning P>0.05 and the ratio of the standard deviation equals 1.0085, the null hypothesis cannot be rejected.

The conclusion of this two-sample comparison test is that there is a statistically significant difference between the x_d values of the compared two samples, meaning that, at 95% confidence level, the chloride penetration depth in the case of all samples is influenced by the exposed surface.

3.5.5.2.2. Influence of cracks

Two-sample comparison tests based on the comparison of two means and the comparison of standard deviation methods were realized in order to determine the possible influence of the existence of cracks. These comparisons were made for different considered cases using the values of x_c (chloride penetration depth near the crack) and taking into consideration the influence of the exposed surface.

3.5.5.2.2.1. Two-sample comparison: depth x_c by sample type for top surface exposed

The two samples of data considered in this case are the values of x_c obtained for reference samples and for samples with cracks having the top surface exposed. These values were previously presented in Table 3.10. It is important to mention that in the case of reference samples, considering they have no cracks, the value of x_d was used (Table 3.12).

Sample 1, representing reference samples type S and SR, consists in 9 values ranging from 15.7 to 26.3 while sample 2, representing samples with cracks type SC and SCR, consists in 13 values ranging from 20.6 to 37.0. These two samples of data are compared by means of various statistics and graphs and by running several tests in order to determine whether there are statistically significant differences between the two samples.

The samples characteristics are further presented in Table 3.33.

Table 3.33. Summary statistics: depth x_c by sample type for top surface exposed

	Sample Type=R	*Sample Type=S*
Count	9	13
Average	20,8222	29,8077
Standard deviation	3,56783	4,63797
Coeff. of variation	17,1347%	15,5596%
Minimum	15,7	20,6
Maximum	26,3	37,0
Range	10,6	16,4
Stnd. skewness	0,191175	-0,0674505
Stnd. kurtosis	-0,742232	0,0187035

The standardized skewness and standardized kurtosis can be used to determine whether the samples come from normal distributions. Values of these statistics outside the range of -2 to +2 indicate significant departures from normality, which would tend to invalidate the tests which compare the standard deviations. In this case, both standardized skewness standardized kurtosis are within the range expected.

Comparison of means for depth x_c

A t-test is run to compare the means of the two samples and it also constructs confidence intervals for each mean and also for the difference between the means. Of particular interest is the confidence interval for the difference between the means, which extends from -12.8229 to –5.14804. Since the interval does not contain the value 0, there is a statistically significant difference between the means of the two samples at the 95% confidence level. The test is also used to investigate the null hypothesis about the difference between the means of the populations from which the two samples come. Considering that in the present test t=-4.88436 and P=0.0000897041, meaning P<0.05 the null hypothesis is rejected in favour of the alternative.

Comparison of standard deviations for depth x_c

The previously presented results assume that the variances of the two samples are equal. These assumptions are made based on the results of an F-test to compare the standard deviations presented in Table 3.34.

Table 3.34. Comparison of standard deviations: depth x_c by sample type for top surface exposed

	Sample Type=R	*Sample Type=S*
Standard deviation	3,56783	4,63797
Variance	12,7294	21,5108
Df	8	12

An F-test is run to compare the variances of the two samples and it also constructs confidence intervals for each standard deviation and for the ratio of the variances. Of particular interest is the confidence interval for the ratio of the variances, which extends from 0.16851 to 2.48524. Since the interval contains the value 1, there is not a statistically significant difference between the standard deviations of the two samples at the 95% confidence level. The test is also used to investigate the null hypothesis about the standard deviations of the populations from which the two samples come. Considering that in this test F=0.591771 and P=0.464524, meaning P>0.05 and the ratio of the standard deviation equals 0.591771, the null hypothesis cannot be rejected.

The conclusion of this two-sample comparison test is that there is a statistically significant difference between the x_c values of the compared two samples, meaning that, at 95% confidence level, when having the top surface exposed the chloride penetration depth is influenced by the existence of cracks.

3.5.5.2.2.2 Two-sample comparison: depth x_c by sample type for bottom surface exposed

The two samples of data considered in this case are the values of x_c obtained for reference samples and for samples with cracks having the bottom surface exposed. These values were previously presented in Table 3.11. It is important to mention that in the case of reference samples, considering they have no cracks, the value of x_d was used (Table 3.13).

Sample 1, representing reference samples type S and SR, consists in 9 values ranging from 10.3 to 20.6 while sample 2, representing samples with cracks type SC and SCR, consists in 7 values ranging from 12.2 to 27.1. These two samples of data are compared by means of various statistics and graphs and by running several tests in order to determine whether there are statistically significant differences between the two samples.
The samples characteristics are further presented in Table 3.35.

Table 3.35. Summary statistics: depth x_c by sample type for bottom surface exposed

	Sample Type=R	*Sample Type=S*
Count	9	7
Average	14,4889	21,6143
Standard deviation	4,00763	4,71785
Coeff. of variation	27,66%	21,8275%
Minimum	10,3	12,2
Maximum	20,6	27,1
Range	10,3	14,9
Stnd. skewness	1,00155	-1,49336
Stnd. kurtosis	-0,69528	1,62526

The standardized skewness and standardized kurtosis can be used to determine whether the samples come from normal distributions. Values of these

statistics outside the range of -2 to +2 indicate significant departures from normality, which would tend to invalidate the tests which compare the standard deviations. In this case, both standardized skewness standardized kurtosis are within the range expected.

Comparison of means for depth x_c

A t-test is run to compare the means of the two samples and it also constructs confidence intervals for each mean and also for the difference between the means. Of particular interest is the confidence interval for the difference between the means, which extends from -11.8016 to -2.4492. Since the interval does not contain the value 0, there is a statistically significant difference between the means of the two samples at the 95% confidence level. The test is also used to investigate the null hypothesis about the difference between the means of the populations from which the two samples come. Considering that in the present test t=-3.26815 and P=000560658, meaning P<0.05 the null hypothesis is rejected in favour of the alternative.

Comparison of standard deviations for depth x_c

The previously presented results assume that the variances of the two samples are equal. These assumptions are made based on the results of an F-test to compare the standard deviations presented in Table 3.36.

Table 3.36. Comparison of standard deviations: depth x_c by sample type for bottom surface exposed

	Sample Type=R	*Sample Type=S*
Standard deviation	4,00763	4,71785
Variance	16,0611	22,2581
Df	8	6

An F-test is run to compare the variances of the two samples and it also constructs confidence intervals for each standard deviation and for the ratio of the variances. Of particular interest is the confidence interval for the ratio of the variances, which extends from 0.128863 to 3.35659. Since the interval contains the value 1, there is not a statistically significant difference between the standard deviations of the two samples at the 95% confidence level. The test is also used to investigate the null hypothesis about the standard deviations of the populations from which the two samples come. Considering that in this test F=0.721585 and P=0.651655, meaning P>0.05 and the ratio of the standard deviation equals 0.591771, the null hypothesis cannot be rejected.

The conclusion of this two-sample comparison test is that there is a statistically significant difference between the x_c values of the compared two samples, meaning that, at 95% confidence level, when having the bottom surface exposed the chloride penetration depth is influenced by the existence of cracks.

3.5.5.2.3. Influence of crack widths

One-way ANOVA tests were performed in order to determine the possible influence of the crack width on D_c (diffusion coefficient measured near the crack) for samples having the top surface exposed. The considered crack widths were previously presented in Table 4.1 and Table 4.3.

3.5.5.2.3.1. One-way ANOVA: diffusion coefficient D_c by average crack widths

This procedure performs a one-way analysis of variance for diffusion coefficient D_c considering the average crack width previously presented in Table 4.1. Various tests and graphs are constructed to compare the mean values of D_c for the considered 16 cores type SC and SCR with 4 different levels of crack width. The result characteristics of the one-way ANOVA are further presented in Table 3.37.

Table 3.37. Summary statistics: diffusion coefficient D_c by crack width

Source	*Sum of Squares*	*Df*	*Mean Square*	*F-Ratio*	*P-Value*
Between groups	51,4673	3	17,1558	5,28	0,0149
Within groups	39,0063	12	3,25052		
Total (Corr.)	90,4736	15			

The ANOVA table decomposes the variance of Dc into two components: a between-group component and a within-group component. The F ratio, which in this case F= 5.27785, is a ration of the between-group estimate to the within-group estimate. Since P=0.0149, P<0.05 there is a statistically significant difference between the mean Dc from one level of crack width to another at the 95% confidence level.

The table of means for Dc by crack width is further presented in Table 3.38. Also, the table shows the standard error of each mean which is a measure of its sampling variability. The standard error is formed by dividing the pooled standard deviation by the square root of the number of observations at each level. The table also displays an interval around each mean. The intervals are based on Fisher's least significant difference (LSD) procedure and are constructed in such a way that if two means are the same, the intervals will overlap 95% of the time.

Table 3.38. Table of means for Dc by crack width with 95% LSD intervals

			Stnd. error		
Level	*Count*	*Mean*	*(pooled s)*	*Lower limit*	*Upper limit*
0	3	8,38333	1,04092	6,77964	9,98703
0,1	5	13,47	0,80629	12,2278	14,7122
0,15	3	12,7167	1,04092	11,113	14,3204
0,3	5	11,994	0,80629	10,7518	13,2362
Total	16	11,9137			

To determine which means are significantly different from which others the Multiple Range Test is carried on. Table 3.39 presents which means are significantly different from which others by using a multiple comparison procedure.

Table 3.39. Multiple Range Tests results for 95% LSD- Dc by crack width

Level	*Count*	*Mean*	*Homogeneous Groups*
0	3	8,38333	X
0,3	5	11,994	X
0,15	3	12,7167	X
0,1	5	13,47	X

Contrast	*Sig.*	*Difference*	*+/- Limits*
0 - 0,1	*	-5,08667	2,86878
0 - 0,15	*	-4,33333	3,20739
0 - 0,3	*	-3,61067	2,86878
0,1 - 0,15		0,753333	2,86878
0,1 - 0,3		1,476	2,48443
0,15 - 0,3		0,722667	2,86878

The bottom half of the output shows the estimated difference between each pair of means. An asterisk has been placed next to 3 pairs, indicating that these pairs show statistically significant differences at the 95% confidence level.

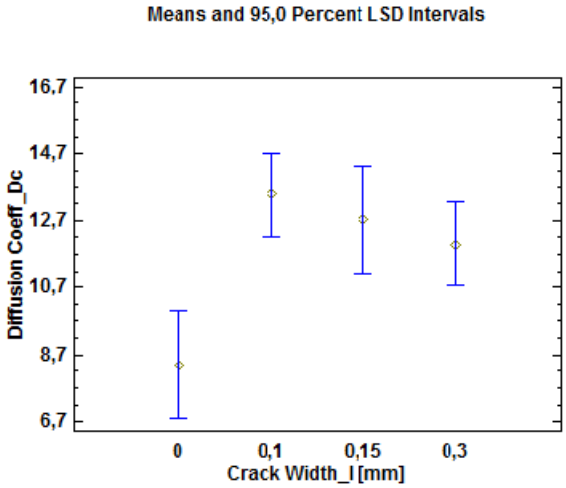

Figure 3.36. Interval plot (95% confidence) of D_c for crack width

Figure 3.36 presents the interval plots at 95% confidence of diffusion coefficient D_c for each crack width. It can be observed that there is a statistical significant difference between the values obtained for the reference samples and the values obtained for samples with cracks, but no statistical significant difference is between the different considered widths.

3.5.5.2.3.2. One-way ANOVA: diffusion coefficient D_c by total crack widths

This procedure performs a one-way analysis of variance for diffusion coefficient D_c considering the total crack width previously presented in Table 4.3. Various tests and graphs are constructed to compare the mean values of D_c for the considered 16 cores type SC and SCR with 5 different levels of crack width. The results of the one-way ANOVA are further presented in Table 3.40.

Table 3.40. Summary statistics: diffusion coefficient D_c by total crack width

Source	*Sum of Squares*	*Df*	*Mean Square*	*F-Ratio*	*P-Value*
Between groups	61,003	4	15,2508	5,69	0,0099
Within groups	29,4706	11	2,67914		
Total (Corr.)	90,4736	15			

The ANOVA table decomposes the variance of Dc into two components: a between-group component and a within-group component. The F ratio, which in this case F= 5.6924, is a ration of the between-group estimate to the within-group estimate. Since P=0.0099, P<0.05 there is a statistically significant difference between the mean Dc from one level of crack width to another at the 95% confidence level.

The table of means for D_c by crack width is further presented in Table 3.41. Also, the table shows the standard error of each mean which is a measure of its sampling variability. The standard error is formed by dividing the pooled standard deviation by the square root of the number of observations at each level. The table also displays an interval around each mean. The intervals are based on Fisher's least significant difference (LSD) procedure and are constructed in such a way that if two means are the same, the intervals will overlap 95% of the time.

Table 3.41. Table of means for Dc by total crack width with 95% LSD intervals

			Stnd. error		
Level	*Count*	*Mean*	*(pooled s)*	*Lower limit*	*Upper limit*
0	3	8,38333	0,945012	6,91258	9,85409
0,1	2	15,005	1,1574	13,2037	16,8063
0,15	5	12,826	0,732003	11,6868	13,9652
0,2	5	11,994	0,732003	10,8548	13,1332
0,25	1	11,36	1,63681	8,81258	13,9074
Total	16	11,9138			

To determine which means are significantly different from which others the Multiple Range Test is carried on. Table 3.42 presents which means are significantly different from which others by using a multiple comparison procedure.
The bottom half of the output shows the estimated difference between each pair of means. An asterisk has been placed next to 3 pairs, indicating that these pairs show statistically significant differences at the 95% confidence level.

Table 3.42. Multiple Range Tests results for 95% LSD- Dc by total crack width

Level	*Count*	*Mean*	*Homogeneous Groups*
0	3	8,38333	X
0,25	1	11,36	XX
0,2	5	11,994	X
0,15	5	12,826	X
0,1	2	15,005	X

Contrast	*Sig.*	*Difference*	*+/- Limits*
0 - 0,1	*	-6,62167	3,28871
0 - 0,15	*	-4,44267	2,63097
0 - 0,2	*	-3,61067	2,63097
0 - 0,25		-2,97667	4,15992
0,1 - 0,15		2,179	3,01415
0,1 - 0,2		3,011	3,01415
0,1 - 0,25		3,645	4,41226
0,15 - 0,2		0,832	2,27848
0,15 - 0,25		1,466	3,94645
0,2 - 0,25		0,634	3,94645

Figure 3.37 presents the interval plots at 95% confidence of diffusion coefficient D_c for each crack width. It can be observed that there is a statistical significant difference between the values obtained for the reference samples and the values obtained for samples with cracks, but no statistical significant difference is between the different considered widths. The existence of an insignificant difference between the diffusion coefficient obtained for the samples with no cracks and the sample having a crack with a 0,25 mm width can be explained by the fact that there was a single sample with this width, which caused a greater confidence interval.

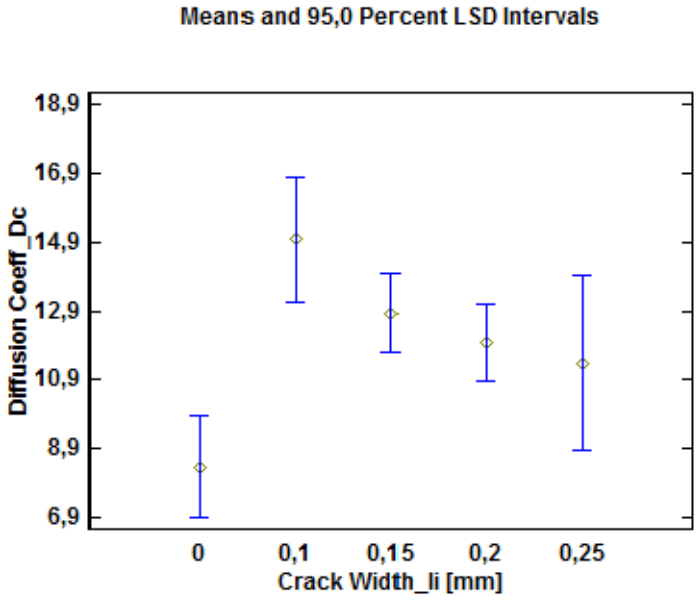

Figure 3.37. Interval plot (95% confidence) of D_c for crack width

3.5.5.2.4. Influence of exposed surface and rebars on D_d

A multifactor ANOVA test was performed in order to determine the effect of the exposed surface and the reinforcement existence on D_d (average diffusion coefficient) for the 6 reference samples type S and 6 reference samples type SR having the top and bottom surface exposed. The considered values of D_d were previously presented in Table 3.16.

A multifactor analysis of variance for the D_d was performed constructing various tests and graphs to determine which of the considered factors, exposed surface and rebar existence, have a significant effect on the average diffusion coefficient. Also, it tests for significant interactions amongst the factors. The results of the multifactor ANOVA are further presented in Table 3.43.

Table 3.43. Analysis of variance for D_d

Source	*Sum of Squares*	*Df*	*Mean Square*	*F-Ratio*	*P-Value*
MAIN EFFECTS					
A:Exposed surface	35,9148	1	35,9148	27,42	0,0005
B:Reinforcement	9,72	1	9,72	7,42	0,0234
Experimental error	11,7883	9	1,30981		
TOTAL (CORRECTED)	57,4231	11			

The variability of D_d are decomposed into contributions due to various factors. Since Type III sums of squares have been chosen, the contribution of each factor is measured having removed the effects of all other factors. Since 2P values are less than 0.05 these factors have a statistically significant effect on D_d at 95% confidence level.

The table of means for D_c by crack width is further presented in Table 3.44. This table shows the mean D_d for each level of the factors and it shows the standard error of each mean, which is a measure of its sampling variability. The rightmost two columns show 95% confidence intervals for each of the means.

Table 3.44. Table of least squares means for D_d with 95% confidence intervals

Level	Count	Mean	*Stnd. Error*	*Lower Limit*	*Upper Limit*
GRAND MEAN	12	7,31667			
Exposed surface					
bottom	6	5,58667	0,467227	4,52972	6,64361
top	6	9,04667	0,467227	7,98972	10,1036
Reinforcement existence					
no	6	8,21667	0,467227	7,15972	9,27361
yes	6	6,41667	0,467227	5,35972	7,47361

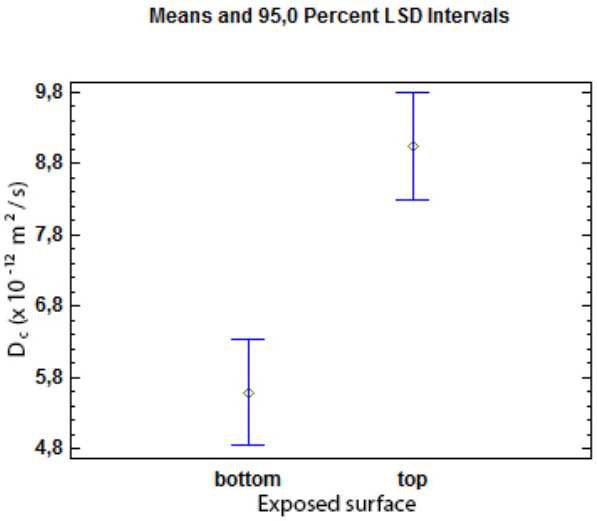

Figure 3.38. Interval plot (95% confidence) of D_d for exposed surface

Figure 3.38 and Figure 3.39 present the interval plot at 95% confidence of D_d for the exposed surface and for the reinforcement existence, respectively.

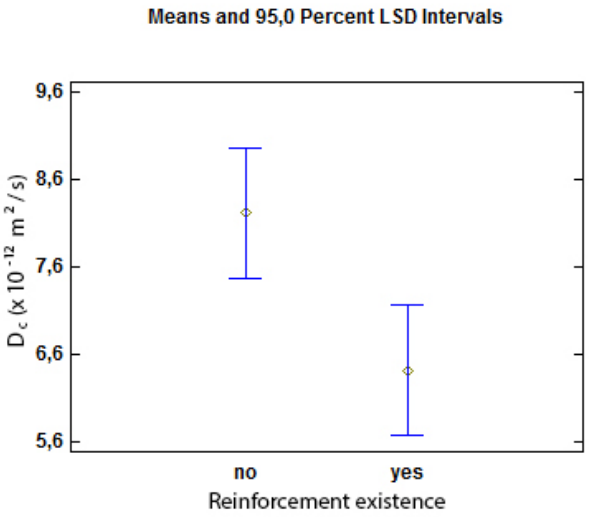

Figure 3.39. Interval plot (95% confidence) of D_d for reinforcement existence

3.5.5.2.5. Summary and conclusions of statistical analysis

A statistical analysis was performed in order to investigate whether certain parameters have an influence on chloride penetration, based on the obtained experimental data. Therefore the possible influence of: the exposed surface, the presence of the cracks, the crack width and the existence of the rebars were studied, by means of different statistical methods such as the comparison of means, the comparison of standard deviation and the analysis of variance (ANOVA). Also, the values of the measured crack widths (Section 3.5.1) were considered as independent variables in some tests.

The values of the chloride penetration depth (x_d- average chloride penetration depth, x_c- chloride depth near the crack), respectively of the migration coefficient corresponding to the previously mentioned chloride penetration values (D_d, D_c), presented in Section 3.4.3, Section 3.4.4, respectively, were used in the statistical analyse as response functions (dependent variables).

After studying the influence of the exposed surface on chloride penetration by the comparison of means method at a 95% confidence interval, the following results were obtained:

- the average chloride penetratio (x_d) is influenced by the exposed surface, when considering only samples type S (samples without cracks and rebars);
- the average chloride penetration (x_d) is influenced by the exposed surface,

when considering only samples type SC (samples with cracks) and type SCR (samples with cracks and with rebars);

- the chloride penetration depth near the crack (x_c) is influenced by the exposed surface when considering only samples type SC (samples with cracks) and SCR (samples with cracks and rebars);
- the average chloride penetration depth (x_d) is influenced by the exposed surface when considering all sample types (S- samples without cracks and rebars, SC- samples with cracks and without rebars, SR- samples without cracks and with rebars and SCR- samples with cracks and rebars).

The possible influence of the presence of cracks was further investigated, by the comparison of means method at a 95% confidence interval, separately for the two cases of exposure, in order to eliminate its influence:

- the chloride penetration depth near the crack (x_c) is influenced by the existence of cracks when having the top surface exposed and taking into consideration all sample types (S- samples without cracks and rebars, SC- samples with cracks and without rebars, SR- samples without cracks and with rebars and SCR- samples with cracks and rebars);
- the chloride penetration depth near the crack (x_c) is influenced by the existence of cracks. when having the bottom surface exposed and taking into consideration all sample types(S- samples without cracks and rebars, SC- samples with cracks and without rebars, SR- samples without cracks and with rebars and SCR- samples with cracks and rebars).

Next, the possible influence of the crack widths on the available samples was investigated by performing a one-way ANOVA test at a 95% confidence interval and considering both the average crack width and the total crack width, as previously presented in Table 4.1 and Table 4.3, respectively:

- the values of D_c (migration coefficient near the crack) are used considering the average crack widths of: 0.1; 0.15 and 0.3. It seems that no statistical significant difference is between the considered crack widths;
- the values of D_c (migration coefficient near the crack) are used considering the total crack widths of: 0.1; 0.15; 0.2 and 0.3. It seems that no statistical significant difference is between the considered crack widths.

Finally, the effect of the exposed surface and the presence of the rebars were studied by performing a multifactor ANOVA test at a 95% confidence interval comparing sample type S (samples without cracks and rebars) with sample type SR (samples without cracks and with rebars) having the top and the bottom surface exposed. The results show that their combined effect have a statistically significant effect on D_d (average diffusion coefficient).

3.6. Summary and conclusions

In this chapter, the influence of chloride penetration on RC structures with cracks was studied. 40 cores drilled from different locations from a RC slab subjected to compressive stress, with different characteristics were analysed and subjected to a non-steady state migration test according to NT Build 492. After the non-steady state migration test, the chloride penetration depth and the migration coefficient were determined and based on the obtained values, the influence of different parameters such as: exposed surface to chloride solution, rebar position and influence of cracks on chloride ingress was studied. Further more, the possible effect of carbonation on chloride penetration was taken into consideration. Based on this study, the following conclusions can be drawn:

- Chloride penetration is affected by the characteristics of the concrete on the exposed surface. The surface layer of concrete affects the transport characteristics of the material and can enhance the chloride ingress.
- No significant conclusions could be drawn regarding the influence of rebars on chlorde ingress.
- The presence of cracks has a significant influence on chloride ingress, increasing it.
- It appears that carbonation pushes the chloride front and decreases significantly the chloride concentration. Still, a more complex study must be performed in order to have a better image on the influence of carbonation on chloride ingress.
- Still, based on the existent information, the statistical analysis was realized in order to investigate the possible influence of crack width on chloride ingress.

Even though having a limited number of replicas, a statistical analysis was realized in order to investigate the possible influence of crack width on chloride ingress. Also, the influence of the exposed surface, the presence of cracks and the existence of rebars was once again investigated. It must be noted that the statistical analyse was performed by using the following methods: comparison of means, comparison of standard deviation and analysis of variance (ANOVA) at a 95% confidence level. The following conclusions can be drawn from this study:

- Chloride penetration depth is statistically significant influenced by the exposed surface when taking into consideration all samples, but also when considering its influence on particular sample categories (S- samples without cracks and rebars, SC- samples with cracks and without rebars, SR- samples without cracks and with rebars and SCR- samples with cracks and rebars).
- Chloride penetration depth near the crack is statistically significant influenced by the existence of cracks.
- No statistically significant influence of the crack width on chloride ingress was determined within the available data.
- The combined effect of the exposed surface and the presence of rebars has a statistically significant influence on chloride diffusion.

4. NUMERICAL APPROACH

4.1. Overview of numerical simulation

After completing the experimental part, sufficient information was obtained in order to continue with the numerical analysis consisting in creating a model that can realistically simulate chloride penetration in cracked reinforced concrete.

As earlier mentioned, three steps must be taken into consideration when simulating chloride transport in cracked concrete: creating the geometry of the crack, determining the chloride transport behaviour and determining the numerical method to simulate chloride ingress.

In order to determine the most appropriate numerical method, prior to simulating chloride ingress in the cracked samples considered in the present research, preliminary investigations were made on mortar samples with notches where chloride transport was simulated using the Abaqus/Standard software based on the FEM using the mass diffusion tool. Due to the fact that the numerical results obtained using the FEM were in good agreement with the experimental ones, the numerical method taken into consideration is considered to be a good tool for simulating chloride transport in concrete and is further used in the present research.

Based on the geometry characteristics of the samples, previously determined in **Section 3.3**, 3D representations of type SC and SCR samples were realized in order to have a better view of the crack orientation and positioning, respectively of the rebars inside the samples. These representations were also taken in consideration when determining the geometry of the model considered in the numerical simulations.

Parameters such as: the diffusion coefficient D, initial chloride concentration c and applied chloride concentration C, determined from the experimental part were used as simulation parameters.

Initially, chloride penetration was simulated in reference samples, on cylinders with 100 mm diameter and 50 mm thickness, in accordance with the reference samples used in the experimental part; the obtained numerical results were compared to the experimental ones and were in good agreement. Afterwards, chloride penetration was simulated on samples with cracks, this time, in order to reduce the size of the model half of cylinder was modelled; the obtained numerical results were compared to the experimental ones and were in good agreement.

A schematic overview of the numerical approach is presented in Figure 4.1.

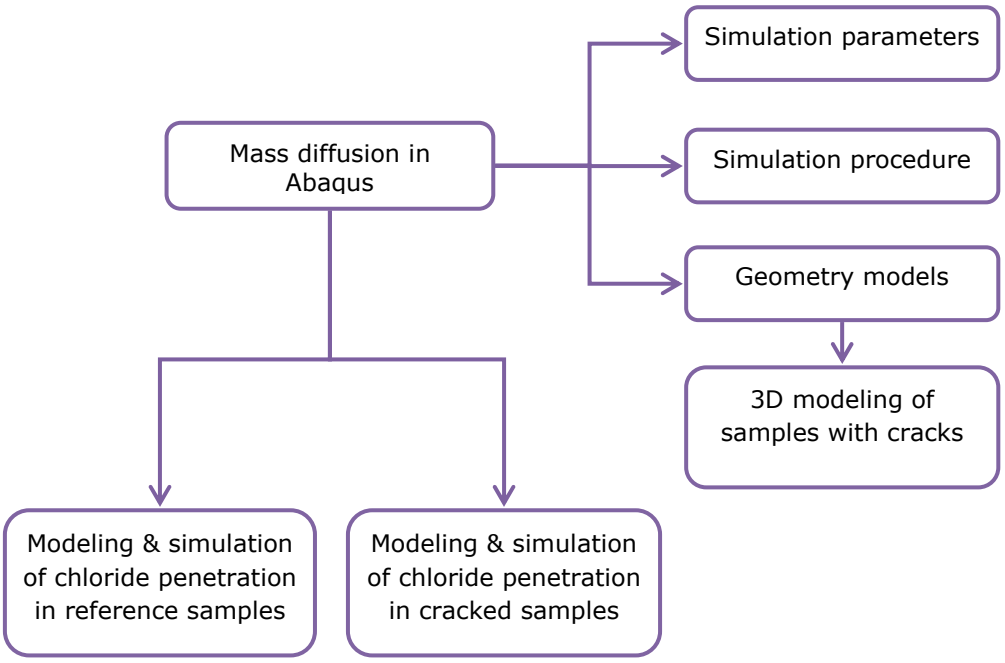

Figure 4.1. Schematic overview of the numerical approach

4.2. Background of the numerical analysis

As previously presented in Section 2.7, a considerable number of numerical models were proposed in order to simulate chloride ingress so that the initiation of chloride-induced corrosion and its consequences of RC structures could be better understood and controlled. Still, even though these studies consider concrete at various levels of complexity, the geometric characteristics of real cracks are disregarded, most of the studies consider the cracks to be rectangular, while very limited research is focused on developing models with a realistic crack design.

In the following, two of these models which consider a realistic crack design are presented: the model developed by (Lu, 2012) and the model developed by (Savija, 2014).

In his study, (Lu, 2012) developed a model predicting the chloride diffusion profile in cracked concrete while considering the real microstructure including cement paste, voids and aggregates. He used a 3D image-based microstructure simulation procedure in order to model the chloride ingress in cracked mortar. In his study the COMSOL Multiphysics package was used in order to have a better understanding of diffusion and binding (reaction) in cracked concrete. In the simulations, two different 3D microstructures with cracks were used: a 3D X-ray CT image-based measured mortar microstructure and a 3D virtual microstructure created using a spherical harmonic analysis-based approach (Garboczi, 2002). The microstructure study focused on concrete composed of a matrix of cement paste (hydrated cement), sand and gravel inclusions (aggregates) and voids. The crack

was made by inserting a stainless steel shim into the casting specimen from the top, and then pulling it out after final set of the mortar has occurred. These 3D models and a schematic representation of their development are presented in Figure 4.2 and Figure 4.3. Both of these 3D image-based microstructures were converted into a FE mesh and then a 3D mesh representing the true multiphase microstructure was written as Nastran mesh and imported into the COMSOL Multiphysics package so that the influence of cracking on chloride diffusion with binding could be examined.

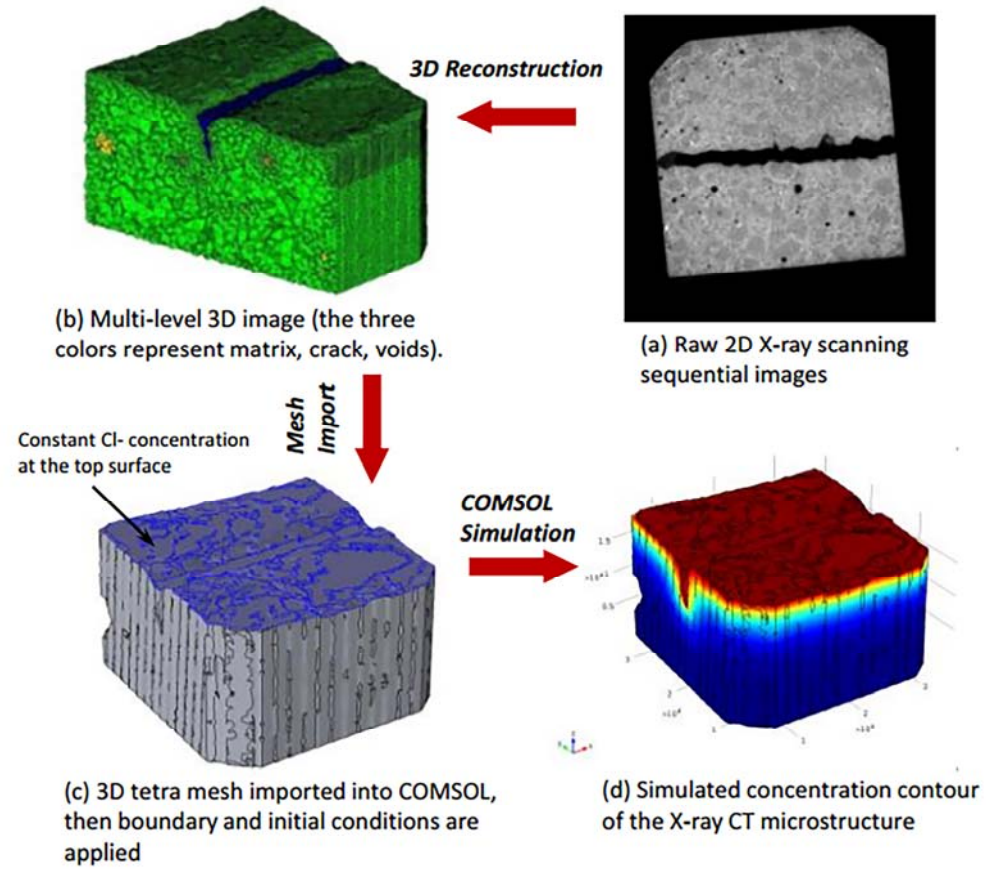

Figure 4.2. 3D dimensional diffusion and binding simulation procedure with an X-ray microtomography image set (Lu, 2012)

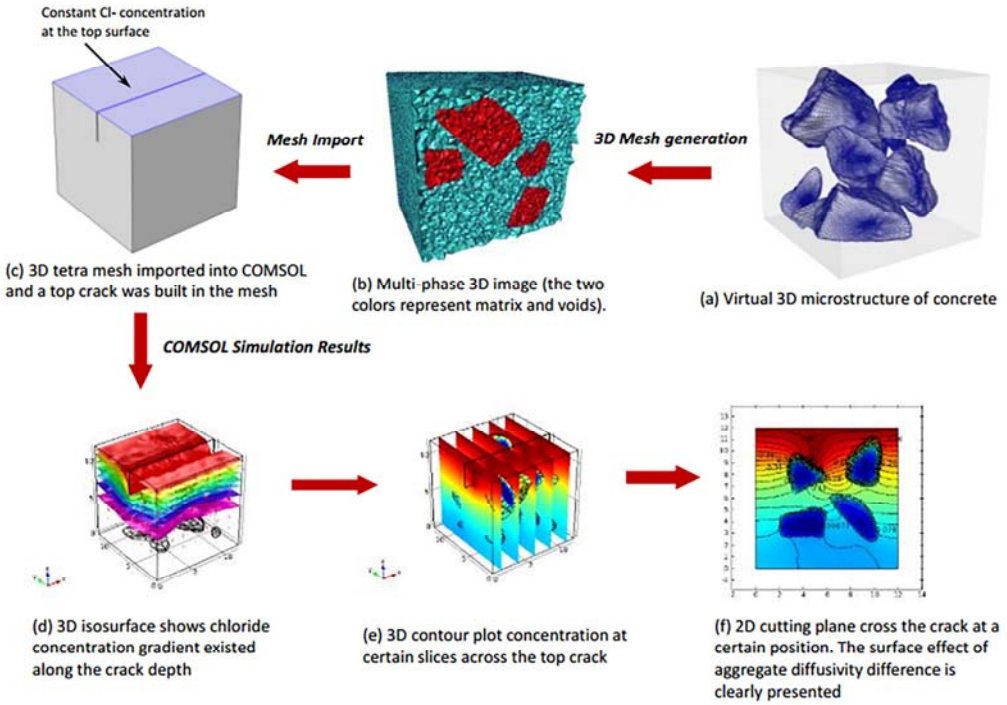

Figure 4.3. 3D virtual concrete simulation made by real aggregares represented in spherical harmonic analysis (Lu, 2012)

Also, an experimental ponding test was performed, exposing a mortar specimen for 30 days into a salt solution at a constant concentration. An epoxy layer was coated on all surfaces except the top surface in order to block chloride penetration from bottom and side surfaces. For the purpose of validation, when the chloride ponding test finished, a micro X-ray fluorescence test was performed (μXRF) to measure the chloride concentration profile on the mortar samples. Figure 4.4. presents a comparison between the experimental results obtained using the μXRF technique and the 2D chloride ingress simulation. The considered surface is 25 mm wide and 17 mm high. The experimental results were then compared with the numerical ones so that the 3D X-ray CT image-based microstructure is used to study the crack effect on chloride transport. Virtual lines located at different values on the sample's surface were made to plot the simulation results.

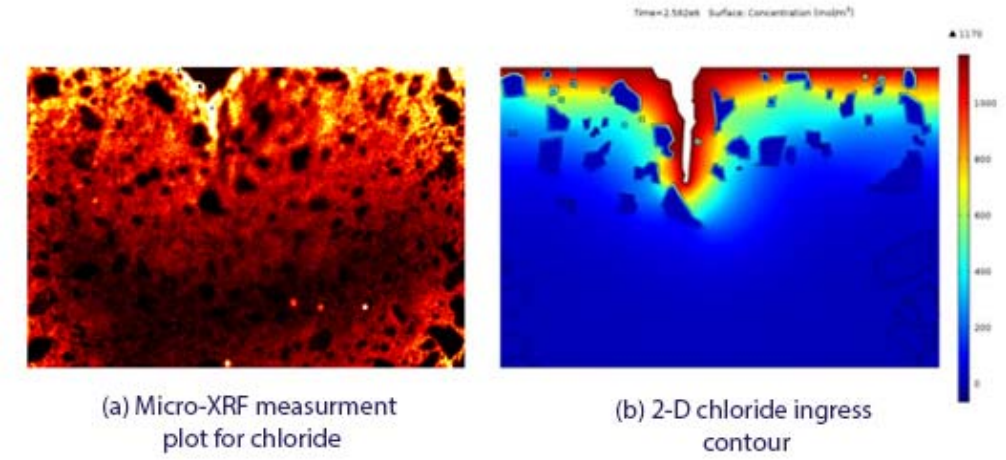

Figure 4.4. μXRF measurement result of chloride concentration contour plot and the 2D chloride ingress simulation contour comparison (Lu, 2012)

A concentration contour plot of 3D X-ray CT image based model at 30 days is presented in Figure 4.5. Due to the fact that the constant concentration boundary condition was applied on the top surface, there is a higher concentration in the upper part and a lower value at the bottom. In order the see the influence of the crack on the concentration profile, cut surfaces transverse to the crack length are presented (Figure 4.6).

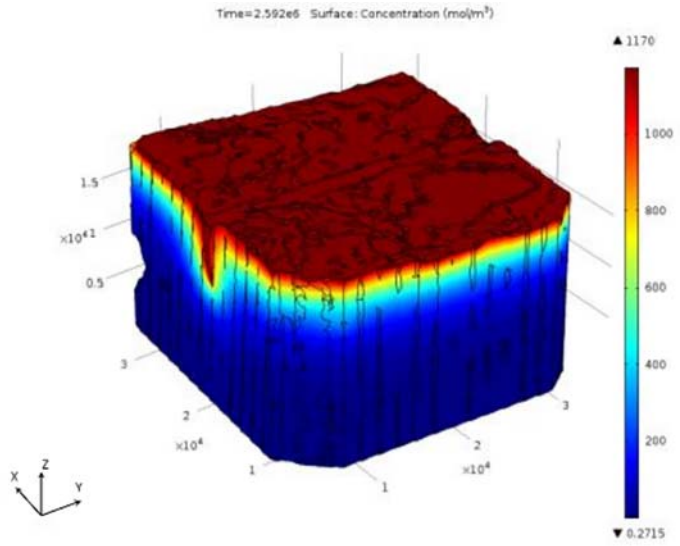

Figure 4.5. Concentration contour plot of 3D X-ray image-based model at 30 days (Lu, 2012)

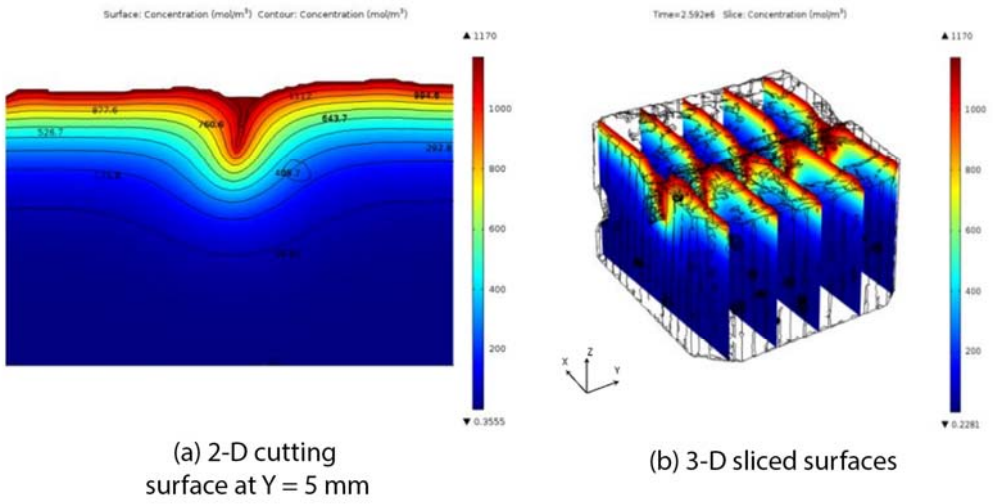

Figure 4.6. Concentration contour plot of 3D X-ray image-based concrete model simulation result at 30 days (Lu, 2012)

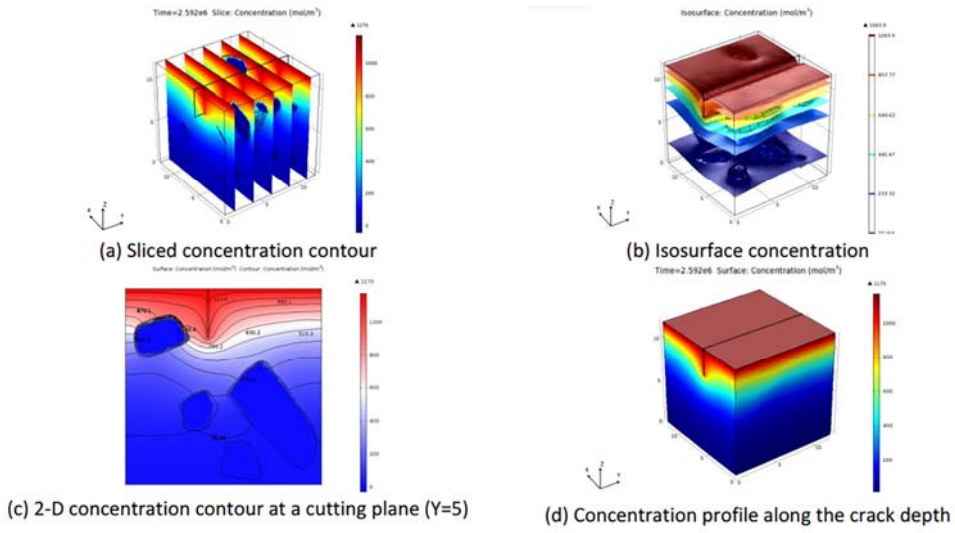

Figure 4.7. Concentration contours of 3D virtual concrete model simulation result, shown in sliced contour, isosurface and 2D cutting surface and overall profile (Lu, 2012)

In order to explore the diffusivity difference between aggregate and cement paste, the virtual concrete microstructure was also simulated in the COSMOL Multiphysics package. A smaller diffusivity value was given to the aggregate, while a much larger value was used in the mortar matrix. The same as in the X-ray CT

microstructure, a constant concentration boundary condition was applied on the top surface. Figure 4.7 presents the concentration contour of 3D virtual concrete model simulation result, shown in sliced contour, isosurface concentration and overall profile. It can be observed that the chloride concentration changes at the aggregate surface. It can also be seen that the presence of crack leads to a quick ingress channel of saturated chloride solution.

It can be concluded that both X-ray CT image-based and spherical harmonic based microstructures were successfully applied to build realistic heterogeneous cracked concrete models in which chloride ingress was accurately simulated using the COSMOL Multiphysics package. It was observed that the existence of cracks has an accelerating effect on chloride diffusion in concrete, while binding generally retards the chloride penetration.

In his study, (Savija, 2014) uses a coupled analysis consisting of a mechanical analysis followed by the chloride transport analysis, based on the lattice model, in order to study the transport in heterogeneous concrete and also to simulate chloride migration in cracked concrete. Two lattice models are used: the fracture lattice model also known as the Delft lattice model (Schlangen, 1993) and the transport lattice model. Coupling of mechanical and transport analysis is as follows: first, the fracture simulation is performed and its output is then used as an input for the transport simulation. In the fracture lattice approach, the material is discretized as a set of truss or beam elements. For transport simulations, the material is treated as a set of one-dimensional pipe elements (sometimes called conduit elements), through which the transport takes place.

Figure 4.8 presents the mechanism for spatial discretization in 3D: first a prismatic domain is described, which is first divided into a number of cubic cells and then a sub-cell is defined in the center of each cell. Within each sub-cell a node is randomly placed using a pseudo-random number generator. Then, a Voronoi tessellation of the domain is performed with the generated set of nodes. Nodes with adjacent Voronoi cells are connected by lattice elements.

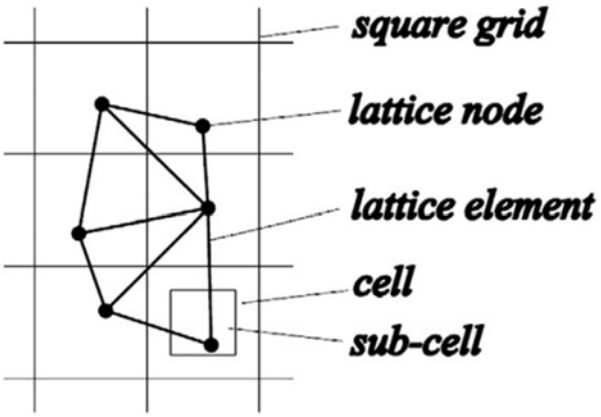

Figure 4.8. Node placement procedure in two-dimensions (Savija, 2014)

The degree of randomness built in the lattice is controlled by the ratio between the sub-cell and the cell size. Heterogeneous material behavior can be considered by employing the particle overlay procedure (Figure 4.9). This way, different mechanical or transport properties can be assigned to different material

phases. As an input, either a computer generated material structure or a material structure obtained by scanning (2D) or CT-scanning (3D) can be used. Each node in the mesh is assigned with a pixel/ voxel value (2D and 3D, respectively) from the used material structure. Properties assigned to each element depend on the pixel/voxel value at its end nodes.

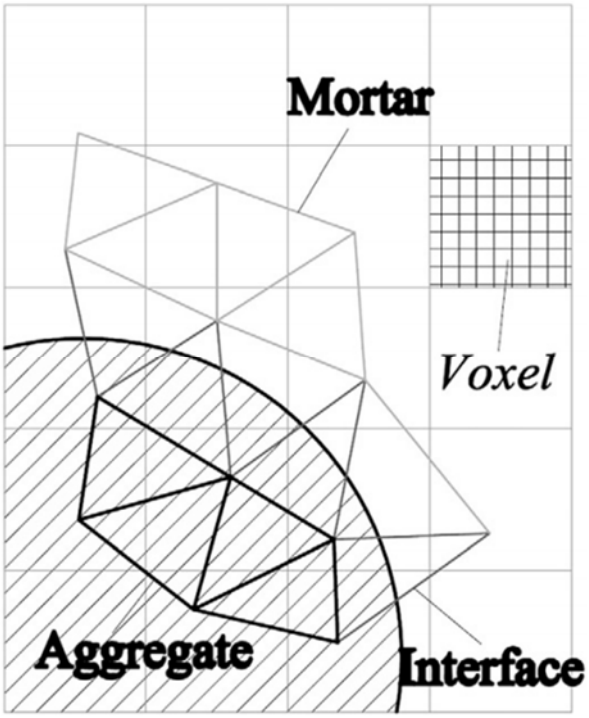

Figure 4.9. Particle overlay procedure in two dimensions (Savija, 2014)

In the Delft lattice model, the material structure is discretized as an assembly of beam elements and the fracture simulation is achieved by performing a linear elastic analysis of the lattice under loading and removing an element which exceeds a prescribed fracture criterion. In the chloride migration model, concrete is discretized as a set of one-dimensional "pipe" elements through which chlorid transport takes place. The governing equation is used to model chloride ion diffusion under the action of an electrical field (Tang, 1993).

As earlier mentioned, a coupled analysis is performed. A material structure with about 60% of circular aggregates was generated and a lattice cell size of 0.125 mm was projected on top of it and mechanical and transport properties were assigned to each phase using the particle overlay-procedure. Cracking is induced by exposing the bottom surface of the numerical specimen to splitting; the left half is subjected to displacement to the left and the right half to displacement to the right. A crack forms in the middle of the bottom surface. The cracked specimen is then subjected to an RCM test with 25 V applied for 6 hours. A surface concentration C_0=

2.2045 kg/m^3 was applied for the exposed surface and cracks wider than 12 μm. The results are shown in Figure 4.10.

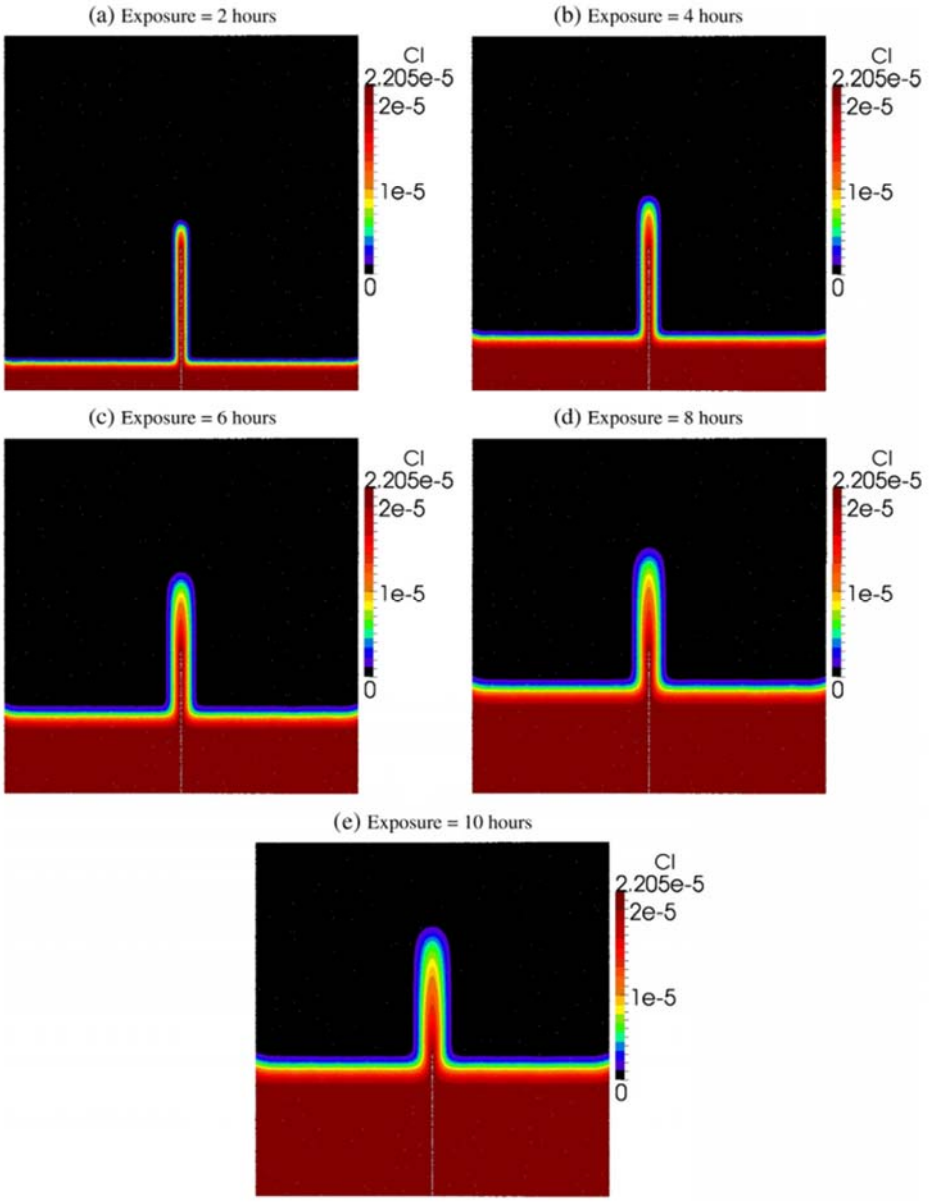

Figure 4.10. Chloride ion distribution for different crack widths (only cracks wider than 12 μm are depicted on the left hand side) (Savija, 2014)

It can be concluded that the model can successfully reproduce the analytical solution of the governing equation. Also, the heterogeneous nature of concrete

causes deviation from the theoretical migration profile by taking into account the tortuosity of concrete. As expected, cracks cause a sharp increase in penetration in front of the defect.

4.3. Preliminary state: mass diffusion in Abaqus

It must be noted that the results presented in this subchapter are a part of the study previously presented in (Sosdean, 2015). As earlier mentioned, the influence of artificial cracks on chloride penetration was studied both experimentally and numerically. The experimental results were obtained using chloride penetration tests on mortar specimens with different mortar compositions, with and without artificial cracks subjected to chloride exposure. Numerical results were obtained using transient FE analysis by simulating chloride mass diffusion. Comparisons between experimental and numerical results are in good agreement.

It has to be specified that in the present work, the emphasis is on the numerical part, while the experimental part is briefly presented; more details about the experimental part can be found in (Sosdean, 2015). Mortar specimens of size 40 mm x 40 mm x 160 mm, with six different mortar compositions, in which artificial cracks/notches with different widths and depths were induced using the notch method (De Schutter, 1999; Marsavina, 2009), were subjected to chloride diffusion while being stored in a 3.5% NaCl solution for 28 days. An epoxy coating was applied to all surfaces except the surface containing the crack, to prevent them from chloride ingress. At regular time intervals (8, 12, 16 ….28 weeks), the chloride penetration was examined experimentally in order to determine the depth of the chloride penetration.

4.3.1. Algorithm for solving the mass diffusion equations

In the cracked concrete, the simulation of chloride diffusion is investigated with the Abaqus/Standard software based on the FEM, using the mass diffusion tool (Abaqus Analysis User's Manual, 2010).

The basic solution variable (used as the degree of freedom at the nodes of the mesh) is the "normalized concentration" (often also referred to as the "activity" of the diffusing material), $\phi \stackrel{def}{=} c/s$, c is the mass concentration of the diffusing material and s is the solubility in the base material. Therefore, when the mesh includes dissimilar materials that share nodes, the normalized concentration is continuous across the interface between the different materials.

In Abaqus, mass diffusion can be defined using two methods: the general chemical potential, or an extended form of Fick's law.

Diffusion is assumed to be driven by the gradient of a general chemical potential, which gives the behavior:

$$J = -sD \cdot \left[\frac{\partial \theta}{\partial x} + k_s \frac{\partial}{\partial x}\left(ln\left(\theta - \theta^z \right) \right) + k_p \frac{\partial p}{\partial x} \right] \tag{4.1}$$

where D(c, θ, f) is the diffusivity; s(θ, f) is the solubility; k_s(c, θ, f) is the "Soret effect" factor, providing diffusion because of temperature gradient; θ is the temperature; θ^Z is the absolute zero on the temperature scale used; k_p(c, θ, f) is the pressure stress factor, providing diffusion driven by the gradient of the equivalent pressure stress, $p \stackrel{def}{=}$ - trace(σ)/3; σ is stress; and f are any predefined

field variables. The Sorret effect factor and the pressure stress factor can be defined optionally to introduce mass diffusion caused by temperature and pressure gradients, respectively.

Since mass diffusion behaviour is often described by Fick's law:

$$J = -D\frac{\partial C}{\partial x} \tag{4.2}$$

Fick's law is offered in Abaqus/Standard as a special case of the general chemical potential relation. In the present study, mass diffusion was simulated using the general chemical potential option, in which the Sorret effect and the pressure stress factor were not taken into consideration and also the solubility coefficient was considered unity. Also, due to the fact that the model simulates chloride diffusion using a concentration dependent diffusion coefficient within the case of one-dimensional diffusion and there are no chlorides initially present, no chloride binding is considered in the model.

4.3.2. Modeling of mass diffusion in Abaqus

Six geometries were considered according to (Table 4.1). Plane 2D - 8 node quadratic elements were used for the mesh. A convergence study was carried out in order to determine the proper mesh density, and the element size of 0.1 mm × 0.1 mm was considered acceptable. The total number of elements and nodes for the six studied geometries are presented in (Table 4.1).

Table 4.1. Geometries and mesh parameters for numerical calculations

Geometries	Crack dimensions		Mesh parameters	
	Depth (mm)	Width (mm)	Number of elements	Number of nodes
I	0	0	160000	481601
II	5	0.2	159900	481401
III	5	0.3	159850	481301
IV	5	0.5	159750	480951
V	10	0.3	159700	480901
VI	10	0.5	159500	480301

The boundary conditions which have been applied are presented in (Figure 4.11).

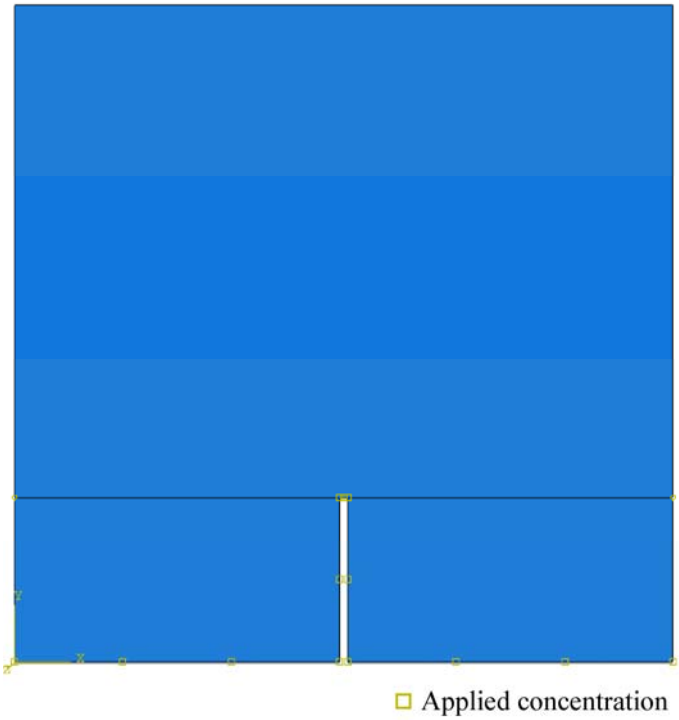

Figure 4.11. Applied boundary conditions

The boundary conditions were applied on the model as follows: the total chloride concentration was applied only on the cracked edges and on the edges of the crack; the un-cracked edges being considered insulated (0 flux), this being the default boundary condition in ABAQUS for mass diffusion. For the 3,5 % NaCl solution that was used in the experiments, a concentration of 21.23 ppm was applied (Figure 4.12).

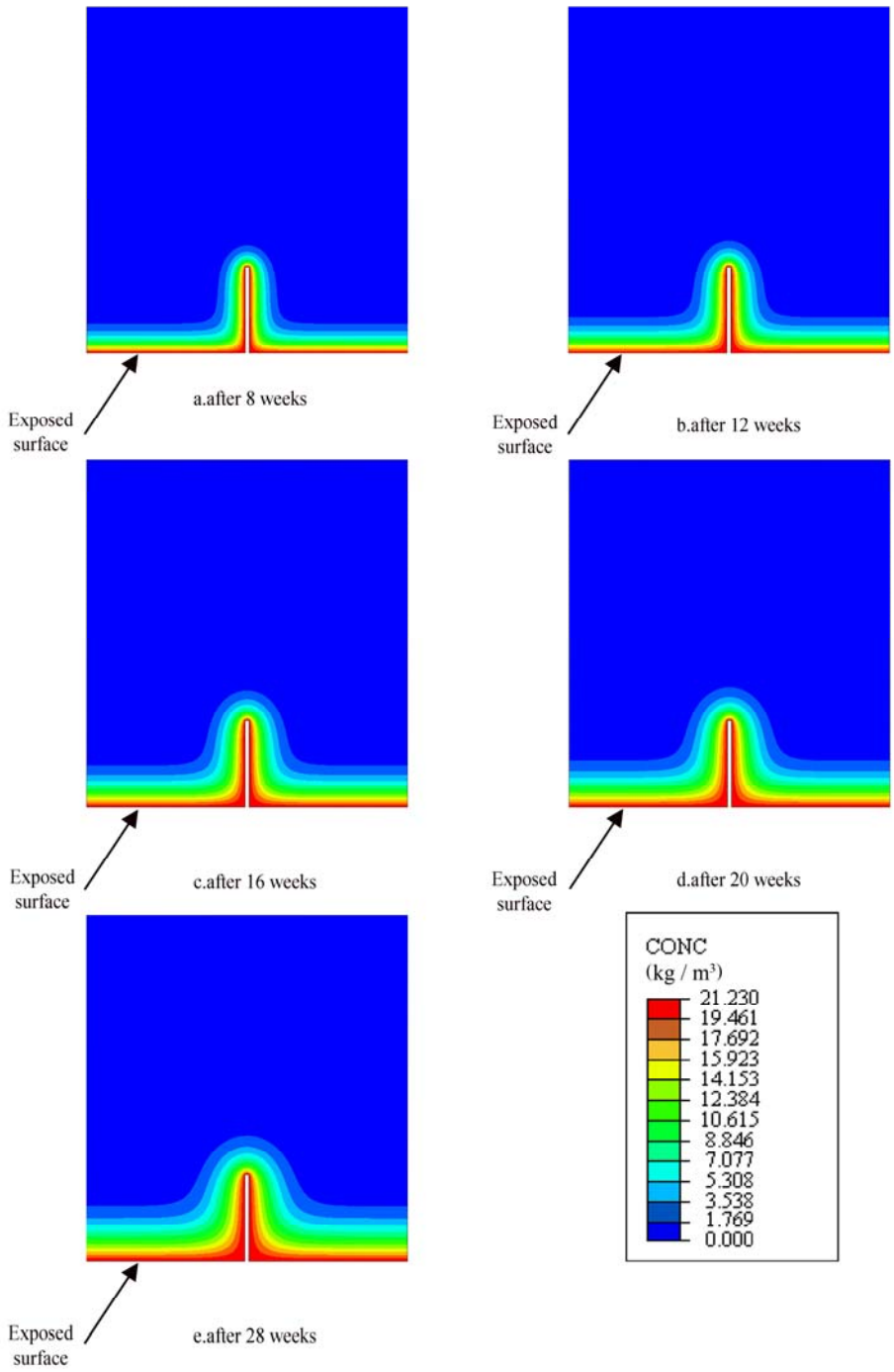

Figure 4.12. Chloride concentration distribution

Previous studies conducted by (Djerbi et al., 2008) concluded that the diffusion coefficient in crack was increasing linearly with the increasing of crack width from 30 to 80 μm, but was almost constant when the crack width was approximately 80 μm or more. In their studies, (Savija, 2013) used the equation presented below in order to simulate the diffusion process in the crack and in the cracked concrete using effective diffusion coefficients for different crack widths:

$D_{cr}=2\times10^{-11}\cdot w-4\times10^{-10}$ (m^2/s) for $30\mu m\leq w<80\mu m$ (4.3)

$D_{cr}=1.4\times10^{-9}$ (m^2/s) for $w\geq80\mu m$. (4.4)

It seems that only when dealing with cracks between 30μm and 80 μm the crack width influences the transport mechanism of chlorides. If the crack width is bigger than 80 μm the crack width has no significant effect on the chloride transport process in cracked concrete and the chloride diffusion coefficient is not influenced by the crack width and cracks behave like the exposed concrete surface. Based on the studies presented above, and considering that the present research deals with crack widths higher than 80 μm, a constant value for the diffusion coefficient (Table 4.2) was used as material property for the whole model.

Tabel 4.2. Diffusivity constants and the total chloride concentration

Series	Cement	Diffusivity constant [10^{-12} m/s^2]	Total Chloride Concentration [kg/m^3]
1	CEM I 42.5 R, 1 part	0.57	15.63
2	CEM III/B 32.5 HSR LA, 1 part	0.65	15.75
3	CEM V/A 32.5, 1 part	0.78	15.68
4	CEM I 42.5 R, 0.85 part	0.78	15.63
5	CEM III/B 32.5 HSR LA	0.81	15.75
6	CEM I 42.5 R, 0.9 part	0.40	15.63

The values for the diffusivity constants and for the total chloride concentration are shown in (Table 4.2) for the 6 considered mortar compositions. These values were determined experimentally from the diffusion tests on un-notched specimens.

A linear interpolation was applied in order to determine the penetration corresponding to the same concentration that was obtained experimentally by using the silver nitrate solution (1.183 $kgCl^-/m^3$).

Comparisons between experimental and numerical results on chloride penetration are presented in (Figure 4.13) for mortar Series 5.

It seems that even though in the first steps of the simulation, there is a minor discrepancy between the numerical and the experimental results, after 28 weeks, they seem to have the same pattern. However, the numerical results seem to be slightly higher than the experimental ones: 1.76% at the crack tip and 2.85% in the uncracked region. The higher difference is observed at the edge of the specimen, more than 13%, but this can be due to boundary effects in the sample.

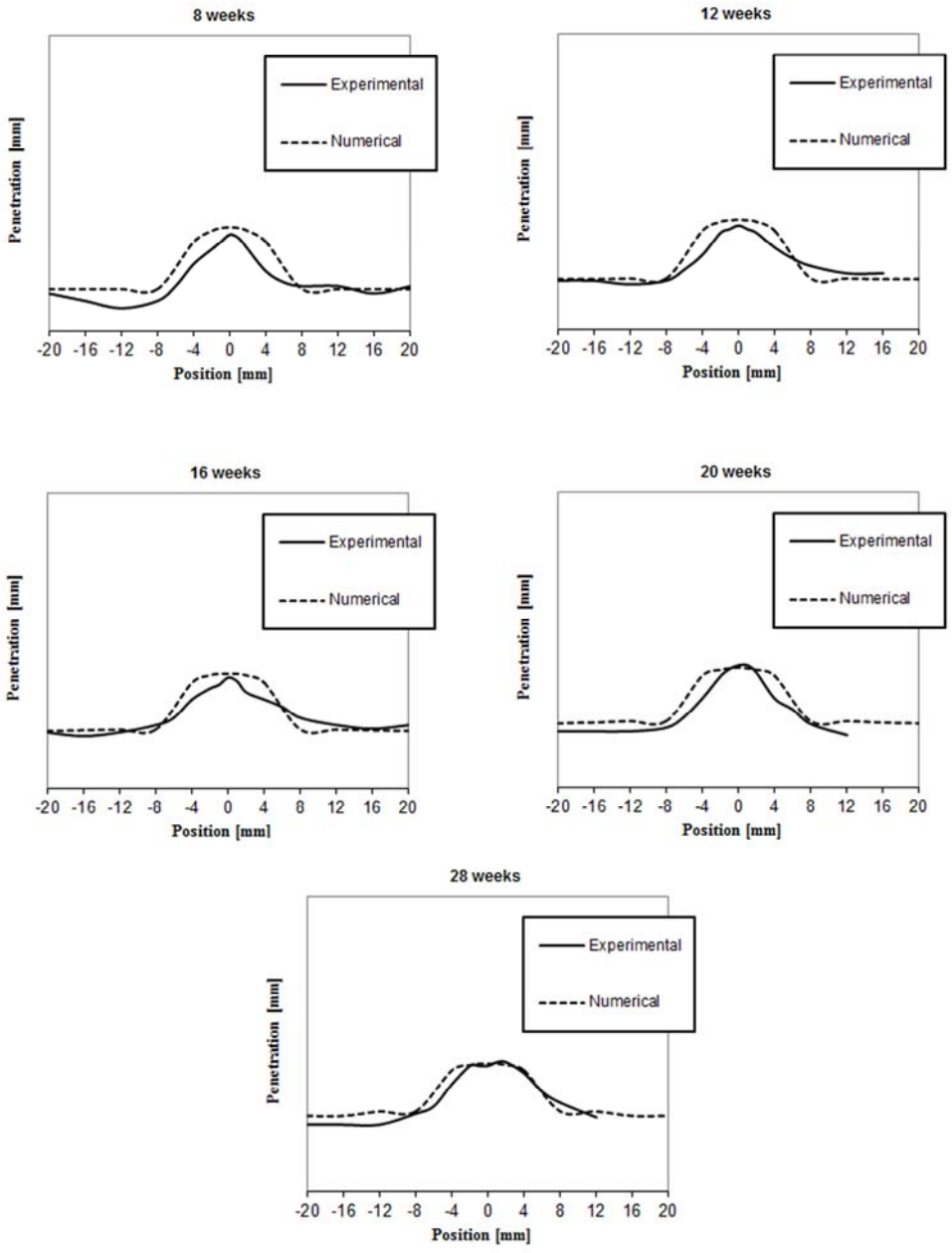

Figure 4.13. Comparison between experimental and numerical results on chloride penetration for notched specimen 10 x 0.5 mm- Series 5.

4.3.3. Results and discussions

In this section, only results related with the present work are presented, such as: the influence of crack width and crack depth on penetration depth and the influence of the diffusion coefficient. Results relating to the exposure time, cement type are presented in (Sosdean, 2015).

4.3.3.1. Influence of crack width on chloride penetration

As earlier mentioned in Section 2.5.1 many studies were focused in determining whether and if crack width affects chloride ingress in concrete. Figure 4.14 and Figure 4.15 show how the chloride front is indeed influenced by the different crack widths. It seems that starting with the first weeks the experimental results show a minor difference between the samples with different crack widths and that the chloride front slightly increases with increasing crack width. Referring to the numerical results, it can be seen that even though the crack widths are different, the results seem to be very similar.

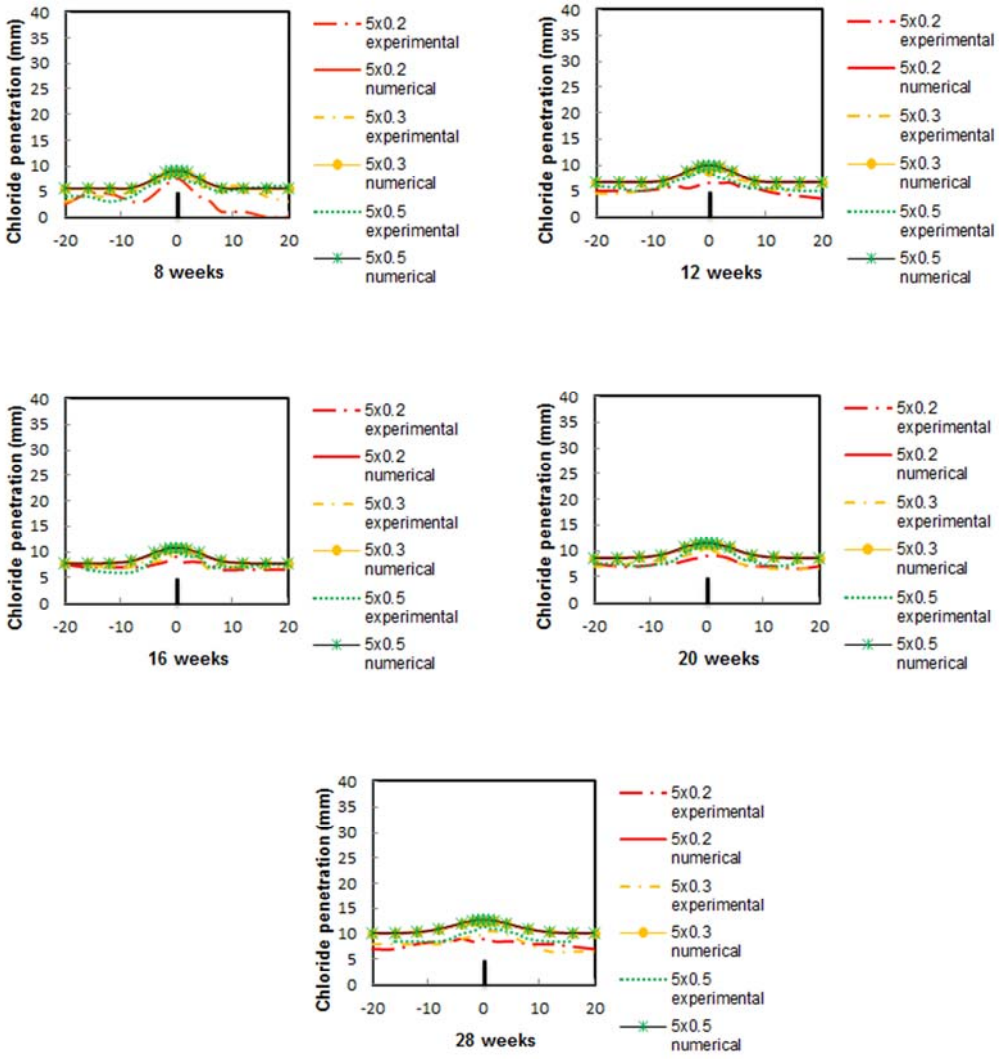

Figure 4.14. Comparisons between different crack widths- 5 mm notch depth

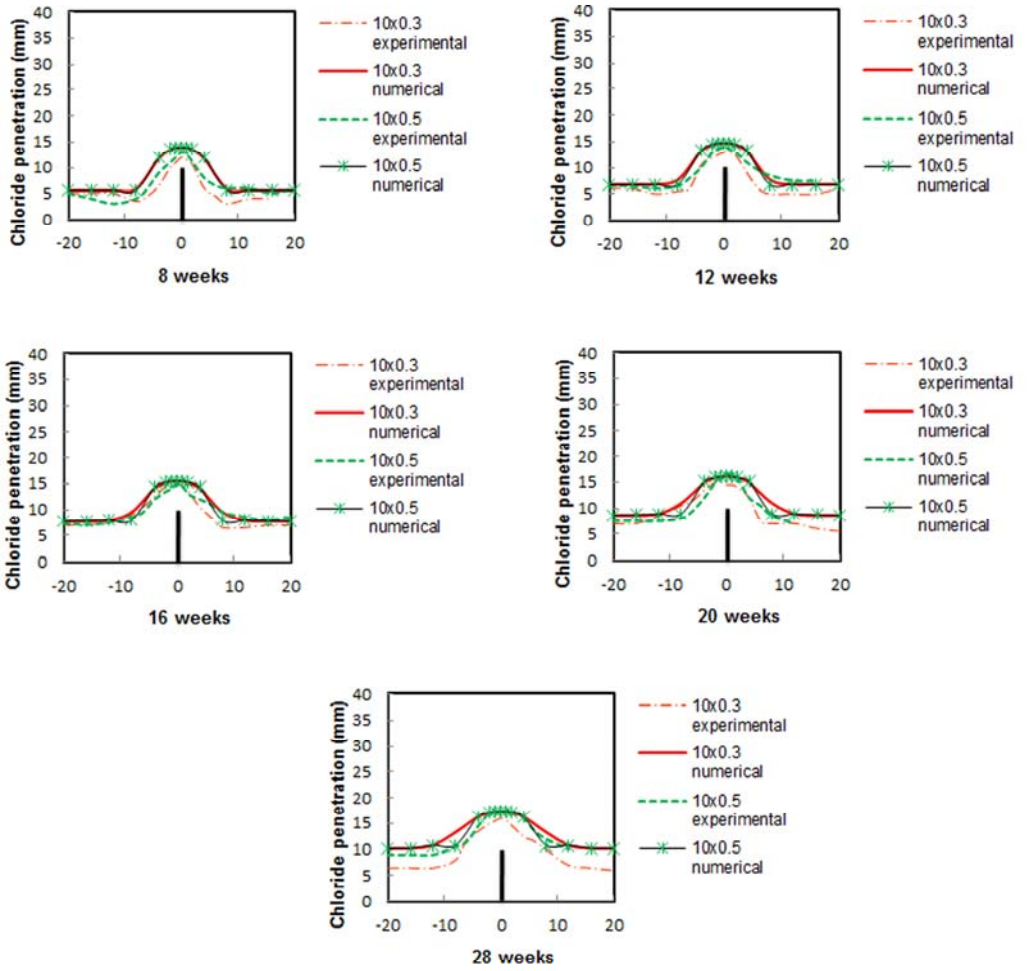

Figure 4.15. Comparisons between different crack widths- 10 mm notch depth

4.3.3.2. Influence of crack depth on chloride penetration

Figure 4.16 and Figure 4.17 show how the chloride front increases with increasing crack depth. It can be observed that the maximum penetration occurs in the region -10 to 10 mm from notch. This is in accordance with (Marsavina, 2009).

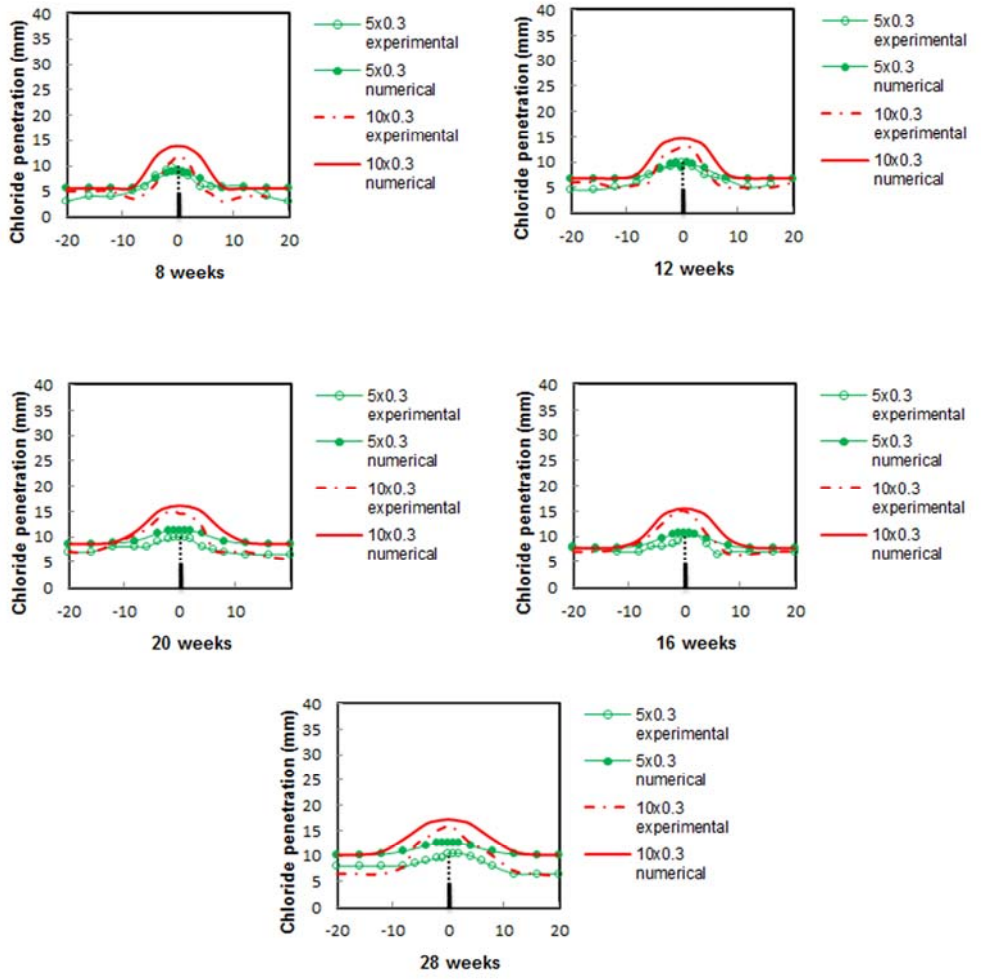

Figure 4.16. Comparison between different crack depths- 0.3 mm crack width

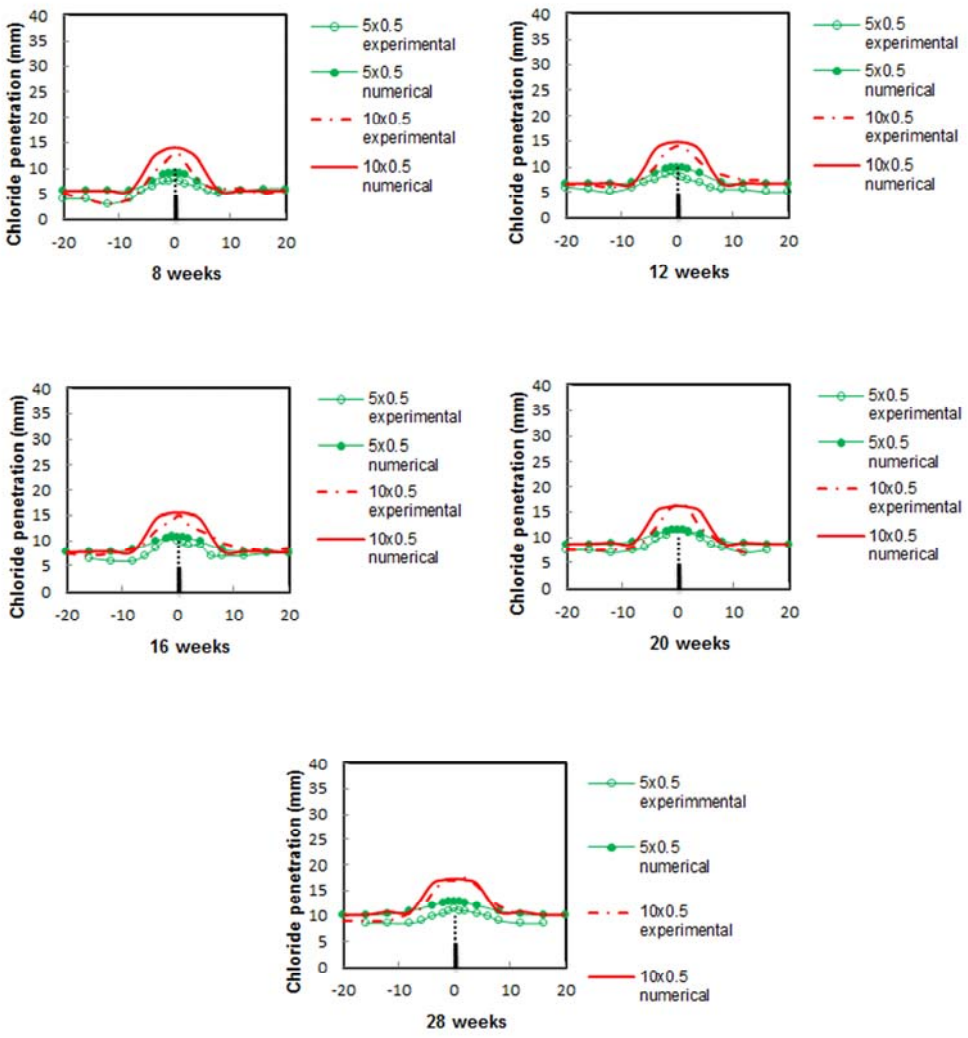

Figure 4.17. Comparison between different crack depths- 0.5 mm crack width

4.3.3.3. Influence of material diffusion coefficients

Starting from the hypothesis that the colorimetric method used to determine the diffusion coefficient is not the most accurate one; simulations have been made in order to see how much influence the increase/decrease with 50% of the initial value of the diffusion coefficient will have on the modelling on chloride ingress. A mean value of the diffusion coefficients of the samples used in the experiment was determined, and simulations were carried out by modeling the crack geometry having 10 mm depth and 0.5 mm width. The chloride profiles show only a 20% difference, even though the diffusion coefficients varied with 50%, Figure 4.18. This

shows that the chloride penetration depth is having a reduced sensitivity to changes in the diffusion coefficient.

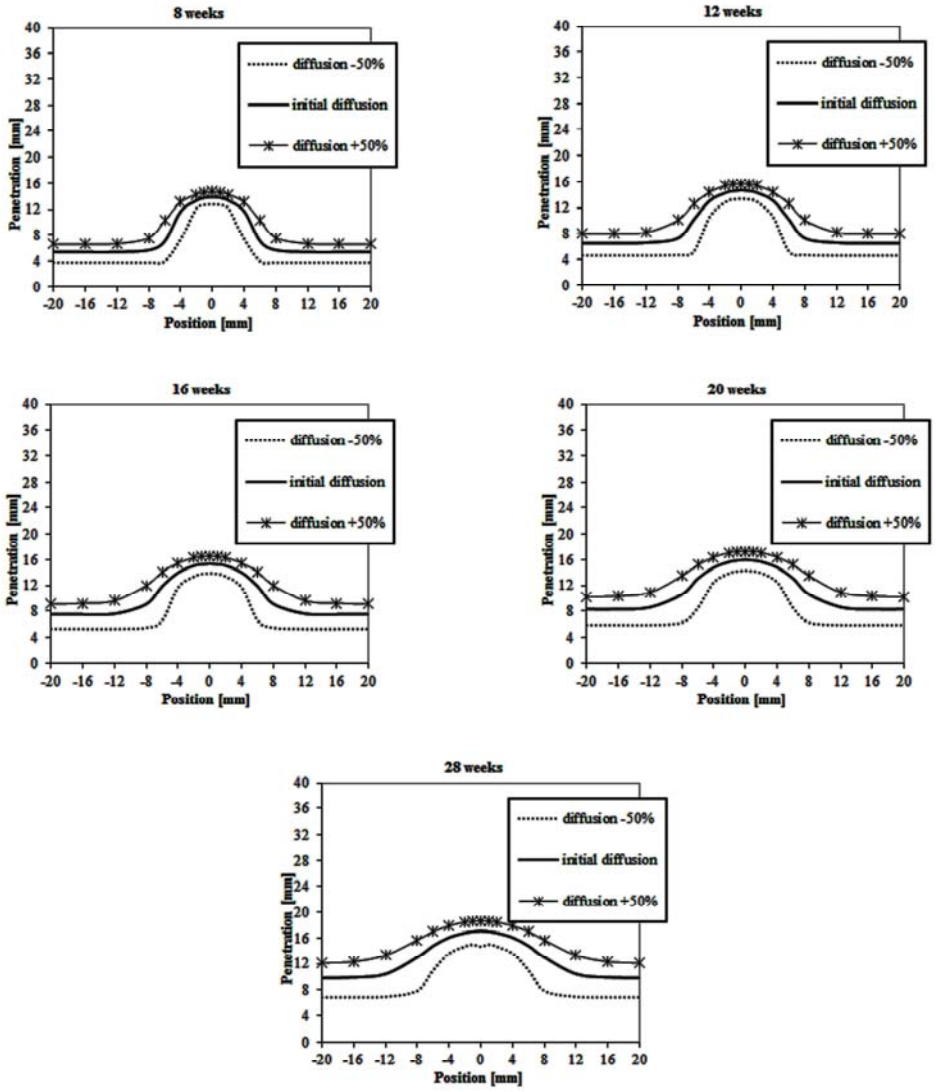

Figure 4.18. Numerical simulation- influence of the diffusion coefficient

4.3.4. Conclusions

In this study, the influence of artificial cracks, notches, with different considered crack widths and depths on the chloride penetration is experimentally

and numerically studied. With regards to the present study, the following conclusions can be drawn: within the parameter range considered the chloride transport property of concrete is not influenced by the considered crack widths, but only by the crack depths. Also, the numerical results obtained by using the FEM are in very good agreement with the experimental ones and it seems that is a good tool for simulating chloride transport in concrete.

4.4. 3D modeling of sample geometries used in the experimental part

Based on the individual geometrical characteristics of each sample, including the crack pattern and rebar position, used in the experimental part and previously described in Section 3.2, respectively Section 3.3, 3D representation of each sample was made. 3D solid cylinders of 100 mm diameter and 50 mm width were modeled in Autocad. Cracks were constructed by taking into consideration their position on the top and bottom of the sample and with regards to their average width, previously presented in Table 4.1. Also, the rebar was positioned in the model, based on the locations obtained when slicing each sample in order to determine the chloride penetration, described in Section 3.3.2. The 3D geometry of Sample 4 is further presented in Figure 4.19. The modeled 3D geometries of all type SC and SCR samples are presented in Appendix 1.

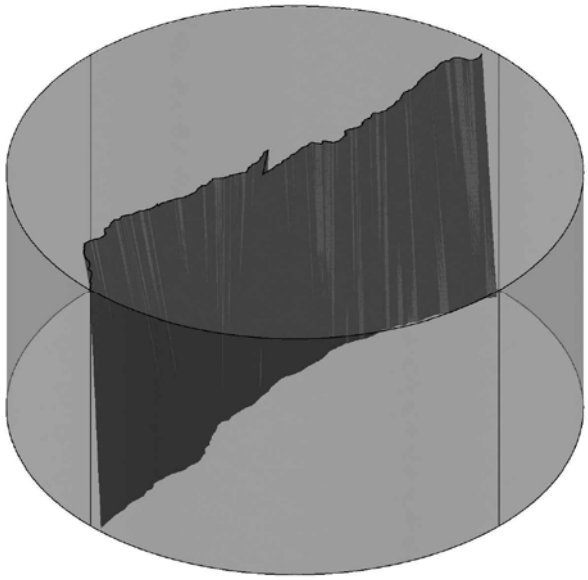

Figure 4.19. 3D representation of Sample 4

4.5. Simulation of chloride penetration in cracked concrete

4.5.1. Simulation of chloride penetration in uncracked concrete

The aim of this study is to simulate chloride ingress in the reference samples type S having the top surface exposed. Three geometries consisting in a cylinder with 100 mm diameter and 50 mm thickness were considered, in accordance with the reference samples used in the experimental part. The mesh was realized using 3D 20- node quadratic elements, each element having the size of 2mm x 2 mm x 2mm. The boundary conditions which have been applied and the chloride concentration distribution are presented in Figure 4.20.

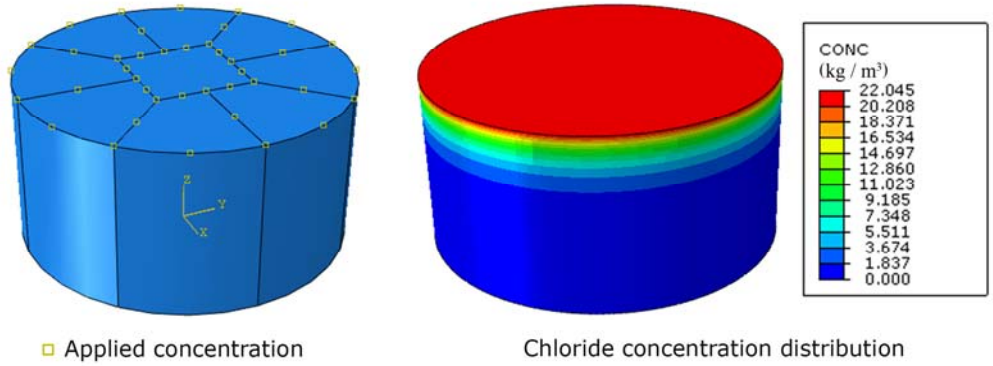

Figure 4.20. Applied boundary conditions and chloride concentration distribution

The boundary conditions were applied on the model as follows: the total chloride concentration was applied on the top surface, corresponding to the top exposed surface in the experiments, while the other surfaces were considered insulated (0 flux), this being the default condition in Abaqus for mass diffusion. For the 10% NaCl solution used in the experiments, a concentration C_{tot} of 22.045 kg/m^3 was applied (Figure 4.20). The values for the diffusivity constants were previously determined experimentally and presented in Table 3.7. The value of the initial chloride concentration of 0.03%, corresponding to c_i= 0.7955 kg/m^3, was also determined experimentally by titration, Section 3.5.4. An exponential interpolation was applied to determine the concentration corresponding to the same concentration that was obtained using the silver nitrate solution (1.70 kg/m^3). Comparisons between experimental and numerical results on chloride penetration are further presented in Figure 4.21. It can be seen that the numerical results are in good agreement with the experimental ones.

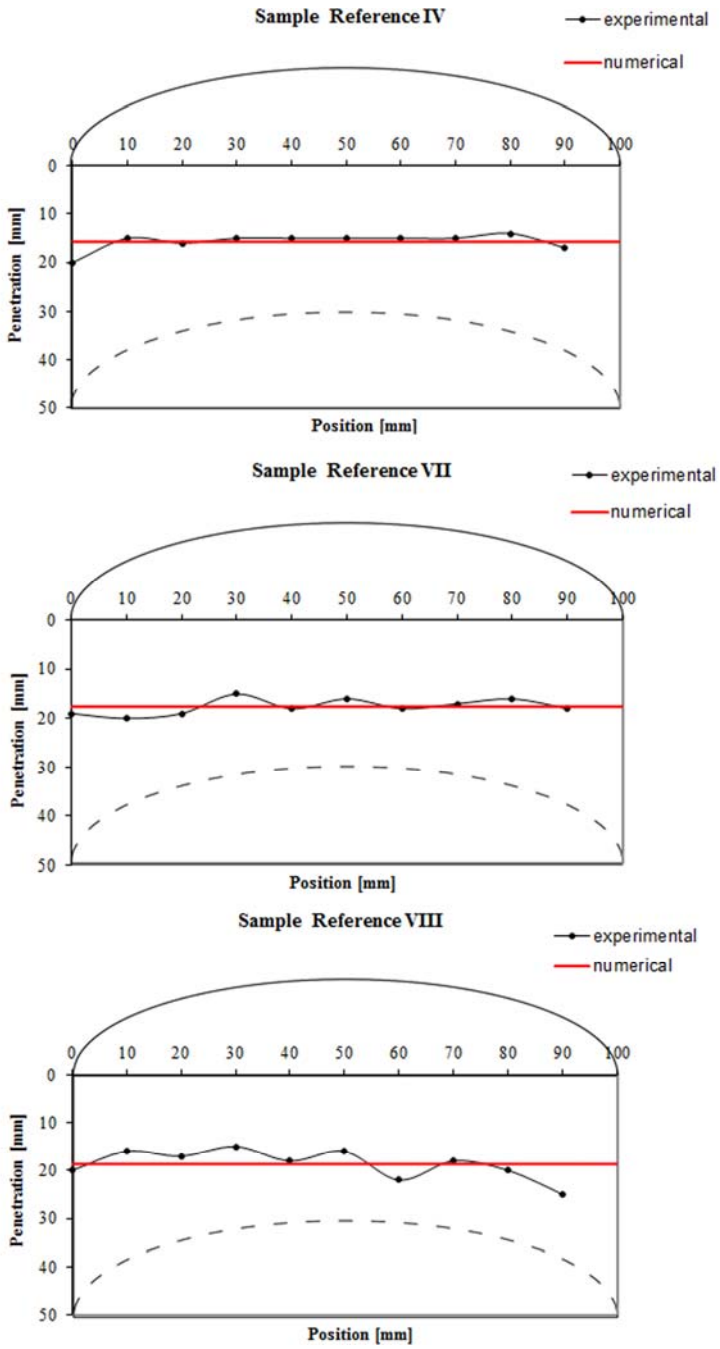

Figure 4.21. Comparison between experimental and numerical results for reference samples type S having the top surface exposed

4.5.2. Simulation of chloride penetration in cracked concrete

Following the same procedure previously presented, chloride ingress is simulated in cracked type SR, Sample 4. This time, the geometry consists in a disc, which is actually half the cylinder of 100 mm diameter and 50 mm thickness previously presented. This simplification was made due to the fact that it could be observed that the crack passes right through the middle of the sample.

It can be obesrved that the disc is divided to 6 parts, this being in accordance to the cutting planes used in the experimental part, in order to determine the chloride penetration on each of these parts. The mesh also consists in 3D 20- node quadratic elements, each element having the size of 2mm x 2 mm x 2mm. The boundary conditions which have been applied are presented in Figure 4.22. The boundary conditions were applied on the model as follows: the total chloride concentration was applied on the top surface and the left surface, which repreesents the crack edge. The same concentration is applied on both the top surface and the left surface which is considered to be the crack edge, due to the fact that in the present study it was concluded that the considered transecting cracks behave like a free concrete surface exposed to chloride ingress. The same conclusion was found in the study of (Rodriguez, 2001).

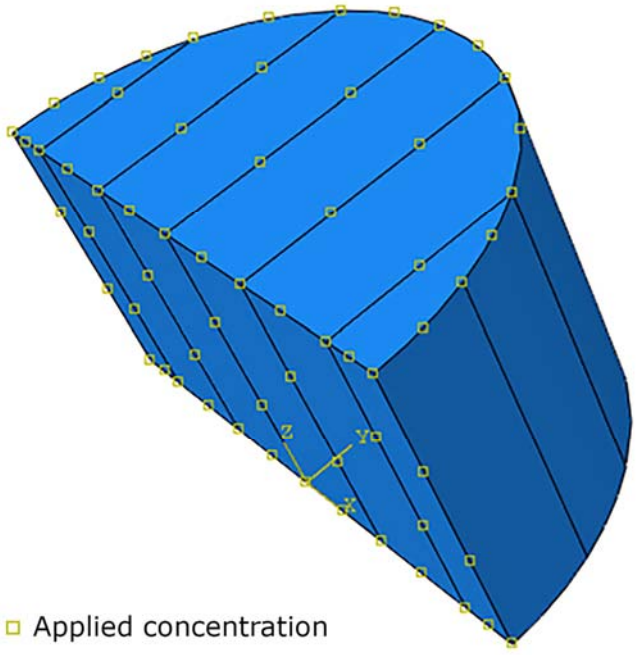

Figure 4.22. Applied boundary conditions

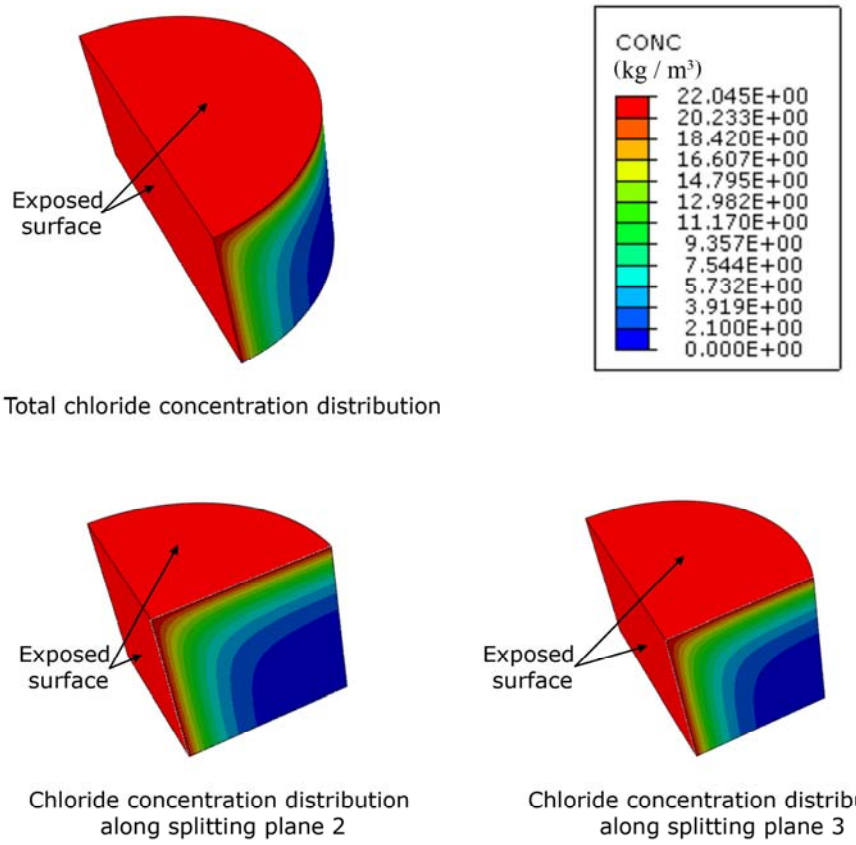

Figure 4.23. Chloride concentration distribution

For the 10% NaCl solution used in the experiments, a concentration C_{tot} of 22.045 kg/m^3 was applied (Figure 4.23). The value of the diffusivity constant is D= 6.1 x 10^{-12} m/s^2, the medium value of the three diffusion coefficient values, determined in the non-steady state migration test on reference samples type S, and previously presented in Section 5.5.1. The same value of c_i= 0.7955 kg/m^3, was considered the initial chloride concentration. A polynomial interpolation was applied to determine the concentration corresponding to the same concentration that was obtained using the silver nitrate solution (1.70 kg/m^3). Comparisons between experimental and numerical results on chloride penetration are further presented in Figure 4.23.

The simulation time was calculated with equation (2.3), based on the diffusion coefficient and the mean penetration experimentally obtained.

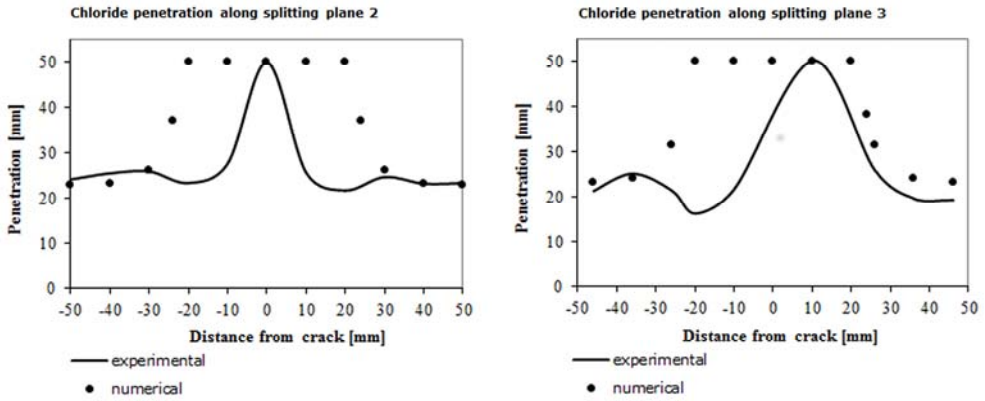

Figure 4.24. Comparison between experimental and numerical results

It can be seen that the numerical results are in good agreement with the experimental ones.

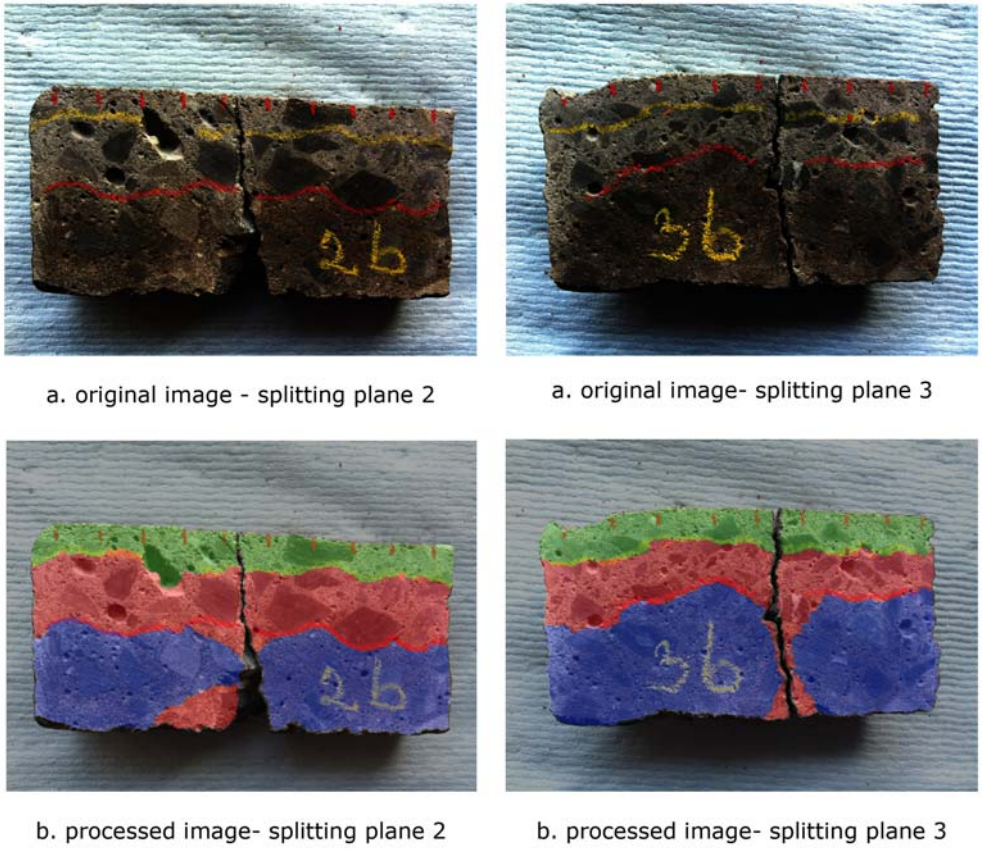

Figure 4.25. Chloride ingress along Sample 4- splitting planes 2 and 3

Figure 4.25 presents the chloride penetration on sample 4, along splitting planes 2 and 3. The 2D effect of the diffusion can be observed, even though the presence of aggregates interrupts further chloride penetration.

4.6. Summary and conclusions

In this chapter, a numerical model that can realistically simulate chloride ingress in cracked concrete was presented. Experimental results were compared to numerical results in order to validate the model. Parameters such as: the diffusion coefficient D, initial chloride concentration c and applied chloride concentration C, were determined experimentally and were used as simulation parameters.

Initially, a 2D model was developed to simulate chloride transport on mortar samples with artificial cracks (notches), with different widths and depths, using the Abaqus/Standard software based on the FEM using the mass diffusion tool. The following conclusions can be drawn:

- The numerical results obtained by using the FEM are in very good agreement with the experimental ones and it seems that is a good tool for simulating chloride transport in concrete.
- Within the parameter range considered the chloride transport property of concrete is not influenced by the considered crack widths, but only by the crack depths.
- Chloride penetration depth has a reduced sensitivity to changes in the diffusion coefficient, when simulating chloride diffusion.

Then, a 3D model that can accurately simulate chloride ingress in the cracked samples considered in the present research was studied. First, chloride ingress was simulated in uncracked concrete (reference samples type S) and afterwards it was simulated on cracked concrete (Sample 4- sample type SC- samples with cracks and without rebars. When comparing the numerical results with the experimental ones, good agreement was found.

5. FINAL CONCLUSIONS, PERSONAL CONTRIBUTIONS AND FURTHER RESEARCH

5.1. Final conclusions

Conclusions related to the respective part of the work were given in every chapter. Some general conclusions are presented below:

- *The presence of cracks has a significant influence on chloride diffusion.*

This effect was noticed in Section 3. By analysing the experimental results of chloride penetration on concrete samples with cracks, it was discovered that the chloride penetration values, and also the migration coefficients corresponding to them, were significantly higher for samples with cracks, compared to those without cracks. This particular fact was also determined by statistical analysis (Section 3.5.5).

- *No significant influence of the crack width was observed within the considered range of values.*

In Section 3.5.5, after using the one-way ANOVA analysis statistical method at a 95% confidence interval, it was concluded that the crack width, one of the most controversial parameter, has no statistically significant influence on chloride penetration when considering the values of the average and total crack widths. Still, it must be mentioned that due to the fact that the crack geometries were not induced artificially but were indeed drilled from a real-scale slab, that collapsed, the number of equal replicas for each test was almost impossible, therefore a more accurate result could have been obtained if using a higher number of samples.

- *Chloride ingress is influenced by the chloride depth.*

This aspect was observed in Section 4.3.3, when studying artificial cracks (notches) with different imposed depths in mortar samples were studied, but also it was observed when studying samples with through-thickness of the samples cracks, when the 2D effect of the diffusion can be observed.

- *The exposed surface has a significant influence on chloride penetration.*

It was observed that chloride penetration is dependent on the concrete material. This aspect was studied in Section 3, where it was concluded that the surface layer of concrete affects the transport characteristics of the material and can enhance the chloride ingress. This idea was also emphasised by statistical analysis (Section 3.5.5).

- *Carbonation influences chloride penetration*.

In the present research, it was observed in Section 3.5.4, that carbonation pushes the chloride front and decreases significantly the chloride concentration. Still, a more complex study must be performed in order to have a better image on the influence of carbonation on chloride ingress.

- *The proposed FE model can accurately simulate chloride diffusion in cracked and uncracked concrete.*

A model was developed (Section 4) in order to simulate chloride ingress in the samples used in the experimental part of the present research. Due to the fact that the numerical results agree fairly well with the experimental ones, this model seems to be a good tool to simulate chloride ingress in uncracked and cracked concrete.

5.2. Personal contributions

As mentioned in Section 1, the purpose of the present research was to obtain more information about the complex mechanism of chloride ingress and its effect on RC structures. Below are presented some original contributions:

- For studying the influence of chloride diffusion on samples with real cracks, cores of 100 mm diameter and 50 mm thickness were drilled from a RC structure exposed to a simulated accidental failure of the central support and subsequent vertical loading until collapse and were subjected to a non-steady state migration test according to NT Build 492, in order to obtain samples with the same characteristics as in structures from the real environment.
- Due to the uniqueness of each drilled core, a thoroughly examination of the sample characteristics, including of the crack patterns and rebar position, was realized. In total, 40 samples were used in this study, categorized in four main groups: samples without cracks and without rebars (S) (a), samples with cracks and without rebars (SC) (b), samples without cracks and with rebars (SR) (c), samples with cracks and with rebars (SCR).
- The influence of different parameters (crack existence, crack width, carbonation and existence of rebars) was determined by statistical analysis.
- Parameters such as: the diffusion coefficient D, initial chloride concentration c and applied chloride concentration C, were determined experimentally and were used as simulation parameters in developing a numerical model that can accurately simulate chloride ingress in cracked and uncracked concrete.
- In order to calibrate the numerical model, preliminary investigations were made when chloride penetration was simulated on samples with notches previously subjected to chloride diffusion for 28 weeks; after the validation of the FE model, chloride penetration was simulated on the samples used in this study, subjected to non-steady state migration tests.

5.3. Further research

In the future, the following could be done:

- Developing an experimental program in which a more considerable amount of samples are studied;
- Studying chloride penetration on samples subjected to natural diffusion;
- Studying the corrosion aspect of the rebars embedded in concrete while subjected to chloride penetration;
- Developing a FE model that can realistically simulate chloride ingress in which both the crack and the rebar are accurately represented, including the geometrical characteristics of cracks (tortuosity, length…).

6. BIBLIOGRAPHY

Abaqus Analysis User's Manual. (2010). *Abaqus 6.10, Dessault Systemes Simulia*. Providence, RI: Dessault Systemes Simulia Corp.

ACI 222. *Corrosion of metals in concrete*. Comitee and American Concrete Institute and International Organization for Standardization, 1992

ACI Committee 224. *Control of cracking in concrete structures (ACI 224R-90)*, ACI Manual of Concrete Practice, Part 3, ACI (1999)

Adiyastuti, S.M. (2005). *Influence of cracks on chloride induced corrosion in reinforced concrete flexural members* (PhD thesis), University of New South Wales, Sydney, Australia

Akhavan, A. (2012). *Characterizing saturated mass transport in fractured cementitious materials* (Doctoral dissertation, The Pennsylvania State University).

Aldea, C. M., Song, W. J., Popovics, J. S., & Shah, S. P. (2000). *Extent of healing of cracked normal strength concrete*. Journal of materials in civil engineering, 12(1), pp. 92-96.

Aldea, C.M. and Shah, S.P. (1999). *Effect of cracking on water and chloride permeability of concrete*. Journal of Materials in Civil Engineering, ASCE, vol. 11(3), pp. 181-187

Angst, U., & VENNESLAND, Ø. (2009). *Critical chloride content in reinforced concrete–State of the art*. Concrete repair, rehabilitation and retrofitting II. Taylor & Francis Group, London, ISBN, 978-0-415-46850-3.

Antoni, Antoni. (2008). *Chloride penetration into fiber reinforced concrete under static and cyclic compressive loading.* Civil Engineering Dimension 10, no. 2, pp-63

Arya, C., & Ofori-Darko, F. K. (1996). Influence of crack frequency on reinforcement corrosion in concrete. *Cement and Concrete Research*, *26*(3), 345-353.

Audenaert, K., De Schutter, G. and Marsavina, L. (2008, b). *Modelling of chloride penetration in concrete with artificial cracks*. In: Schlangen E, De Schutter G (Eds), Proceedings pro058: international RILEM symposium on concrete modeling- ConMod '08, pp. 439-446,Delft, The Netherlands

Audenaert, K., De Schutter, G. and Marsavina, L. *The influence of cracks on chloride penetration in concrete structures. Part one: experimental evaluation*. In: Audenaert K., Marsavina L., De Schutter G. (Eds), International RILEM workshop on transport mechanisms in cracked concrete. Acco, Leuven pp 35-43, 2007

Audenaert, K., De Schutter, G., & Marsavina, L. (2009). *Influence of cracks and crack width on penetration depth of chlorides in concrete.* European journal of environmental and civil engineering, 13(5), 561-572.

Audenaert, K., De Schutter, G., Marsavina, L. *Influence of artificial cracks on chloride diffusion. Concrete in Aggressive Aqueous Environments, Performance, Testing and Modelling.* Toulouse, 2009

Audenaert, K., Marsavina, L. and De Schutter, G. (2008, a). *Influence of cracks on the service life of concrete structures in a marine environment*. Key Engineering Materials, vol. 399, pp. 153-160

Bentz, D. P., Garboczi, E. J., Lu, Y., Martys, N., Sakulich, A. R., & Weiss, W. J. (2013). *Modeling of the influence of transverse cracking on chloride penetration into concrete*. Cement and Concrete Composites, 38, pp. 65-74.

Bertolini, L. (2008). *Steel corrlosion and service life of reinforced concrete structures*. Structure and Infrastructure Engineering, 4(2), 123-137.

Borges, P. H., Costa, J. O., Milestone, N. B., Lynsdale, C. J., & Streatfield, R. E. (2010). *Carbonation of CH and C–S–H in composite cement pastes containing high amounts of BFS*. Cement and Concrete Research, 40(2), 284-292.

British Standards Institution. BS 8110:Part 1, BSI, London (1997)

British Standards Institution. *ENV 1991-1-1*, BSI, London (1992)

Brühwiler, E. and Wittmann, F.H. (1990). *The wedge splitting test, a new method of performing stable fracture mechanics tests.* Engineering Fracture Mechanics, vol. 35, pp. 117-125

BS 8110-1. *Structural use of concrete. Part 1: Code of practice for design and construction* (British Standards Institution, 1997)

Cao, H. T., & Sirivivatnanon, V. (2001). *Service life modelling of crack-freed and cracked reinforced concrete members subjected to working load*. In Proceedings CIB Building Congress, Wellington, New Zeeland

Clear, C. A. (1985). The effects of autogenous healing upon the leakage of water through cracks in concrete (No. Tech Rpt. 559).

Cousin, B., and B. Martin-Perez. *Chloride Ingress in Pre-Tensioned Prestressed Concrete Beams and the Effect of Corrosion on Their Structural Behaviour*. In: Sixth International Conference on Concrete under Severe Conditions: Environment and Loading. (2010).

De Rooij, M. R., & Schlangen, E. (2011). Self-healing phenomena in cement-based materials. Draft of State-of-the-Art report of RILEM Technical Committee Report 221-SHC.

De Schutter, G. (1999, a*). Quantification of the influence of cracks in concrete structures on carbonation and chloride penetration*. Magazine of Concrete Research, 51(6), 427-435.

De Schutter, G. (1999, b). *Influence of early age thermal cracking on durability of massive concrete structures in marine environment*. In: M.A. Lacasse and D.J. Vanier (Eds), Durability of Building Materials and Components 8, Vol. 1, NRC Research Press, Ottawa

De Sitter, W. R. (1984, May). *Costs for service life optimization: The Law of Fives*. In Durability of Concrete Structures, Workshop Report (pp. 131-134).

Deif, A. K. (2010). *Chloride ingress into reinforced concrete sustaining in-service loads*. (PhD thesis), University of Ottawa, Ottawa, Canada

Di Benedetti, M., Loreto, G., Matta, F., & Nanni, A. (2012). *Acoustic emission monitoring of reinforced concrete under accelerated corrosion*. Journal of Materials in Civil Engineering, 25(8), 1022-1029.

Djerbi, A., Bonnet, S., Khelidj, A. and Baroghel-bouny, V. (2008). *Influence of traversing crack on chloride diffusion into concrete*. Cement and Concrete Research, vol. 38(6), pp. 877-883

dSagues, A. A., Moreno, E. I., Morris, W., & Andrade, C. (1997). *Carbonation in concrete and effect on steel corrosion* (No. WPI 0510685,).

Edvardsen, C. (1999). *Water permeability and autogenous healing of cracks in concrete*. ACI Materials Journal, 96(4).

Eurocode 2. *Design of Concrete Structures. Part 1: General Rules and Rules for Buildings* (European Committee for Standardization, 1992)

François, R. and Arliguie, G. (1998). *Influence of service cracking on reinforcement steel corrosion*. Journal of Materials in Civil Engineering, vol. 10(1), pp. 14-20

François, R., Castel, A., Vidal, T. and Vu, N.-A. (2006). *Long term corrosion behavior of reinforced concrete structures in chloride environment*. Journal de Physique IV(Proceedings), vol. 136, pp. 285-293

Fu, Chuanqing, Xianyu Jin, Hailong Ye, and Nanguo Jin. *Theoretical and experimental investigation of loading effects on chloride diffusion in saturated concrete*. Journal of Advanced Concrete Technology 13, no. 1, pp 30-43 (2015)

Garboczi, E. J. (2002). *Three-dimensional mathematical analysis of particle shape using X-ray tomography and spherical harmonics: Application to aggregates used in concrete*. Cement and concrete research, 32(10), 1621-1638.

Gérard, B. and Marchand, J. (2000). *Influence of cracking on the diffusion properties of cement-based materials: Part I: Influence of continuous cracks on the steady-state regime*. Cement and Concrete Research, vol. 30(1), pp. 37-43

Gouverneur, D. (2014). *Experimental and Numerical Analysis of Tensile Membrane Actionin Reinforced Concrete Slabs in the Framework of Structural Robustness.* (PhD thesis), Ghent University, Gent, Belgium

Gowripalan, N., Sirivivatnanon, V., Lim, C.C. (2000). *Chloride diffusivity of concrete cracked in flexure.* Cement and Concrete Research, vol. 30(5), pp. 725-730

Granju, J.L. and Balouch, S.U. (2005). *Corrosion of steel fibre reinforced concrete from the cracks*. Cement and Concrete Research, vol 35(3), pp. 572-577

Gu, C. P., Ye, G., & Sun, W. (2015). *A review of the chloride transport properties of cracked concrete: experiments and simulations*. Journal of Zhejiang University SCIENCE A, 16(2), 81-92.

Guo, L., Guo, X., & Mi, C. (2012). *Multi-scale finite element analysis of chloride diffusion in concrete incorporating paste/aggregate ITZs*. Science China Physics, Mechanics and Astronomy, 55(9), 1696-1702.

Hirao, H., Yamada, K., Takahashi, H. and Zibara, H. (2005). *Chloride Binding of Cement Estimated by Binding Isotherms of Hydrates.* Journal of Advanced Concrete Technology, vol. 3, no. 1, pp 77-84

Hooton, R. D., Charmchi, G., Karkar, E. (2001). *Development and standardization of rapid methods for assessing the fluid penetration resistance of concrete*. Materials Science of Concrete: Fluid and Ion Transport Rates in Concrete, A. Cer. S., pp. 1-12,

Igarashi, S. I., Hosoda, A., Hitomi, T., & Imamoto, K. I. Technical Committee on Self-healing/Repairing Technology in Cement-based Materials, Technical Committee Report JCI- TC091A, 2011

Iqbal, P. O. N., & Ishida, T. (2009). *Modeling of chloride transport coupled with enhanced moisture conductivity in concrete exposed to marine environment*. Cement and Concrete Research, 39(4), 329-339.

Ishida, T., Iqbal, P. O. N., & Anh, H. T. L. (2009). *Modeling of chloride diffusivity coupled with non-linear binding capacity in sound and cracked concrete*. Cement and Concrete Research, 39(10), 913-923.

Ismail, M., Toumi, A., François, R. and Gagné, R. (2004). *Effect of crack opening on the local diffusion of chloride in inert materials*. Cement and Concrete Research, vol. 34(4), pp. 711-716

Ismail, M., Toumi, A., François, R. and Gagné, R. (2008). *Effect of crack opening on the local diffusion of chloride in cracked mortar samples*. Cement and Concrete Research, vol. 38(8-9), pp. 1106-1111

Jacobsen, S. and Sellevold, E. J. (1996 b). *Self healing of high strength concrete after deterioration by freeze/thaw.* Cement and Concrete Research, 26(1), pp. 55-62.

Jacobsen, S., Marchand, J., Boisvert, L. (1996 a). *Effect of cracking and healing on chloride transport in OPC concrete*. Cement and Concrete Research, 26(6), pp. 869-881.

Jaffer, S. J., & Hansson, C. M. (2009). *Chloride-induced corrosion products of steel in cracked-concrete subjected to different loading conditions*. Cement and Concrete Research, 39(2), pp. 116-125

Jang, S.Y., Kim, B.S. and Oh, B.H. (2011). *Effect of crack width on chloride diffusion coefficients of concrete by steady-state migration tests*. Cement and Concrete Research, vol. 41(1), pp. 9-19

Jin, W. L., Yan, Y. D., & Wang, H. L. (2006). *Chloride diffusion in the cracked concrete*. In: B. H. Oh, et al.(Eds), Fracture Mechanics of Concrete and Concrete Structures -Assessment, Durability, Monitoring and Retrofitting of Concrete Structures, Korea Concrete Institute, Seoul, pp. 880-886, 2010S

Karam, A. (2014). *Chloride ingress into submerged concrete under sustained load*. (PhD thesis), University of Ottawa, Ottawa, Canada

Karihaloo, B.L, Abdalla H.M and Xiao, Q.Z. (2006). *Deterministic size effect in the strength of cracked concrete structures*. Cement and Concrete Research, vol. 36(1), pp. 171-188

Kato, E., Kato, Y., & Uomoto, T. (2005). *Development of simulation model of chloride ion transportation in cracked concrete*. Journal of Advanced Concrete Technology, 3(1), 85-94.

Knudsen, A., Jensen, F. M., Klinghoffer, O., & Skovsgaard, T. (1998, December). *Cost-effective enhancement of durability of concrete structures by intelligent use of*

stainless steel reinforcement. In Conference on Corrosion and rehabilitation of reinforced concrete structures, Florida.

Kobayashi, K., Shiraki, R., Kawai, K. *Carbonation of Concrete*. Proceedings of JSCE, no. 443, pp. 1-14, 1991

Koch, G. H., Brongers, M. P., Thompson, N. G., Virmani, Y. P., & Payer, J. H. (2002). *Corrosion cost and preventive strategies in the United States* (No. FHWA-RD-01-156,).

Konin, A., R. Francois, and G. Arliguie. (1998). *Penetration of chlorides in relation to the microcracking state into reinforced ordinary and high strength concrete*. Materials and structures 31, no. 5, pp310-316

Kropp, T. A. B. J., & Hilsdorf, H. K. (1989). *Formation of silica gel during carbonation of cementitious systems containing slag cements*. *ACI Special Publication*, *114*.

Li, C.Q. (2001). *Initiation of chloride-induced reinforcement corrosion in concrete structural members-experimentation.* ACI Structural Journal, vol. 98(4), pp. 502-510

Lin, G., Liu, Y., & Xiang, Z. (2010). Numerical modeling for predicting service life of reinforced concrete structures exposed to chloride environments. Cement and concrete composites, 32(8), 571-579.

Lippiatt, B. C., & Ahmad, S. (2004, April). *Measuring the life-cycle environmental and economic performance of concrete: the BEES approach*. In Proceedings of the International workshop on sustainable development and concrete technology (pp. 213-230).

Liu, R., Jiang, L., Xu, J., Xiong, C., & Song, Z. (2014). Influence of carbonation on chloride-induced reinforcement corrosion in simulated concrete pore solutions. *Construction and Building Materials*, *56*, 16-20.

Lu, Y., Garboczi, E., Bentz, D., & Davis, J. (2012*). Modeling of Chloride Transport in Cracked Concrete: A 3-D Image–based Microstructure Simulation.* In Proceedings of the 2012 COMSOL Conference.

Ma, B., Mu, S. and De Schutter, G. (2013*). Non-steady state chloride migration and binding in cracked self-compacting concrete*. Journal of Wuhan University of Technology Materials Science, vol. 28(5), pp. 921-926

Maes, M., & De Belie, N. (2013). *Resistance of cracked concrete to chloride attack*. In 3rd International conference on sustainable construction materials & technologies. Kyoto Research Park (pp. 1-10).

Malheiro, R., Camões, A., Ferreira, R. M., Meira, G., & Amorim, M. T. (2014). *Effect of carbonation on the chloride diffusion of mortar specimens exposed to cyclic wetting and drying*. In: XIII International Conference on Durability of Building Materials and Components, pp. 482-489

Marcotte, T.D. and Hansson, C.M. (2003). *The influence of silica fume on the corrosion resistance of steel in high performance concrete exposed to simulated sea water*. Journal of Materials Science, vol. 38(23), pp. 4765-4776

Marsavina, L., Audenaert, K., De Schutter, G, Faur, N. and Marsavina, D. (2009). *Experimental and numerical determination of the chloride penetration in cracked concrete*. Construction and Building Materials, vol. 23(1), pp. 264-274

Martin- Perez, B. (1999). *Service life modelling of RC highway structures exposed to chlorides*, (PhD Thesis), University of Toronto.

Mihashi, H., & Nishiwaki, T. (2012). *Development of engineered self-healing and self-repairing concrete-state-of-the-art report. Journal of Advanced Concrete Technology*, 10(5), 170-184

Mohamed, T.U., Otsuki, N., Hisada, M. and Shibata T. (2001). *Effect of crack width and bar types on corrosion of steel in concrete*. Journal of Materials in Civil Engineering, vol. 13(3), pp. 194-201

Mohammed, T. U., Otsuki, N., & Hamada, H. (2003). *Corrosion of steel bars in cracked concrete under marine environment*. Journal of Materials in Civil Engineering, 15(5), pp. 460-469.

Montgomery, D. C. (2008). *Design and analysis of experiments*. John Wiley & Sons

Mu, S. (2012). Chloride penetration and service-life prediction of cracked self-compacting concrete. (PhD thesis), Faculty of Engineering and Architecture, Gent, Belgium

Mu, S., De Schutter, G and Ma, B. (2013). *Non-steady state chloride diffusion in concrete with different crack densities*. Materials and Structures, vol. 46(1-2), pp. 123-133

Ngala, V. T., & Page, C. L. (1997). *Effects of carbonation on pore structure and diffusional properties of hydrated cement pastes*. Cement and Concrete Research, 27(7), 995-1007.

Nieves-Mendoza, D., Gaona-Tiburcio, C.,Hervert-Zamora, H.L. & Almeraya-Calderón, F. (2012). Statistical Analysis of Factors Influencing Corrosion in Concrete Structures. *Int. J. Electrochem. Sci*, *7*, 5495-5509.

Nord Test Build 443, 1995. *Concrete, hardened: accelerated chloride penetration*

Nord Test Build 492, 1999*. Concrete, mortar and cement-based materials: chloride migration*

Otieno, M. B., M. G. Alexander, and H-D. Beushausen. (2010). *Corrosion in cracked and uncracked concrete–influence of crack width, concrete quality and crack reopening*. Magazine of Concrete Research 62, no. 6, pp. 393-404

Otsuki, N., Miyazato, S., Diola, N.B. and Suzuki, H. (2000). *Influences of bending crack and water-cement ratio on chloride-induced corrosion of main reinforcing bars and stirrups*. ACI Materials Journal, vol. 97(4), pp. 454-464

Otsuki, N., Nagataki, S., & Nakashita, K. (1993*). Evaluation of the AgNO 3 solution spray method for measurement of chloride penetration into hardened cementitious matrix materials*. Construction and Building Materials, 7(4), 195-201.

Ožbolt, J., Balabanić, G., & Kušter, M. (2011). *3D Numerical modelling of steel corrosion in concrete structures*. Corrosion science, 53(12), 4166-4177.

Ožbolt, J., Balabanić, G., Periškić, G., & Kušter, M. (2010). *Modelling the effect of damage on transport processes in concrete.* Construction and Building Materials, 24(9), pp. 1638-1648.

Ožbolt, J., Oršanić, F., & Balabanić, G. (2014). *Modeling pull-out resistance of corroded reinforcement in concrete*: Coupled three-dimensional finite element model. Cement and Concrete Composites, 46, 41-55.

Papadakis, V. G., Fardis, M. N., & Vayenas, C. G. (1992). *Effect of composition, environmental factors and cement-lime mortar coating on concrete carbonation*. Materials and Structures, 25(5), 293-304.

Papakonstantinou, K. G., & Shinozuka, M. (2013). *Probabilistic model for steel corrosion in reinforced concrete structures of large dimensions considering crack effects*. Engineering Structures, 57, 306-326.

Park, S. S., Kwon, S. J., & Jung, S. H. (2012). *Analysis technique for chloride penetration in cracked concrete using equivalent diffusion and permeation*. Construction and Building Materials, 29, 183-192.

Paul, S. K., Chaudhuri, S., & Barai, S. V. (2014). *Chloride diffusion study in different types of concrete using finite element method (FEM)*. Advances in Concrete Construction, 2(1), pp. 39-56

Pease, B.J.(2010). *Influence of concrete cracking on ingress and reinforcement corrosion*, (PhD thesis), Technical University of Denmark, Lyngby, Denmark

Picandet, V., Khelidj, A. and Bellegou, H. (2009). *Crack effects on gas and water permeability of concretes*. Cement and Concrete research, vol. 39(6), pp. 537-547

Pour-Ghaz, M., Rajabipour, F., Couch, J. and Weiss, J. (2009, a) *Modelling fluid transport in cementitious systems with crack-line (Notch) geometries*. In: Kovler K. (Ed), Proceedings of the 2nd international RILEM workshop on concrete durability and service life planning, pp. 71-79, RILEM Publications SARL, Haifa, Israel

Pour-Ghaz, M., Rajabipour, F., Couch, J. and Weiss, J. (2009, b) *Numerical and experimental assessment of unsaturated fluid transport in saw-cut (Notched) concrete elements*. ACI Special Publication SP266-06, vol. 266, pp. 73-86

Rahman, M. K., Al-Kutti, W. A., Shazali, M. A., & Baluch, M. H. (2012). Simulation of chloride migration in compression-induced damage in concrete.*Journal of Materials in Civil Engineering*, *24*(7), 789-796.

Ramezanianpour, A. A., Ghahari, S. A., & Esmaeili, M. (2014). *Effect of combined carbonation and chloride ion ingress by an accelerated test method on microscopic and mechanical properties of concrete*. Construction and Building Materials, 58, 138-146.

Ramm, W., & Biscoping, M. (1998). *Autogenous healing and reinforcement corrosion of water-penetrated separation cracks in reinforced concrete*. Nuclear Engineering and Design, 179(2), pp. 191-200.

Reddy, B., Glass, G. K., Lim, P. J., & Buenfeld, N. R. (2002). *On the corrosion risk presented by chloride bound in concrete.* Cement and Concrete Composites, 24(1), 1-5.

Reinhardt, H. W., & Jooss, M. (2003). *Permeability and self-healing of cracked concrete as a function of temperature and crack width*. Cement and Concrete Research, 33(7), pp. 981-985.

Reinhardt, H. W., Jonkers, H., Van Tittelboom, K., Snoeck, D., De Belie, N., De Muynck, W., ... & Mechtcherine, V. (2013). *Recovery against Environmental Action*. In Self-Healing Phenomena in Cement-Based Materials (pp. 65-117). Springer Netherlands.

Reinhardt, H.W. *Fluid transport in wedge-splitted cracked concrete*. In: Audenaert K., Marsavina L., De Schutter G. (Eds), International RILEM workshop on transport mechanisms in cracked concrete. Acco, Leuven pp 13-18, 2007

Rodriguez, O.G. and Hooton, R.D. (2003). *Influence of cracks on chloride ingress into concrete*. ACI Materials Journal, vol. 100(2), pp. 102-126 (2003)

Rodriguez,O.G. (2001). *Influence of cracks on chloride ingress into concrete*. (PhD thesis), University of Toronto, Toronto, Canada

Rostam, S. *SERVICE LIFE DESIGN OF CONCRETE STRUCTURES-AN EXPERIENCE-BASED DISCIPLINE BECOMING SCIENTIFIC*. In: Papers in Structural Engineering

and Materials- A Centenary Celebration, Department of Structural Engineering and Materials, Technical University of Denmark, 2000.

Saeki, T. (2002). Effect of carbonation on chloride penetration in concrete. In*Proceedings of The 3 rd International RILEM Workshop on Testing and Modelling the Chloride Ingress into Concrete, Madrid, Spain* (pp. 381-394).

Şahmaran, M. *Effect of flexure induced transverse crack and self-healing on chloride diffusivity of reinforced mortar*. (2007). Journal of Materials Science, vol. 42(22), pp. 9131-9136

Sahmaran, M., & Yaman, I. Ö. (2008, b). *Influence of transverse crack width on reinforcement corrosion initiation and propagation in mortar beams*. Canadian Journal of Civil Engineering, 35(3), 236-245.

Şahmaran, M., Keskin, S. B., Ozerkan, G., & Yaman, I. O. (2008, a). *Self-healing of mechanically-loaded self-consolidating concretes with high volumes of fly ash*. Cement and Concrete Composites, 30(10), pp. 872-879.

Saito, M., & Ishimori, H. (1995). Chloride permeability of concrete under static and repeated compressive loading. Cement and Concrete Research, 25(4), 803-808.

Savija, B. (2014) *Experimental and numerical investigation of chloride ingress in cracked concrete.* (PhD thesis), Delft University of Technology, Delft, The Netherlands

Šavija, B., Luković, M., & Schlangen, E. (2014). *Lattice modeling of rapid chloride migration in concrete.* Cement and Concrete Research, 61, 49-63.

Šavija, B., Pacheco, J., & Schlangen, E. (2013*). Lattice modeling of chloride diffusion in sound and cracked concrete.* Cement and Concrete Composites, 42, 30-40.

Schießl, P. and Raupach, M. (1997). *Laboratory studies and calculations on the influence of crack width on chloride-induced corrosion of steel in concrete*. ACI Materials Journal, vol. 94(1), pp. 56-62

Schlangen, E, Yoon I.-S. and De Rooij, M.R. *Measurement of chloride ingress in cracked concrete*. In: Audenaert K., Marsavina L., De Schutter G. (Eds), International RILEM workshop on transport mechanisms in cracked concrete. Acco, Leuven pp 19-25, 2007

Schlangen, E. (1993). *Experimental and numerical analysis of fracture processes in concrete*. TU Delft, Delft University of Technology.

Seung, Y.J., Kim, B.S. and Oh, B.H. (2011). *Effect of crack width on chloride diffusion coefficients of concrete by steady-state migration tests*. Cement and Concrete Research, vol. 41(1), pp. 9-19

Song, H.W., Kwon, S.J., Byun, K.J. and Park, C.K. (2006). *Predicting carbonation in early-aged cracked concrete*. Cement and Concrete Research, vol. 36(5), pp. 979-989

Sosdean, C., Marsavina, L., & De Schutter, G. (2015). *Experimental and numerical determination of the chloride penetration in cracked mortar specimens*. European Journal of Environmental and Civil Engineering, (ahead-of-print), 1-19.

Stanish, K.D., Hooton, R.D., Thomas, M.D.A. (1997). *Testing the chloride resistance of concrete: a literature revie*w, University of Toronto, Ontario, Canada

Statgraphics. (1997). Statgraphics plus, version 3.0.

Taheri-Motlagh, A.(1998). *Durability of reinforced concrete structures in aggressive marine environment*. (PhD thesis), Delft University of Technology, Delft, The Netherlands

Tang, L., & Nilsson, L. (1993). Rapid determination of the chloride diffusivity in concrete by applying an electric field. *ACI Materials Journal*, *89*(1).

Tumidajski, P. J., & Chan, G. W. (1996). Effect of sulfate and carbon dioxide on chloride diffusivity. *Cement and Concrete Research*, *26*(4), 551-556.

Tuutti, K. (1982). *Corrosion of steel in concrete*. Swedish foundation for concrete research, Stockholm, 1982.

Van den Heede, P., Maes, M., De Belie, N. (2014). *Influence of active crack width control on the chloride penetration resistance and global warming potential of slabs made with fly ash +silica fume concrete.* Construction and Building Materials, vol. 67, pp. 74-80

Vesikari, E. (2009). *Carbonation and chloride penetration in concrete with special objective of service life modelling by the Factor Approach*. VTT Technical Research Centre of Finland. VTT

Wang, H., Chunhua, L., Weiliang J., and Yun B. (2011). *Effect of external loads on chloride transport in concrete*. Journal of Materials in Civil Engineering 23, no. 7, pp. 1043-1049

Wang, J., Nanukuttan, S.V., Basheer, P.A. and Bai, Y. *Influence of Micro and Macro Cracks Due to Sustained Loading on Chloride-Induced Corrosion of Reinforced Concrete Beams*. In: 4th International Conference on the Durability of Concrete Structures, Purdue University (2014)

Wang, K., Jansen, D.C. Shah, S.P. (1997). *Permeability study of cracked concrete*. Cement and Concrete Research, vol. 27(3), pp. 381-393

Wang, L., & Ueda, T. (2011). *Mesoscale modelling of the chloride diffusion in cracks and cracked concrete*. Journal of Advanced Concrete Technology, 9(3), 241-249.

Wang, L., Soda, M., & Ueda, T. (2008). *Simulation of chloride diffusivity for cracked concrete based on RBSM and truss network model*. Journal of Advanced Concrete Technology, 6(1), 143-155.

Win, P.P., Watanabe, M. and Machida, A. (2004). *Penetration profile on of chloride ion in cracked reinforced concrete*. Cement and Concrete Research, vol. 34(7), pp. 1073-1079

Ye, H., Jin, N., Jin, X., & Fu, C. (2012). *Model of chloride penetration into cracked concrete subject to drying–wetting cycles*. Construction and Building Materials, 36, 259-269.

Ye, H., Tian, Y., Jin, Y., Jin, X. and Fu, C. (2013). *Influence of cracking on chloride diffusivity and moisture influential depth in concrete subjected to simulated environmental conditions*. Construction and Building Materials, vol. 47, pp. 66-79

Yoon, I. S. (2007). *Deterioration of concrete due to combined reaction of carbonation and chloride penetration: experimental study*. Key Engineering Materials, 348, 729-732

Yoon, I.S. and Schlangen, E. (2009). *Long/short term experimental study on chloride penetration in cracked concrete*. Key Engineering Materials, vol. 417-418, pp. 765-768

Yuan, Q. (2009 b). *Fundamental Studies on Test Methods for the Transport of Chloride Ions in Cementitious Materials* (Doctoral dissertation, Ghent University).

Yuan, Q., Shi, C., De Schutter, G., Audenaert, K., & Deng, D. (2009 a). *Chloride binding of cement-based materials subjected to external chloride environment–a review.* Construction and Building Materials, 23(1), 1-13.

Yuan, Q., Shi, C., De Schutter, G., Deng, D., & He, F. (2010). *Numerical model for chloride penetration into saturated concrete.* Journal of Materials in Civil Engineering, 23(3), 305-311.

APPENDIX

3D representation of samples

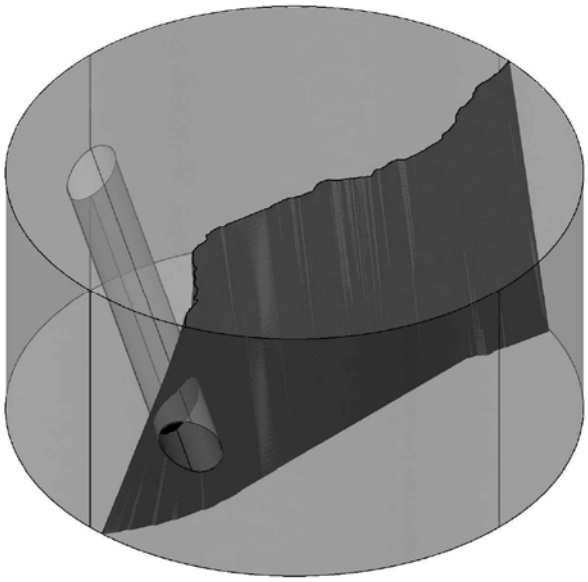

Figure A1. 3D representation of sample 6

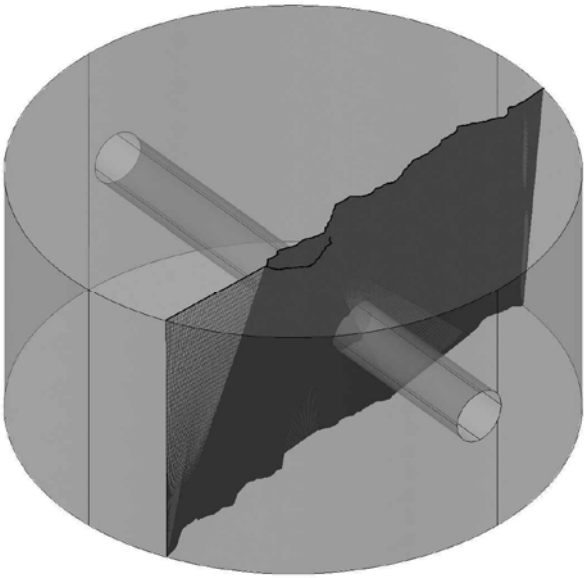

Figure A2. 3D representation of sample 7

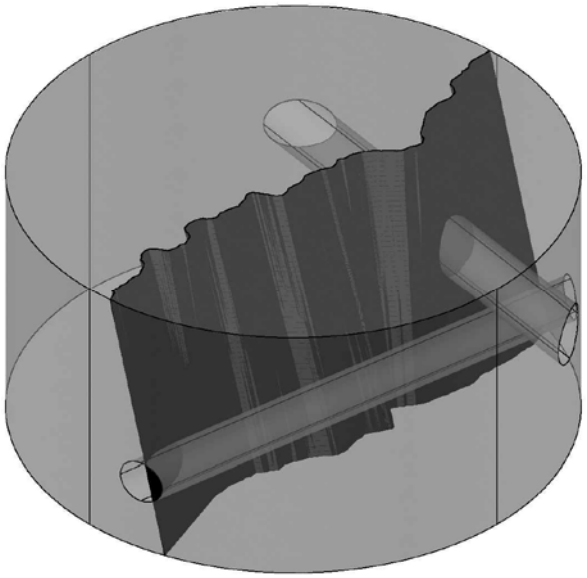

Figure A3. 3D representation of sample 13

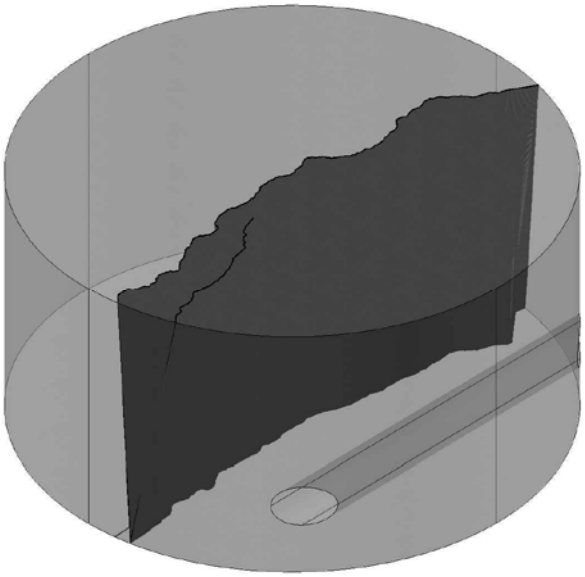

Figure A4. 3D representation of sample 16

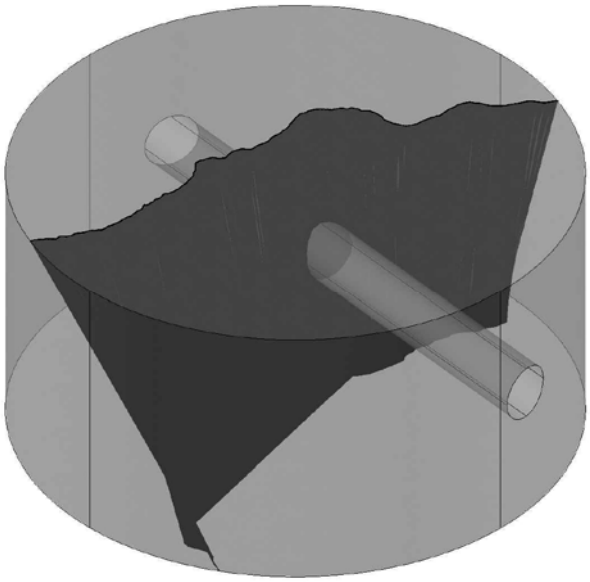

Figure A5. 3D representation of sample 25

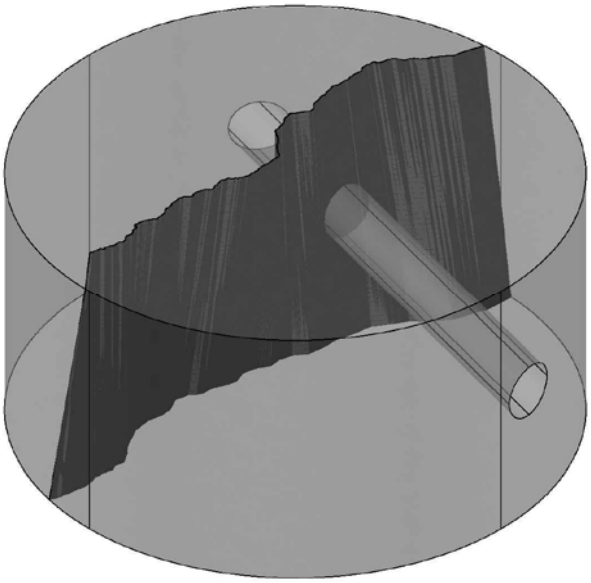

Figure A6. 3D representation of sample A

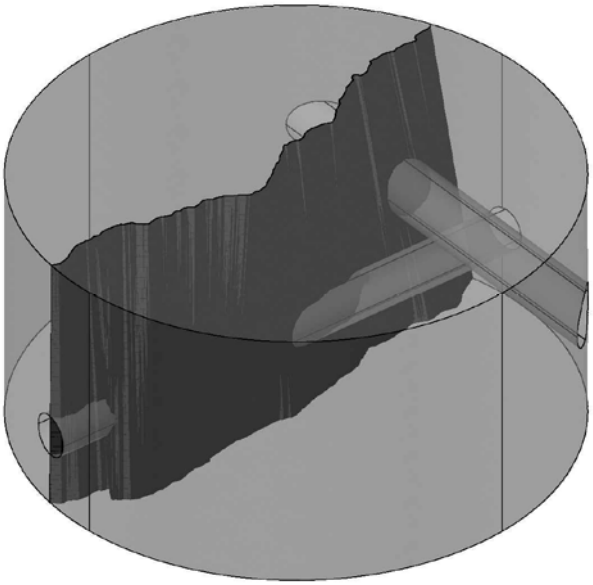

Figure A7. 3D representation of sample A2

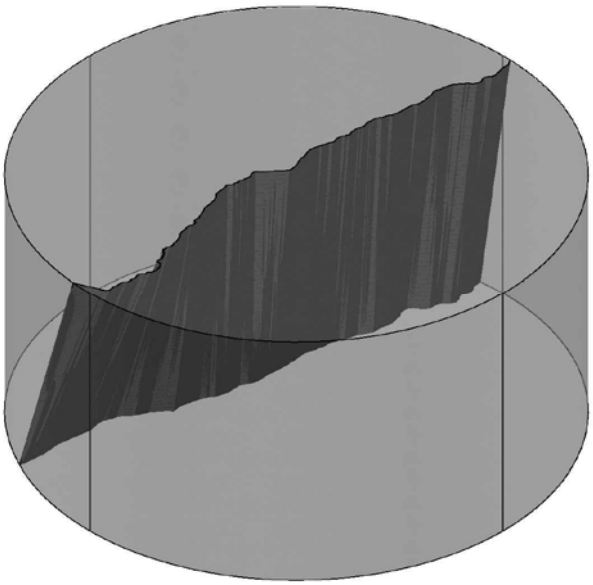

Figure A8. 3D representation of sample B

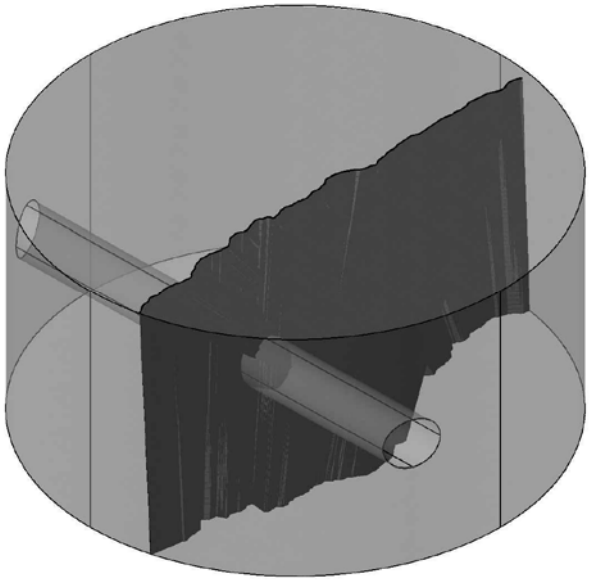

Figure A9. 3D representation of sample B2

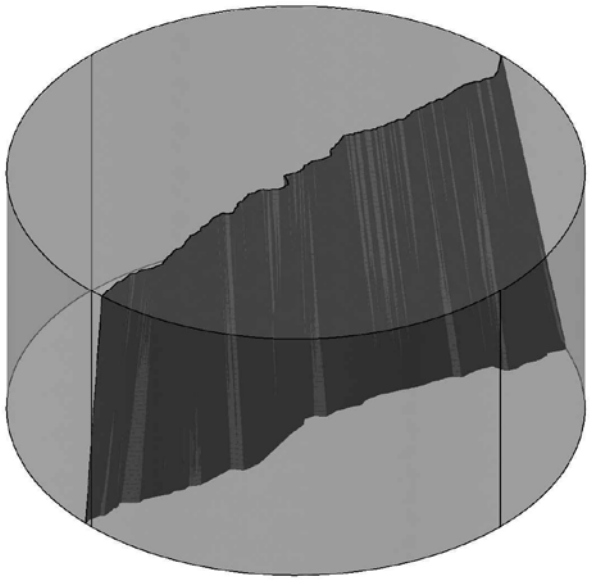

Figure A10. 3D representation of sample C

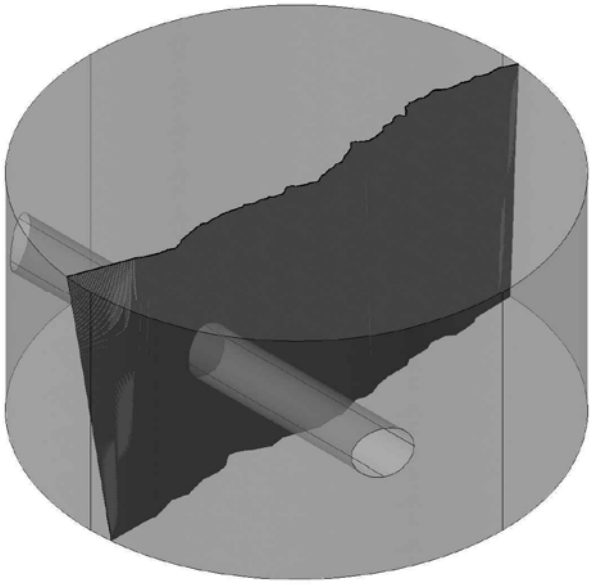

Figure A11. 3D representation of sample D

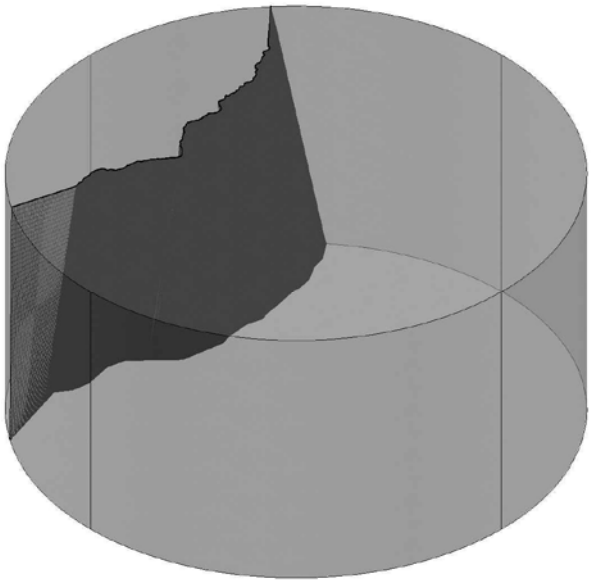

Figure A12. 3D representation of sample E

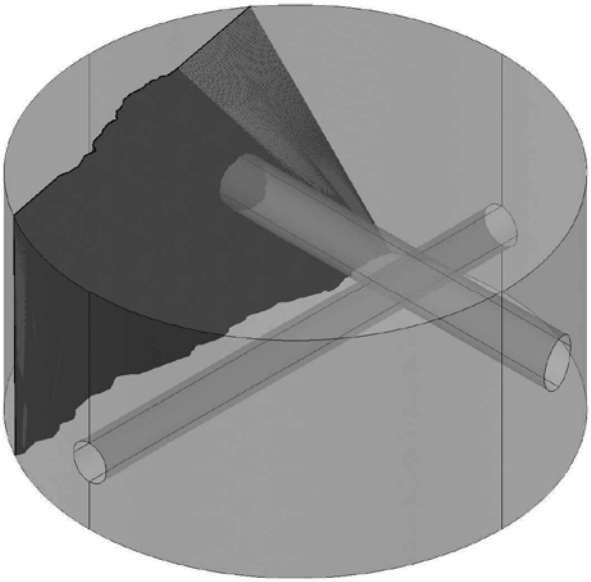

Figure A13. 3D representation of sample F

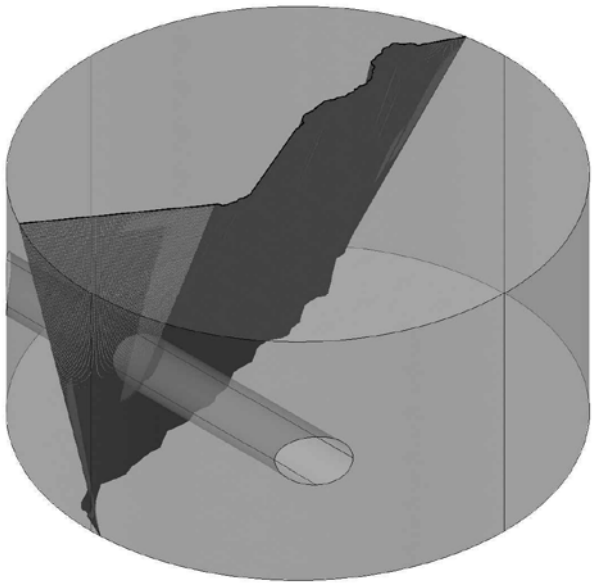

Figure A14. 3D representation of sample G

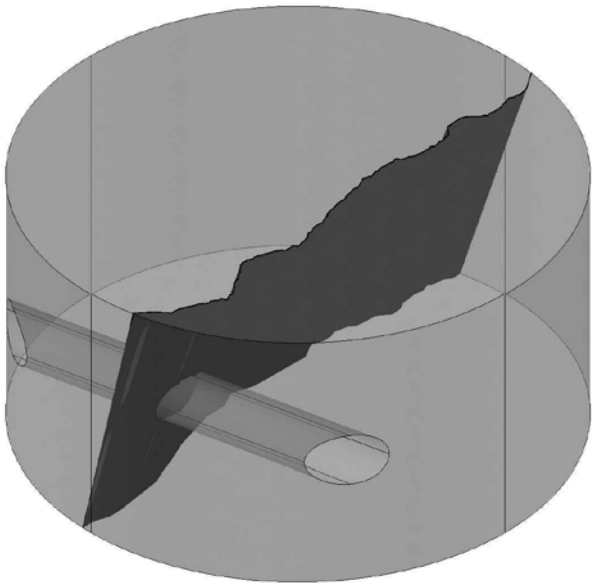

Figure A15. 3D representation of samples H

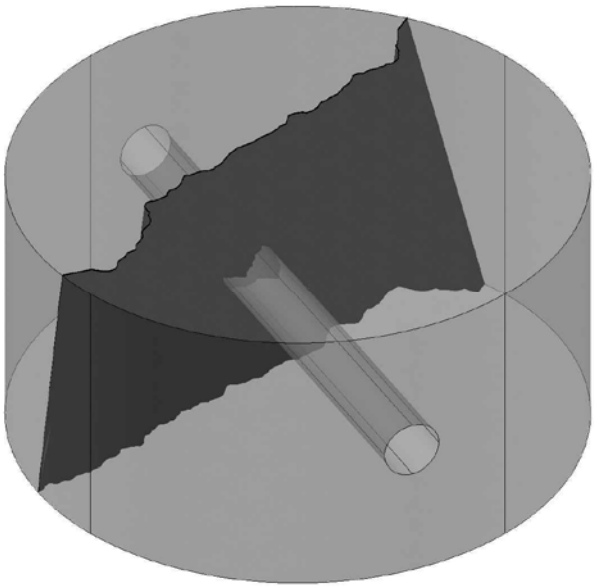

Figure A16. 3D representation of sample I

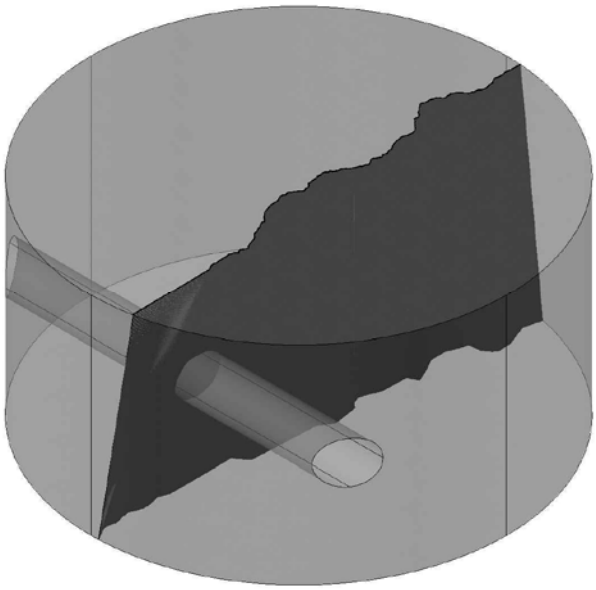

Figure A17. 3D representation of sample J

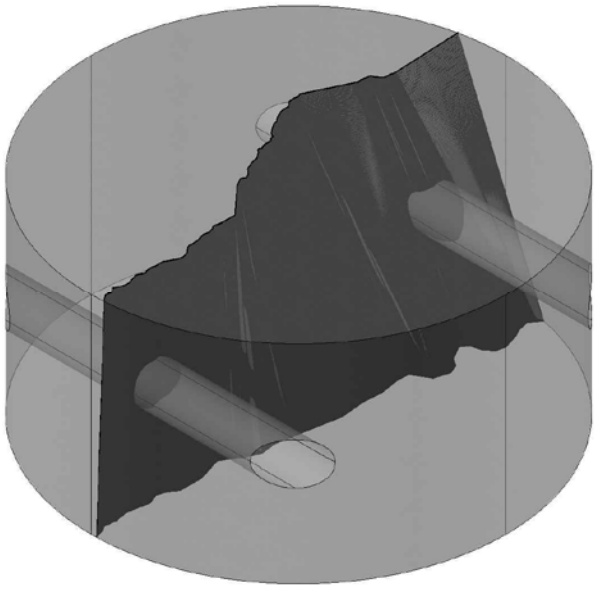

Figure A18. 3D representation of sample K

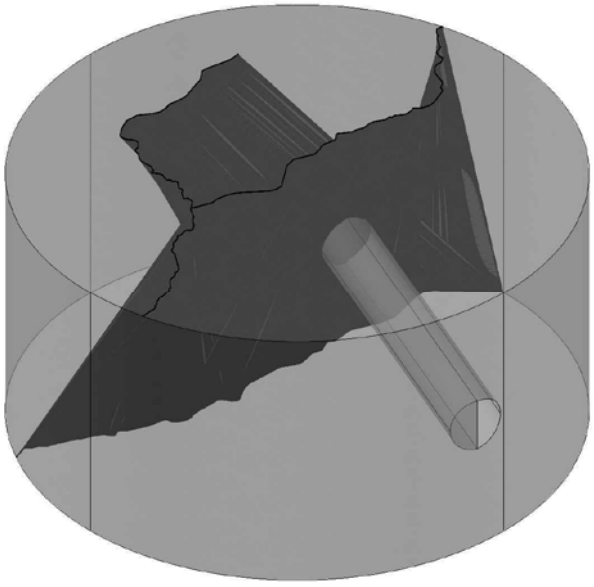

Figure A19. 3D representation of sample L

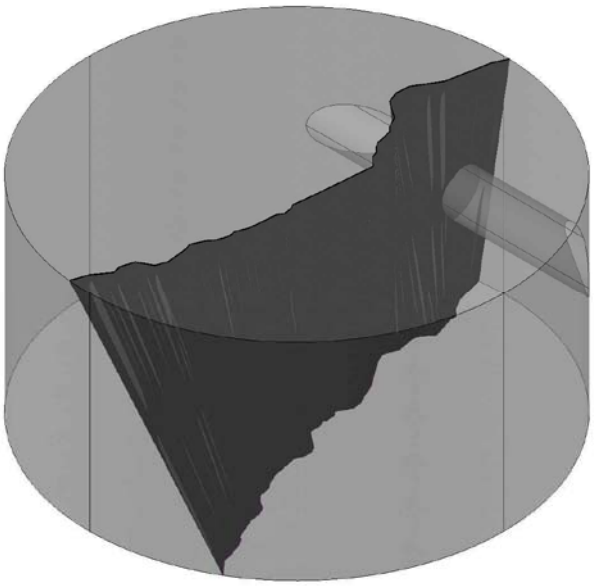

Figure A20. 3D representation of sample M

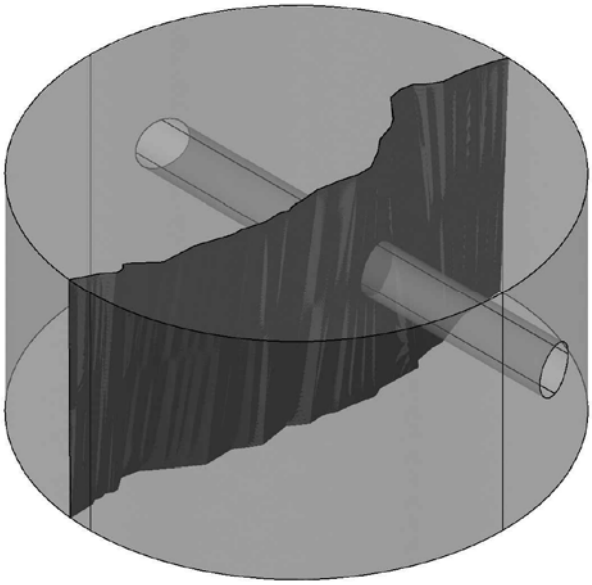

Figure A21. 3D representation of sample N